Dynamic Aggregation of Grid-tied Inverters

A DISSERTATION
SUBMITTED TO THE FACULTY OF THE GRADUATE SCHOOL
OF THE UNIVERSITY OF MINNESOTA
BY

Victor Chris Samuel Purba

IN PARTIAL FULFILLMENT OF THE REQUIREMENTS
FOR THE DEGREE OF
DOCTOR OF PHILOSOPHY

Prof. Sairaj Dhople, Advisor

July, 2020

Acknowledgements

I would like to express my sincere gratitude to my research advisor Prof. Sairaj Dhople for his guidance starting from the senior honor project until my Ph.D. study. I am grateful for his support, patience, and motivation through these years. His insight and knowledge on power systems and power electronics have deepened my understanding on the subjects.

I would like to thank my committee members: Prof. Ned Mohan, Prof. Jungwon Choi, and Prof. Peter Seiler for their advice and insightful comments on this dissertation. I would also extend my gratitude to Prof. Bruce Wollenberg for his courses on power systems, and to Prof. Mihailo Jovanović for his courses on control systems and the research opportunity in my undergraduate and early graduate years.

I would like to thank my fellow collaborators: Brian Johnson, Saber Jafarpour, Francesco Bullo, Miguel Rodriguez, and Yashen Lin for their valuable comments and feedback on the ideas that matter to this Ph.D. study. This dissertation would not have been possible without their hard work. I also thank my fellow labmates: Swaroop, Mohit, Sanjana, Xinwei, Sukumar, and Hyungjin for all their help and time working together.

Finally, I would like to thank my parents, siblings, and friends for their prayer, support, and encouragement throughout my studies.

Dedication

To my parents, Sintar Purba and Damery Evalyn

Abstract

Power-electronics inverters are being integrated in large numbers in distribution networks with rapid deployment of renewable resources, energy storage, and flexible loads. Since such distributed energy resources will serve a majority of loads in the next-generation power network, it is critical to develop scalable and accurate modeling tools to study the dynamical behavior of systems with large numbers of inverters. Typical dynamical models for grid-tied inverters are nonlinear and composed of a large number of states; therefore it is impractical to study systems with many inverters when their full dynamics are retained. To address this issue, a reduced-order aggregated model for parallel-connected grid-tied three-phase inverters is formulated. A necessary and sufficient set of parametric relationships is derived to ensure that the reduced-order models for an arbitrary number of such paralleled inverters have the same model order and structure as any single inverter. The reduced-order model is extended for photovoltaic (PV) inverters, where a PV array, a maximum power point tracking (MPPT) algorithm, and a dc-link capacitor are incorporated into the three-phase inverter model.

Furthermore, a network-cognizant aggregation approach for distribution networks comprising grid-tied inverters is developed. Inverters are clustered based on effective impedances to an infinite bus (modeling the transmission-distribution boundary) and for each cluster, the reduced-order aggregated model is utilized to replace the inverters in the cluster. The K-means algorithm is leveraged for clustering and a suitable linearization of the power-flow equations reduces computational burden involved in determining terminal voltages for the clusters. Numerical simulation results for a benchmark feeder system demonstrate the accuracy and computational benefits of the aggregation method.

Contents

List of Tables

List of Figures

Chapter 1

Introduction

Large numbers of power-electronics inverters are being integrated in distribution networks to interface renewable sources of generation (e.g., photovoltaic (PV) energy conversion systems), energy storage (e.g., large-scale batteries), and flexible loads (e.g., electric vehicles). For instance, island of Oahu in Hawaii has over $800,000$ microinverters [1]. This number is expected to grow as Hawaii plans to achieve 100% penetration level of renewable resources by 2045 [2].

The ratings of individual inverters are typically less than a few MVA while synchronous generators have ratings of several hundred MVA. This disparity implies that serving the same net load with inverters instead of generators would require an orders-of-magnitude increase in the number of energy-conversion interfaces (from a few thousand generators to potentially millions of inverters). Since systems with large numbers of inverters will be common in the future, it is critical to develop scalable and accurate models for such systems with limited computational burden. To this end, this dissertation focuses on reducing the model complexity of multi-inverter systems. It begins with reduced-order aggregate state-space models for an arbitrary number of grid-tied inverters connected in parallel. An aggregation technique acknowledging the network interconnection between the inverters is then proposed.

In this dissertation, we examine a three-phase voltage source inverter (VSI) and output LCL filter. The control architecture of the inverter is composed of a pulse width modulation (PWM) scheme, an inner current-control loop, an outer power-control loop, and a phase-locked loop (PLL) for grid synchronization. The model is extended to a

three-phase photovoltaic (PV) inverter, where the dc-side components, in this case a PV array and a dc-link capacitor, are acknowledged in the three-phase inverter model. The control architecture is expanded to include a maximum power tracking (MPPT) algorithm and a dc-link controller. The ac-side three-phase and PV inverter models are prototypical in the literature [3–12].

For parallel connection of inverters with the same topology, we develop an aggregate reduced-order inverter model that has a state-space model with the same structure and model order as any single inverter in the collection. To this end, we derive a necessary and sufficient set of parametric relationships between the aggregate model and the individual model by which the aggregate model captures the collective dynamical behavior of the parallel system. For the ac-side three-phase inverter model, we are able to expand their aggregate model for the case when the power ratings of the inverters are all different, and the case when the reference setpoints to the inverters are all different.

With the aggregate models at the foundation, we develop a network-cognizant model reduction technique for distribution networks comprising grid-tied inverters. In addition to the grid-tied inverters, our model for the distribution network includes impedance loads interconnected to the inverters through lines modeled with Π-equivalent circuits. Individually modeling the dynamics of all inverters, interconnecting lines, and loads to glean insights into the collective behavior of the distribution network, with particular emphasis on the real- and reactive-power injected into the feederhead, is computationally intractable. As a solution, we develop an aggregation approach for the distribution network. It involves clustering the inverters based on their electrical distances from the feederhead that leverages the K-means algorithm, transferring the inverters to auxiliary buses based on their clusters with the aid of auxiliary transformers to connect these auxiliary buses to the inverter buses in the original network and linear approximation of the power flow equations to reduce computation burden of solving a nonlinear ac power flow.

This dissertation collects the work that have appeared in various conferences and journals. We report these alongside a discussion of the organization of the dissertation next. Chapter 2 introduces the mathematical notation used in the manuscript. Chapter 3 describes the three-phase grid-tied inverter model, develops the reduced-order aggregate model for parallel-connected inverters, and validates the reduced-order

model with numerical simulations [13]. Chapter 4 extends the results for the three-phase inverter model to include the PV array model and relevant dc-side components and controllers [14]. Chapter 5 develops the distribution-network-cognizant aggregation approach and validates the approach with numerical simulations for the IEEE 37-bus feeder system [15, 16]. Chapter 6 presents concluding remarks of this dissertation and outlines a few recommendations for future research. (This dissertation also includes the work in [17] which developed the reduced-order model for parallel connection of grid-tied single-phase inverters in Appendix A. In addition to numerical simulations, the aggregate model is validated against measurements obtained from an experimental setup of parallel-connected single-phase inverters.) Most of the discussion is presented as it appeared in those manuscripts with slight embellishments and interpolations to connect to the overarching theme. Each chapter includes a survey of the relevant literature.

Chapter 2

Notation

The spaces of $N \times 1$ real- and complex-valued vectors are denoted by $\mathbb{R}^N$ and $\mathbb{C}^N$, respectively; $\mathbb{R}^{M \times N}$ and $\mathbb{C}^{M \times N}$ denote the spaces of $M \times N$ real- and complex-valued matrices, respectively. The matrix transpose is denoted by $(\cdot)^{\mathrm{T}}$. The Moore-Penrose pseudo inverse of a matrix B is denoted by $B^{\dagger}$. A diagonal matrix formed with the entries of vector x is denoted by $\mathrm{diag}(x)$; $\mathrm{bdiag}(A_1, \ldots, A_N)$ denotes a block diagonal matrix of $A_1, \ldots, A_N$. The entrywise natural logarithm and the smallest entry of vector x are denoted by $\log(x)$ and $\min(x)$, respectively; $\mathbb{1}_N$ and $\mathbb{0}_N$ denote N-dimension vectors of all one and all zero entries, respectively; I_N and $\mathbb{0}_{M \times N}$ denote the $N \times N$ identity matrix and an $M \times N$ matrix of all zeros, respectively. Furthermore, $j = \sqrt{-1}$; the magnitude, angle, real and imaginary components of a complex variable x are denoted by $|x|$, $\angle x$, $\mathrm{Re}\{x\}$, and $\mathrm{Im}\{x\}$, respectively, and the matrix conjugate transpose is denoted by $(\cdot)^{\mathrm{H}}$. The cardinality of set $\mathcal{A}$ is denoted by $|\mathcal{A}|$. The maximum of two scalars, a and b, is denoted by $\max(a, b)$.

Chapter 3

Aggregation of Parallel-connected Grid-tied Three-phase Inverters

In this chapter, we examine a three-phase inverter with a full-bridge topology and output LCL filter. As shown in Fig. 3.1, the inverter control system includes: a current controller (that generates the pulse width modulation (PWM) reference signals), a power controller (that responds to real- and reactive-power setpoints and generates current references for the current controller), and a phase-locked loop (PLL) (for grid synchronization). The topology is prototypical and is recognizably popular in the literature [3–8]. Models of this sort generally have more than 10 dynamical states (the particular one we study has 15); and therefore, it is computationally infeasible and analytically unwieldy to study large collections of such inverters with different power ratings. To address these limitations, we derive a structure-preserving reduced-order inverter model for the setting where individual inverters in the parallel setup have the same topology with filter components and controller gains that scale linearly with the power rating in this chapter. By structure preserving, we mean that the reduced-order model itself is a three-phase inverter that is also composed of an LCL filter, a power controller, current controller, and PLL, i.e., it has the same structure and the same number of dynamical states as any individual inverter in the parallel multi-inverter system.

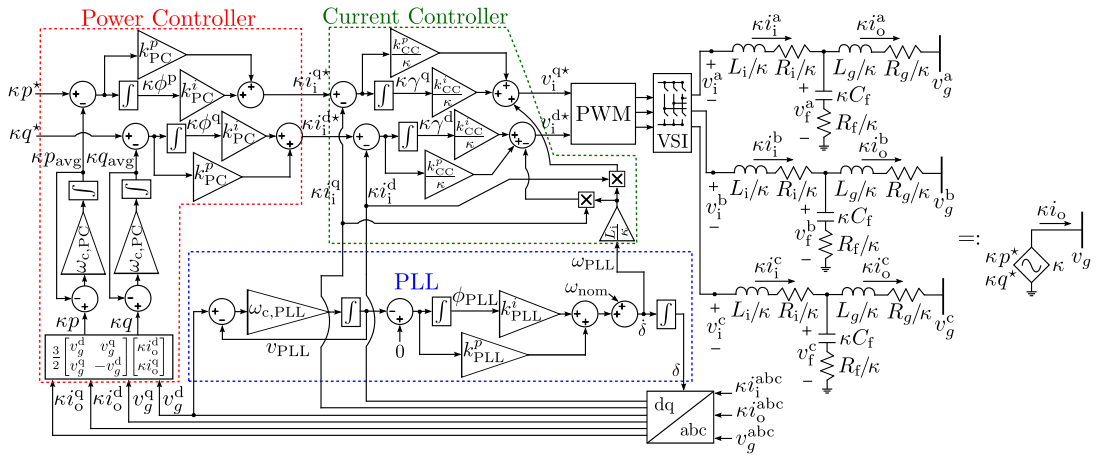

Figure 3.1: Feed-back control loops and output filter of the grid-tied three-phase inverter, and adopted shorthand depicting: i) power rating, with the aid of the power-scaling parameter, κ (see (3.1)), ii) real-power setpoint, $\kappa p^\star$, and iii) reactive-power setpoint, $\kappa q^\star$. Variables super-scripted by a, b, c denote the time-domain ac waveforms for the respective phases, while those super-scripted by d, q correspond to those in the dq reference frame computed with the PLL angle, δ serving as the transformation angle.

A majority of prior literature pertaining to model reduction for energy conversion interfaces has understandably focused on the dynamics of fossil-fuel-driven synchronous generators [18–22]. More recently, there has been increased attention devoted to aggregate models for wind-turbines in utility-scale collector systems [23, 24], electric vehicles [25], and demand response systems [26]. However, these are focused at a macro level that disregards the dynamics at faster time scales which arise from inverter filters and time-domain controllers. With regard to inverter dynamics, most of the related literature has predominantly focused on reduced-order models for *individual* grid-connected [27], islanded [28–30], and resonant inverters [31]. (Tangentially related is literature on model reduction of dc-dc converters [32–34] and induction machines [35, 36].) Model-reduction methods focused on *collections* of inverters have been limited to islanded settings [37, 38] and inverters with virtual-inertia emulation [39]. Both are application domains where inverters are controlled to emulate the dynamics of synchronous generators, and therefore, there is a natural translation of classical model-reduction methods for synchronous generators mentioned previously.

The remainder of this chapter is organized as follows. In Section 3.1, we introduce a three-phase grid-connected inverter model and power scaling laws for the inverter. In Section 3.2, we describe how the states of the inverter are scaled based on its power-scaling parameter, and propose the reduced-order structure-preserving model for parallel-connected inverters. To validate the proposed reduced-order model, we compare numerical simulation of a parallel system to its corresponding reduced-order inverter model in Section 3.3.

3.1 The Inverter Model and Power Scaling Laws

The three-phase inverter is sketched in Fig. 3.1. We assume a voltage source inverter (VSI) with a full-bridge topology and an output LCL filter (L_{i}, C_{f}, L_g). The grid voltage and frequency are denoted by v_g and ω_g, respectively. The control architecture for each inverter includes: an inner-loop current controller, an outer-loop power controller, and a PLL. Since the focus of this chapter is at the ac-side point of common coupling, dynamics of the dc-link and any other converter stages that precede the dc-link are neglected. As shown in Fig. 3.2, we are primarily interested in the collective behavior of N such inverters connected in parallel to the grid. We begin this section with an overview on how the inverters are designed for different power ratings, the features of the reduced-order model sought for the parallel collection of inverters, and then briefly discuss the controller and LCL filter dynamics. Lastly, we represent the dynamics of the inverter in state-space form.

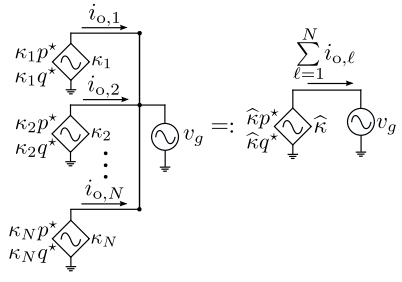

Figure 3.2: For the parallel connection of N inverters, we obtain the power-scaling parameter, $\widehat{\kappa}$, for a reduced-order structure-preserving model.

3.1.1 Scaling Individual Inverters with Power Rating

We first introduce the notion of a *power-scaling parameter*, κ, which is defined as

$$\kappa := \frac{p_{\text{rated}}}{p_{\text{base}}}, \tag{3.1}$$

where p_{rated} is the rated power of a given inverter, and p_{base} is a system-wide base value. We make the assumption that both real and reactive power ratings scale linearly with κ. Suppose we denote the base real- and reactive-power setpoints as $p^\star$ and $q^\star$. Notice from Fig. 3.1 that the reference-power setpoints for the inverter are given by $\kappa p^\star, \kappa q^\star$. Therefore, the output real and reactive power injected by each inverter into the grid are directly proportional to κ. We scale elements of the LCL filter in the manner shown in Fig. 3.1 so that the output current is inversely proportional to the impedance of the filter. With regard to the controllers, we also scale the gains of the current controller by $1/\kappa$ so that its outputs, i.e., the reference for the input voltage of the LCL filter, do not depend on κ, and neither does the voltage drop across the LCL filter. Thus, the output current, and therefore the output power, of the inverter scales directly proportionally to κ.

The scaling approach described above is admittedly assumptive by nature. However, it is a herculean—if not impossible—task to ascertain how commercial inverter manufacturers would scale the cyber-physical architectures of inverters with power rating. Therefore, we base our analysis around this scaling approach, taking solace in the fact that it is grounded in and guided by some fundamental engineering insights.

3.1.2 Desired Features of the Structure-preserving Reduced-order Model

With the control and physical architecture of individual inverters highlighted in Fig. 3.1, and the procedure to scale the inverter design to accommodate different power ratings discussed above, we bring attention to Fig. 3.2 to describe the main goal of this work. We consider a collection of N inverters with different power ratings (described by power-scaling parameters $\kappa_1, \ldots, \kappa_N$) connected in parallel to the grid bus. The dynamics of each inverter include those of the different control blocks and LCL filters illustrated in Fig. 3.1, and are described collectively by a 15-order model (which will be spelled out

subsequently). We derive a structure-preserving reduced-order model for this parallel connection. Particularly, we will show that an inverter model with power-scaling parameter, $\widehat{\kappa} = \sum_{\ell=1}^{N} \kappa_\ell$ perfectly captures the input-output behavior of the N-inverter collection with a dynamical-system model that has the same order and structure as any individual inverter.

3.1.3 Model of an Individual Inverter

With the design procedure adopted for scaling inverters in place, and the goal of this effort described, we next briefly overview individual portions of the dynamical models for the individual inverters in Fig. 3.1. We start with the reference-frame transformation, and then go through the PLL, the current controller, and the power controller. In each case, we describe the model assuming assuming $\kappa = 1$, but indicate how the dynamics are modified for an inverter with a power rating that is not the base value.

3.1.3.1 Reference-frame transformation

Sinusoidally varying three-phase signals $(x^{\mathrm{a}}, x^{\mathrm{b}}, x^{\mathrm{c}})$ in balanced settings are coordinate transformed to equivalent DC signals $(x^{\mathrm{d}}, x^{\mathrm{q}})$ using Park's transformation: [40]

$$\begin{bmatrix} x^{\mathrm{d}} \\ x^{\mathrm{q}} \end{bmatrix} = \frac{2}{3} \begin{bmatrix} \cos(\delta) & \cos(\delta - \frac{2\pi}{3}) & \cos(\delta + \frac{2\pi}{3}) \\ -\sin(\delta) & -\sin(\delta - \frac{2\pi}{3}) & -\sin(\delta + \frac{2\pi}{3}) \end{bmatrix} \begin{bmatrix} x^{\mathrm{a}} \\ x^{\mathrm{b}} \\ x^{\mathrm{c}} \end{bmatrix} =: \frac{2}{3} \Psi \begin{bmatrix} x^{\mathrm{a}} \\ x^{\mathrm{b}} \\ x^{\mathrm{c}} \end{bmatrix}, \tag{3.2}$$

where δ is the instantaneous angle generated by the PLL. The change in coordinates is signified with the abc-dq block in Fig. 3.1. We further note that $[x^{\mathrm{a}}, x^{\mathrm{b}}, x^{\mathrm{c}}]^{\mathrm{T}} = \Psi^{\mathrm{T}}[x^{\mathrm{d}}, x^{\mathrm{q}}]^{\mathrm{T}}$. To illustrate the adopted notation in abc and dq coordinates, consider the grid voltage, v_g, without loss of generality. First, $v_g^{\mathrm{abc}} := [v_g^{\mathrm{a}}, v_g^{\mathrm{b}}, v_g^{\mathrm{c}}]^{\mathrm{T}}$ captures v_g in abc coordinates. In the dq reference frame, we define $v_g^{\mathrm{dq}} := [v_g^{\mathrm{d}}, v_g^{\mathrm{q}}]^{\mathrm{T}}$, and $v_g^{\mathrm{abc}} = \Psi^{\mathrm{T}} v_g^{\mathrm{dq}}$.

3.1.3.2 Phase-locked Loop

The PLL is in feedback with the dq transformation for the grid voltage, and it modulates the angle δ such that $v_g^{\mathrm{d}} \to 0$ asymptotically. (Elementary trigonometric identities coupled with (3.2) illustrate that when $v_g^{\mathrm{d}} = 0$, δ is the instantaneous phase angle of v_g^{a},

i.e., the inverter is *phase locked* with the grid. See Appendix B.1 for a short derivation.) It consists of a low pass filter (with cut-off frequency $\omega_{\mathrm{c,PLL}}$) and a PI controller (with PI gains k^p_{PLL} and k^i_{PLL}). The dynamics of the PLL that generate the angle δ are:

$$\begin{aligned} \dot{v}_{\mathrm{PLL}} &= \omega_{\mathrm{c,PLL}}(v_g^{\mathrm{d}} - v_{\mathrm{PLL}}), \\ \dot{\phi}_{\mathrm{PLL}} &= -v_{\mathrm{PLL}}, \\ \dot{\delta} &= \omega_{\mathrm{nom}} - k^p_{\mathrm{PLL}} v_{\mathrm{PLL}} + k^i_{\mathrm{PLL}} \phi_{\mathrm{PLL}} =: \omega_{\mathrm{PLL}}, \end{aligned} \tag{3.3}$$

where ω_{nom} is the nominal grid frequency (e.g., $2\pi \times 60$ or $2\pi \times 50$ [rad/s]). From the dynamics, we can see that at steady state, $v_g^{\mathrm{d}} = v_{\mathrm{PLL}} = 0$. Furthermore, when the grid frequency is at the nominal, it follows that $\dot{\delta} = \omega_{\mathrm{PLL}} = \omega_{\mathrm{nom}}$.

Remark 3.1 (Dynamics of PLL in scaled inverter)**.** *The same dynamics in* (3.3) *are utilized for inverters with different power ratings, i.e., for the case* $\kappa \neq 1$.

3.1.3.3 Output LCL Filter

The dynamics of the LCL filter (in the dq reference frame) are derived by running pertinent time-domain circuit equations through the dq transformation with angle δ. This yields

$$\begin{aligned} \dot{i}_{\mathrm{i}}^{\mathrm{dq}} &= \frac{1}{L_{\mathrm{i}}}(-R_{\mathrm{i}} i_{\mathrm{i}}^{\mathrm{dq}} + v_{\mathrm{i}}^{\mathrm{dq}} - v_{\mathrm{f}}^{\mathrm{dq}}) + \begin{bmatrix} 0 & 1 \\ -1 & 0 \end{bmatrix} \omega_{\mathrm{PLL}} i_{\mathrm{i}}^{\mathrm{dq}}, \\ \dot{i}_{\mathrm{o}}^{\mathrm{dq}} &= \frac{1}{L_g}(-R_g i_{\mathrm{o}}^{\mathrm{dq}} + v_{\mathrm{f}}^{\mathrm{dq}} - v_g^{\mathrm{dq}}) + \begin{bmatrix} 0 & 1 \\ -1 & 0 \end{bmatrix} \omega_{\mathrm{PLL}} i_{\mathrm{o}}^{\mathrm{dq}}, \\ \dot{v}_{\mathrm{f}}^{\mathrm{dq}} &= R_{\mathrm{d}}(\dot{i}_{\mathrm{i}}^{\mathrm{dq}} - \dot{i}_{\mathrm{o}}^{\mathrm{dq}}) - \begin{bmatrix} 0 & 1 \\ -1 & 0 \end{bmatrix} \omega_{\mathrm{PLL}} R_{\mathrm{d}}(i_{\mathrm{i}}^{\mathrm{dq}} - i_{\mathrm{o}}^{\mathrm{dq}}) \\ &\qquad + \frac{1}{C_{\mathrm{f}}}(i_{\mathrm{i}}^{\mathrm{dq}} - i_{\mathrm{o}}^{\mathrm{dq}}) + \begin{bmatrix} 0 & 1 \\ -1 & 0 \end{bmatrix} \omega_{\mathrm{PLL}} v_{\mathrm{f}}^{\mathrm{dq}}, \end{aligned} \tag{3.4}$$

where $i_{\mathrm{i}}^{\mathrm{dq}} = [i_{\mathrm{i}}^{\mathrm{d}}, i_{\mathrm{i}}^{\mathrm{q}}]^{\mathrm{T}}$, $i_{\mathrm{o}}^{\mathrm{dq}} = [i_{\mathrm{o}}^{\mathrm{d}}, i_{\mathrm{o}}^{\mathrm{q}}]^{\mathrm{T}}$, $v_{\mathrm{i}}^{\mathrm{dq}} = [v_{\mathrm{i}}^{\mathrm{d}}, v_{\mathrm{i}}^{\mathrm{q}}]^{\mathrm{T}}$, and $v_{\mathrm{f}}^{\mathrm{dq}} = [v_{\mathrm{f}}^{\mathrm{d}}, v_{\mathrm{f}}^{\mathrm{q}}]^{\mathrm{T}}$.

Remark 3.2 (Dynamics of LCL filter in scaled inverter)**.** *While the dynamics above correspond to the case where the power-scaling parameter,* $\kappa = 1$*; for inverters with*

power ratings that are scaled values of this base setting, we utilize the filter parameters L_{i}/κ, R_{f}/κ, κC_{f}, R_{d}/κ, L_g/κ, R_g/κ *with* κ *chosen according to* (3.1).

3.1.3.4 Power Controller

The power controller consists of two low pass filters (with cut-off frequency $\omega_{\mathrm{c,PC}}$) and two PI controllers (with PI gains $k^p_{\mathrm{PC}}, k^i_{\mathrm{PC}}$), with its outputs to be the references for the current controller:

$$\begin{aligned} i_{\mathrm{i}}^{\mathrm{d}\star} &= k^p_{\mathrm{PC}}\,(q^\star - q_{\mathrm{avg}}) + k^i_{\mathrm{PC}} \int (q^\star - q_{\mathrm{avg}})dt, \\ i_{\mathrm{i}}^{\mathrm{q}\star} &= k^p_{\mathrm{PC}}\,(p^\star - p_{\mathrm{avg}}) + k^i_{\mathrm{PC}} \int (p^\star - p_{\mathrm{avg}})dt, \end{aligned}$$

where $p^\star, q^\star$ are reference real- and reactive-power setpoints. Furthermore, p_{avg} and q_{avg} are low-pass-filtered versions of the inverter output real and reactive power outputs:

$$\begin{aligned} \dot{p}_{\mathrm{avg}} &= \omega_{\mathrm{c,PC}}(p - p_{\mathrm{avg}}), \\ \dot{q}_{\mathrm{avg}} &= \omega_{\mathrm{c,PC}}(q - q_{\mathrm{avg}}), \end{aligned} \tag{3.5}$$

where p and q are the instantaneous real and reactive output power (measured at the grid terminals) and given by

$$\begin{aligned} p &= \frac{3}{2}(v_g^{\mathrm{d}} i_{\mathrm{o}}^{\mathrm{d}} + v_g^{\mathrm{q}} i_{\mathrm{o}}^{\mathrm{q}}), \\ q &= \frac{3}{2}(v_g^{\mathrm{q}} i_{\mathrm{o}}^{\mathrm{d}} - v_g^{\mathrm{d}} i_{\mathrm{o}}^{\mathrm{q}}). \end{aligned}$$

To ease notation and exposition in subsequent developments, we will find it useful to define:

$$\begin{aligned} \dot{\phi}^{\mathrm{p}} &:= p^\star - p_{\mathrm{avg}}, \\ \dot{\phi}^{\mathrm{q}} &:= q^\star - q_{\mathrm{avg}}. \end{aligned} \tag{3.6}$$

Remark 3.3 (Dynamics of power controller in scaled inverter)**.** *For inverters with* $\kappa \neq 1$*, the power setpoints are scaled as* $\kappa p^\star$ *and* $\kappa q^\star$*; all other dynamics reported above are retained.*

3.1.3.5 Current Controller

The current controller consists of two PI controllers (with PI gains $k^p_{\rm CC}, k^i_{\rm CC}$) and feedforward terms, with its outputs to be the reference for the terminal voltage $v_{\rm i}$:

$$v_{\rm i}^{\rm d\star} = -\omega_{\rm PLL} L_{\rm i} i_{\rm i}^{\rm q} + k^p_{\rm CC}\left(i_{\rm i}^{\rm d\star} - i_{\rm i}^{\rm d}\right) + k^i_{\rm CC}\int (i_{\rm i}^{\rm d\star} - i_{\rm i}^{\rm d})dt,$$
$$v_{\rm i}^{\rm q\star} = \omega_{\rm PLL} L_{\rm i} i_{\rm i}^{\rm d} + k^p_{\rm CC}\left(i_{\rm i}^{\rm q\star} - i_{\rm i}^{\rm q}\right) + k^i_{\rm CC}\int (i_{\rm i}^{\rm q\star} - i_{\rm i}^{\rm q})dt.$$

The addition of the feedforward terms $-\omega_{\rm PLL} L_{\rm i} i_{\rm i}^{\rm q}$ and $\omega_{\rm PLL} L_{\rm i} i_{\rm i}^{\rm d}$ is standard practice, and intended to improve dynamic performance [41]. To ease notation and exposition in subsequent developments, we will find it useful to define:

$$\begin{aligned} \dot{\gamma}^{\rm d} &= i_{\rm i}^{\rm d\star} - i_{\rm i}^{\rm d}, \\ \dot{\gamma}^{\rm q} &= i_{\rm i}^{\rm q\star} - i_{\rm i}^{\rm q}. \end{aligned} \tag{3.7}$$

The (three-phase) PWM modulation signals for the inverter are then obtained as $v_{\rm i}^{\rm abc\star} = \Psi^{\rm T} v_{\rm i}^{\rm dq\star}$. With reference to Fig. 3.1, for an ideal inverter we have that the inverter terminal voltage, $v_{\rm i}^{\rm abc} = v_{\rm i}^{\rm abc\star}$ (and equivalently $v_{\rm i}^{\rm dq} = v_{\rm i}^{\rm dq\star}$). This approximation implies that the inverter terminal voltage follows the commanded reference perfectly and without delay.

Remark 3.4 (Dynamics of current controller in scaled inverter)**.** *While the dynamics above correspond to the case where the power-scaling parameter, $\kappa = 1$; for inverters with power ratings that are scaled values of this base setting, we utilize the parameters $k^p_{\rm CC}/\kappa$, $k^i_{\rm CC}/\kappa$.*

3.1.4 State-space Model for the Inverter Dynamics

For the model in (3.3)–(3.7), we assumed that $\kappa = 1$ and hence, it defines the dynamics in the *unscaled* inverter. For this case, the controller and filter dynamics can be compactly represented in state-space form as follows

$$\dot{x} = Ax + Bu_1 + g(x, u_2), \tag{3.8}$$

where the states are $x = [i_{\mathrm{i}}^{\mathrm{d}}, i_{\mathrm{i}}^{\mathrm{q}}, i_{\mathrm{o}}^{\mathrm{d}}, i_{\mathrm{o}}^{\mathrm{q}}, \gamma^{\mathrm{d}}, \gamma^{\mathrm{q}}, p_{\mathrm{avg}}, q_{\mathrm{avg}}, \phi^{\mathrm{p}}, \phi^{\mathrm{q}}, v_{\mathrm{f}}^{\mathrm{d}}, v_{\mathrm{f}}^{\mathrm{q}}, v_{\mathrm{PLL}}, \phi_{\mathrm{PPL}}, \delta]^{\mathrm{T}}$, and the inputs include $u_1 = [p^\star, q^\star]^{\mathrm{T}}$ and $u_2 = [v_g^{\mathrm{a}}, v_g^{\mathrm{b}}, v_g^{\mathrm{c}}]^{\mathrm{T}} = v_g^{\mathrm{abc}}$. Here, the matrices $A \in \mathbb{R}^{15\times 15}$, $B \in \mathbb{R}^{15\times 2}$, and function $g : \mathbb{R}^{15} \times \mathbb{R}^3 \to \mathbb{R}^{15}$ can be derived from the dynamical-system models in (3.6)–(3.7) straightforwardly. For completeness, their entries are listed in Appendix B.2.

Now, let us consider a *scaled* inverter with $\kappa \neq 1$. If we replace the unscaled model parameters as follows: (see Remarks 3.1–3.4)

$$\left(L_{\mathrm{i}}, R_{\mathrm{i}}, C_{\mathrm{f}}, R_{\mathrm{f}}, L_g, R_g, k_{\mathrm{CC}}^p, k_{\mathrm{CC}}^i\right) \to \left(\frac{L_{\mathrm{i}}}{\kappa}, \frac{R_{\mathrm{i}}}{\kappa}, NC_{\mathrm{f}}, \frac{R_{\mathrm{f}}}{\kappa}, \frac{L_g}{\kappa}, \frac{R_g}{\kappa}, \frac{k_{\mathrm{CC}}^p}{\kappa}, \frac{k_{\mathrm{CC}}^i}{\kappa}\right), \tag{3.9}$$

and the rest of parameters are unchanged, we obtain the *scaled* inverter model

$$\dot{x}^{\mathrm{s}} = A^{\mathrm{s}} x^{\mathrm{s}} + B^{\mathrm{s}} u_1^{\mathrm{s}} + g^{\mathrm{s}}(x^{\mathrm{s}}, u_2^{\mathrm{s}}), \tag{3.10}$$

where the inputs are $u_1^{\mathrm{s}} = \kappa u_1$ and $u_2^{\mathrm{s}} = u_2 = v_g^{\mathrm{abc}}$. The matrices $A^{\mathrm{s}} \in \mathbb{R}^{15\times 15}$, $B^{\mathrm{s}} \in \mathbb{R}^{15\times 2}$, and function $g^{\mathrm{s}} : \mathbb{R}^{15} \times \mathbb{R}^3 \to \mathbb{R}^{15}$ have the same structure as A, B, and g for the unscaled model albeit with parametric scalings given above.

3.2 Inverter Scaling and Reduced-order Model

In this section, we begin with establishing the relationship between the states in the scaled and unscaled inverter models, then we propose a method of aggregating N parallel-connected inverters illustrated in Fig. 3.2. Lastly, we provide a corollary for the case when the reference-power setpoints are arbitrary.

3.2.1 Scaling of Inverter States

Here, we establish the connection between the dynamics of the scaled and unscaled inverters.

Theorem 3.1 (Scaling of three-phase inverter)**.** *Consider the dynamics of the unscaled inverter (with $\kappa = 1$) and scaled inverter (with $\kappa \neq 1$) in* (3.8) *and* (3.10)*, respectively. Suppose the initial conditions for the two dynamical systems at some time $t_0 \geq 0$ are such that $x^{\mathrm{s}}(t_0) = \mathrm{diag}(K)x(t_0)$, with $K := [\kappa \mathbb{1}_{10}^{\mathrm{T}}, \mathbb{1}_5^{\mathrm{T}}]^{\mathrm{T}}$, and the inputs are $u_1^{\mathrm{s}} = \kappa u_1$*

and $u_2^{\mathrm{s}} = u_2$. *It follows that* $x^{\mathrm{s}}(t) = \mathrm{diag}(K)x(t),\ \forall t \geq t_0$ *if and only if the parameters are related as* (3.9).

Proof. We begin by defining $z := x^{\mathrm{s}} - \mathrm{diag}(K)x$. The dynamics of z are given by

$$\begin{aligned}\dot{z} = \dot{x}^{\mathrm{s}} - \mathrm{diag}(K)\dot{x} = A^{\mathrm{s}}x^{\mathrm{s}} + B^{\mathrm{s}}u_1^{\mathrm{s}} + g^{\mathrm{s}}(x^{\mathrm{s}}, u_2^{\mathrm{s}}) - \mathrm{diag}(K)Ax \\ - \mathrm{diag}(K)Bu_1 - \mathrm{diag}(K)g(x, u_2). \end{aligned} \tag{3.11}$$

We will show that $\dot{z} = \mathbb{0}_{15}, \forall t \geq t_0$ when $z(t_0) = x^{\mathrm{s}}(t_0) - \mathrm{diag}(K)x(t_0) = \mathbb{0}_{15}$. This implies that $z(t) = x^{\mathrm{s}}(t) - \mathrm{diag}(K)x(t) = \mathbb{0}_{15}, \forall t \geq t_0$ as claimed in the theorem statement.

We partition x as $[x_1^{\mathrm{T}}, x_2^{\mathrm{T}}]^{\mathrm{T}}$, where $x_1^{\mathrm{T}} = [i_{\mathrm{i}}^{\mathrm{d}}, i_{\mathrm{i}}^{\mathrm{q}}, i_{\mathrm{o}}^{\mathrm{d}}, i_{\mathrm{o}}^{\mathrm{q}}, \gamma^{\mathrm{d}}, \gamma^{\mathrm{q}}, p_{\mathrm{avg}}, q_{\mathrm{avg}}, \phi^{\mathrm{p}}, \phi^{\mathrm{q}}]^{\mathrm{T}}$ and $x_2^{\mathrm{T}} = [v_{\mathrm{f}}^{\mathrm{d}}, v_{\mathrm{f}}^{\mathrm{q}}, v_{\mathrm{PLL}}, \phi_{\mathrm{PPL}}, \delta]^{\mathrm{T}}$, and we also partition x^{s} the same way. Then we write (3.8) and (3.10) as follows

$$\begin{bmatrix}\dot{x}_1 \\ \dot{x}_2\end{bmatrix} = \begin{bmatrix}A_{11} & A_{12} \\ A_{21} & A_{22}\end{bmatrix}\begin{bmatrix}x_1 \\ x_2\end{bmatrix} + \begin{bmatrix}B_1 \\ B_2\end{bmatrix}u_1 + g(x, u_2), \tag{3.12}$$

$$\begin{bmatrix}\dot{x}_1^{\mathrm{s}} \\ \dot{x}_2^{\mathrm{s}}\end{bmatrix} = \begin{bmatrix}A_{11}^{\mathrm{s}} & A_{12}^{\mathrm{s}} \\ A_{21}^{\mathrm{s}} & A_{22}^{\mathrm{s}}\end{bmatrix}\begin{bmatrix}x_1^{\mathrm{s}} \\ x_2^{\mathrm{s}}\end{bmatrix} + \begin{bmatrix}B_1^{\mathrm{s}} \\ B_2^{\mathrm{s}}\end{bmatrix}u_1^{\mathrm{s}} + g^{\mathrm{s}}(x^{\mathrm{s}}, u_2^{\mathrm{s}}). \tag{3.13}$$

By observing the entries of the state-space matrices, it is straightforward to see the following relationships:

$$A_{11}^{\mathrm{s}} = A_{11},\ A_{12}^{\mathrm{s}} = \kappa A_{12}, A_{21}^{\mathrm{s}} = \frac{1}{\kappa}A_{21},\ A_{22}^{\mathrm{s}} = A_{22}, \tag{3.14}$$

$$B_1^{\mathrm{s}} = B_1, B_2^{\mathrm{s}} = \frac{1}{\kappa}B_2. \tag{3.15}$$

Then we have

$$\mathrm{diag}(K)A = \begin{bmatrix}\kappa A_{11} & \kappa A_{12} \\ A_{21} & A_{22}\end{bmatrix} = \begin{bmatrix}\kappa A_{11}^{\mathrm{s}} & A_{12}^{\mathrm{s}} \\ \kappa A_{21}^{\mathrm{s}} & A_{22}^{\mathrm{s}}\end{bmatrix} = A^{\mathrm{s}}\mathrm{diag}(K), \tag{3.16}$$

$$\mathrm{diag}(K)B = \begin{bmatrix}\kappa B_1 \\ B_2\end{bmatrix} = \begin{bmatrix}\kappa B_1^{\mathrm{s}} \\ \kappa B_2^{\mathrm{s}}\end{bmatrix} = B^{\mathrm{s}}(\kappa \mathrm{I}_2). \tag{3.17}$$

Next, we are going to show that $g^{\mathrm{s}}(\mathrm{diag}(K)x, u_2^{\mathrm{s}}) = \mathrm{diag}(K)g(x, u_2)$. Notice that the

PLL dynamics for both inverters are decoupled from the rest of internal states and their parameters are the same, so we can conclude that $v^{\mathrm{s}}_{\mathrm{PLL}} = v_{\mathrm{PLL}}, \phi^{\mathrm{s}}_{\mathrm{PLL}} = \phi_{\mathrm{PLL}}, \delta^{\mathrm{s}} = \delta$. Then, the following identities hold for v^{d}_g and v^{q}_g:

$$\begin{aligned}
v^{\mathrm{d}}_g(\mathrm{diag}(K)x, u^{\mathrm{s}}_2) &= \frac{2}{3}\left(\cos(\delta)v^{\mathrm{a}}_g + \cos(\delta - \frac{2\pi}{3})v^{\mathrm{b}}_g + \cos(\delta + \frac{2\pi}{3})v^{\mathrm{c}}_g\right) \\
&= v^{\mathrm{d}}_g(x, u^{\mathrm{s}}_2) = v^{\mathrm{d}}_g(x, u_2), \\
v^{\mathrm{q}}_g(\mathrm{diag}(K)x, u^{\mathrm{s}}_2) &= -\frac{2}{3}\left(\sin(\delta)v^{\mathrm{a}}_g + \sin(\delta - \frac{2\pi}{3})v^{\mathrm{b}}_g + \sin(\delta + \frac{2\pi}{3})v^{\mathrm{c}}_g\right) \\
&= v^{\mathrm{q}}_g(x, u^{\mathrm{s}}_2) = v^{\mathrm{q}}_g(x, u_2).
\end{aligned}$$

Let $g^{\mathrm{s}}_\ell(\mathrm{diag}(K)x, u^{\mathrm{s}}_2)$ and $g_\ell(x, u_2)$ denote the ℓ-th entry of $g^{\mathrm{s}}(\mathrm{diag}(K)x, u^{\mathrm{s}}_2)$ and $g(x, u_2)$, respectively. The entries of $g^{\mathrm{s}}(\mathrm{diag}(K)x, u^{\mathrm{s}}_2)$ can be written as follows:

$$\begin{aligned}
g^{\mathrm{s}}_1(\mathrm{diag}(K)x, u^{\mathrm{s}}_2) &= 0 = \kappa g_1(x, u_2), \\
g^{\mathrm{s}}_2(\mathrm{diag}(K)x, u^{\mathrm{s}}_2) &= 0 = \kappa g_2(x, u_2), \\
g^{\mathrm{s}}_3(\mathrm{diag}(K)x, u^{\mathrm{s}}_2) &= (-k^p_{\mathrm{PLL}}v_{\mathrm{PLL}} + k^i_{\mathrm{PLL}}\phi_{\mathrm{PLL}})\kappa i^{\mathrm{q}}_{\mathrm{o}} - \frac{\kappa}{L_g}v^{\mathrm{d}}_g(\mathrm{diag}(K)x, u^{\mathrm{s}}_2) \\
&= \kappa g_3(x, u_2), \\
g^{\mathrm{s}}_4(\mathrm{diag}(K)x, u^{\mathrm{s}}_2) &= (k^p_{\mathrm{PLL}}v_{\mathrm{PLL}} - k^i_{\mathrm{PLL}}\phi_{\mathrm{PLL}})\kappa i^{\mathrm{d}}_{\mathrm{o}} - \frac{\kappa}{L_g}v^{\mathrm{q}}_g(\mathrm{diag}(K)x, u^{\mathrm{s}}_2) \\
&= \kappa g_4(x, u_2), \\
g^{\mathrm{s}}_5(\mathrm{diag}(K)x, u^{\mathrm{s}}_2) &= 0 = \kappa g_5(x, u_2), \\
g^{\mathrm{s}}_6(\mathrm{diag}(K)x, u^{\mathrm{s}}_2) &= 0 = \kappa g_6(x, u_2), \\
g^{\mathrm{s}}_7(\mathrm{diag}(K)x, u^{\mathrm{s}}_2) &= \frac{3}{2}\kappa\omega_{\mathrm{c,PC}}\left(v^{\mathrm{d}}_g(\mathrm{diag}(K)x, u^{\mathrm{s}}_2)i^{\mathrm{d}}_{\mathrm{o}} + v^{\mathrm{q}}_g(\mathrm{diag}(K)x, u^{\mathrm{s}}_2)i^{\mathrm{q}}_{\mathrm{o}}\right) \\
&= \kappa g_7(x, u_2), \\
g^{\mathrm{s}}_8(\mathrm{diag}(K)x, u^{\mathrm{s}}_2) &= \frac{3}{2}\kappa\omega_{\mathrm{c,PC}}\left(v^{\mathrm{q}}_g(\mathrm{diag}(K)x, u^{\mathrm{s}}_2)i^{\mathrm{d}}_{\mathrm{o}} - v^{\mathrm{d}}_g(\mathrm{diag}(K)x, u^{\mathrm{s}}_2)i^{\mathrm{q}}_{\mathrm{o}}\right) \\
&= \kappa g_8(x, u_2), \\
g^{\mathrm{s}}_9(\mathrm{diag}(K)x, u^{\mathrm{s}}_2) &= 0 = \kappa g_9(x, u_2), \\
g^{\mathrm{s}}_{10}(\mathrm{diag}(K)x, u^{\mathrm{s}}_2) &= 0 = \kappa g_{10}(x, u_2), \\
g^{\mathrm{s}}_{11}(\mathrm{diag}(K)x, u^{\mathrm{s}}_2) &= (-k^p_{\mathrm{PLL}}v_{\mathrm{PLL}} + k^i_{\mathrm{PLL}}\phi_{\mathrm{PLL}})(-R_{\mathrm{f}}i^{\mathrm{q}}_{\mathrm{i}} + v^{\mathrm{q}}_{\mathrm{f}}) + \frac{R_{\mathrm{f}}}{L_g}v^{\mathrm{d}}_g(\mathrm{diag}(K)x, u^{\mathrm{s}}_2)
\end{aligned}$$

$$
\begin{aligned}
&= g_{11}(x, u_2), \\
g^{\mathrm{s}}_{12}(\mathrm{diag}(K)x, u^{\mathrm{s}}_2) &= (k^p_{\mathrm{PLL}} v_{\mathrm{PLL}} - k^i_{\mathrm{PLL}} \phi_{\mathrm{PLL}})(-R_{\mathrm{f}} i^{\mathrm{d}}_{\mathrm{i}} + v^{\mathrm{d}}_{\mathrm{f}}) + \frac{R_{\mathrm{f}}}{L_g} v^{\mathrm{q}}_g(\mathrm{diag}(K)x, u^{\mathrm{s}}_2) \\
&= g_{12}(x, u_2), \\
g^{\mathrm{s}}_{13}(\mathrm{diag}(K)x, u^{\mathrm{s}}_2) &= \omega_{\mathrm{c,PLL}} v^{\mathrm{d}}_g(x, u_2) = g_{13}(x, u_2), \\
g^{\mathrm{s}}_{14}(\mathrm{diag}(K)x, u^{\mathrm{s}}_2) &= 0 = g_{14}(x, u_2), \\
g^{\mathrm{s}}_{15}(\mathrm{diag}(K)x, u^{\mathrm{s}}_2) &= \omega_{\mathrm{nom}} = g_{15}(x, u_2).
\end{aligned}
$$

Therefore, we have

$$
\mathrm{diag}(K) g(x, u_2) = g^{\mathrm{s}}(\mathrm{diag}(K)x, u^{\mathrm{s}}_2). \tag{3.18}
$$

Let us define function $h(x^{\mathrm{s}}, u^{\mathrm{s}}_2) : \mathbb{R}^{15} \times \mathbb{R}^2 \to \mathbb{R}^{15}$, with its ℓ-th entry is denoted by $h_\ell(x^{\mathrm{s}}, u^{\mathrm{s}}_2)$, to have the same structure as $g^{\mathrm{s}}(x^{\mathrm{s}} u^{\mathrm{s}}_2)$ except the following entries:

$$
\begin{aligned}
h_3(x^{\mathrm{s}}, u^{\mathrm{s}}_2) &= (-k^p_{\mathrm{PLL}} v^{\mathrm{s}}_{\mathrm{PLL}} + k^i_{\mathrm{PLL}} \phi^{\mathrm{s}}_{\mathrm{PLL}}) i^{\mathrm{q,s}}_{\mathrm{o}}, \\
h_4(x^{\mathrm{s}}, u^{\mathrm{s}}_2) &= (k^p_{\mathrm{PLL}} v^{\mathrm{s}}_{\mathrm{PLL}} - k^i_{\mathrm{PLL}} \phi^{\mathrm{s}}_{\mathrm{PLL}}) i^{\mathrm{d,s}}_{\mathrm{o}}, \\
h_{11}(x^{\mathrm{s}}, u^{\mathrm{s}}_2) &= (-k^p_{\mathrm{PLL}} v^{\mathrm{s}}_{\mathrm{PLL}} + k^i_{\mathrm{PLL}} \phi^{\mathrm{s}}_{\mathrm{PLL}}) \left(-\frac{R_{\mathrm{f}}}{\kappa} i^{\mathrm{q,s}}_{\mathrm{i}} + v^{\mathrm{q,s}}_{\mathrm{f}} \right), \\
h_{12}(x^{\mathrm{s}}, u^{\mathrm{s}}_2) &= (k^p_{\mathrm{PLL}} v^{\mathrm{s}}_{\mathrm{PLL}} - k^i_{\mathrm{PLL}} \phi^{\mathrm{s}}_{\mathrm{PLL}}) \left(-\frac{R_{\mathrm{f}}}{\kappa} i^{\mathrm{d,s}}_{\mathrm{i}} + v^{\mathrm{d,s}}_{\mathrm{f}} \right), \\
h_{13}(x^{\mathrm{s}}, u^{\mathrm{s}}_2) &= 0, \\
h_{15}(x^{\mathrm{s}}, u^{\mathrm{s}}_2) &= 0.
\end{aligned}
$$

Then, the following identity holds

$$
\begin{aligned}
g^{\mathrm{s}}(x^{\mathrm{s}}, u^{\mathrm{s}}_2) - \mathrm{diag}(K) g(x, u_2) &= g^{\mathrm{s}}(x^{\mathrm{s}}, u^{\mathrm{s}}_2) - g^{\mathrm{s}}(\mathrm{diag}(K)x, u^{\mathrm{s}}_2) \\
&= h((x^{\mathrm{s}} - \mathrm{diag}\,(K)x), u^{\mathrm{s}}_2)\,.
\end{aligned} \tag{3.19}
$$

Leveraging identities (3.16)–(3.19), we can rewrite (3.11) as

$$
\begin{aligned}
\dot{z} &= A^{\mathrm{s}}(x^{\mathrm{s}} - \mathrm{diag}(K)x) + h((x^{\mathrm{s}} - \mathrm{diag}\,(K)x), u^{\mathrm{s}}_2) \\
&= A^{\mathrm{s}} z + h(z, u^{\mathrm{s}}_2).
\end{aligned} \tag{3.20}
$$

It is straightforward to see $h(\mathbb{0}_{15}, u_2^{\mathrm{s}}) = \mathbb{0}_{15}$. If we initialize $z(t_0) = x^{\mathrm{s}}(t_0) - \mathrm{diag}(K)x(t_0) = \mathbb{0}_{15}$, we have $z(t) = \mathbb{0}_{15}, \forall t \geq t_0$. Therefore we have $x^{\mathrm{s}}(t) = \mathrm{diag}(K)x(t)$, $\forall t \geq t_0$.

For the other direction, given that $z(t) = x^{\mathrm{s}}(t) - \mathrm{diag}(K)x(t) = \mathbb{0}_{15}, \forall t \geq t_0$, the dynamics of z in (3.11) are given by

$$\begin{aligned}\mathbb{0}_{15} = \dot{x}^{\mathrm{s}} - \mathrm{diag}(K)\dot{x} = (A^{\mathrm{s}}\mathrm{diag}(K) - \mathrm{diag}(K)A)x + (\kappa B^{\mathrm{s}} - \mathrm{diag}(K)B)u_1 \\ + g^{\mathrm{s}}(x^{\mathrm{s}}, u_2^{\mathrm{s}}) - \mathrm{diag}(K)g(x, u_2). \qquad (3.21)\end{aligned}$$

It is satisfied when the following identities hold:

$$A^{\mathrm{s}}\mathrm{diag}(K) = \mathrm{diag}(K)A, \quad \kappa B^{\mathrm{s}} = \mathrm{diag}(K)B, \quad g^{\mathrm{s}}(x^{\mathrm{s}}, u^{\mathrm{s}}) = \mathrm{diag}(K)g(x, u_2). \qquad (3.22)$$

By observing the entries of the matrices and functions, it is straightforward to determine the parameters of the scaled inverter with respect to the unscaled one: they are given uniquely by (3.9), and the parameters that are not mentioned in (3.9) are unchanged. □

3.2.2 Aggregation of Inverters

Consider the parallel-connection of N inverters with power-scaling factors $\kappa_1, \ldots, \kappa_N$ illustrated in Fig. 3.2. Define the equivalent power-scaling factor as $\widehat{\kappa} := \sum_{\ell=1}^{N} \kappa_\ell$. For this system, define the reduced-order model

$$\dot{x}^{\mathrm{r}} = A^{\mathrm{r}}x^{\mathrm{r}} + B^{\mathrm{r}}u_1^{\mathrm{r}} + g^{\mathrm{r}}(x^{\mathrm{r}}, u_2^{\mathrm{r}}), \qquad (3.23)$$

where the inputs u_1^{r} and u_2^{r} are given by $u_1^{\mathrm{r}} = \widehat{\kappa}[p^\star, q^\star]^{\mathrm{T}}$, $u_2^{\mathrm{r}} = [v_g^{\mathrm{a}}, v_g^{\mathrm{b}}, v_g^{\mathrm{c}}]^{\mathrm{T}} = v_g^{\mathrm{abc}}$, and we have the same collection of states as the model in (3.10), except with the dynamics of the states being governed with $\kappa = \widehat{\kappa}$. Consequently, $A^{\mathrm{r}} \in \mathbb{R}^{15\times 15}$, $B^{\mathrm{r}} \in \mathbb{R}^{15\times 2}$, $g^{\mathrm{r}} : \mathbb{R}^{15} \times \mathbb{R}^3 \to \mathbb{R}^{15}$ have the same structure as (3.10), except with power-scaling parameter $\widehat{\kappa}$. It is worth emphasizing that the dynamical model of an individual inverter has 15 states, and so modeling the dynamics of every inverter in an N-inverter parallel collection would require a $15N$-order state-space model. By contrast, the reduced-order model has the same structure as any individual inverter, and is hence described only by 15 states.

Lemma 3.2 (Aggregation of parallel-connected scaled three-phase inverters)**.** *Let us denote x_ℓ as the state vector of the ℓ-th inverter in the parallel system. We partition $x_\ell = [\lambda_\ell^{\mathrm{T}}, \xi_\ell^{\mathrm{T}}]^{\mathrm{T}}$, with $\lambda_\ell = [i_{\mathrm{i},\ell}^{\mathrm{d}}, i_{\mathrm{i},\ell}^{\mathrm{q}}, i_{\mathrm{o},\ell}^{\mathrm{d}}, i_{\mathrm{o},\ell}^{\mathrm{q}}, \gamma_\ell^{\mathrm{d}}, \gamma_\ell^{\mathrm{q}}, p_{\mathrm{avg},\ell}, q_{\mathrm{avg},\ell}, \phi_\ell^{\mathrm{p}}, \ \phi_\ell^{\mathrm{q}}]^{\mathrm{T}}$ and $\xi_\ell = [v_{\mathrm{f},\ell}^{\mathrm{d}}, v_{\mathrm{f},\ell}^{\mathrm{q}}, v_{\mathrm{PLL},\ell}, \phi_{\mathrm{PPL},\ell}, \delta_\ell]^{\mathrm{T}}$. We also partition the state vector of the reduced-order model the same way: $x^{\mathrm{r}} = [\lambda^{\mathrm{rT}}, \xi^{\mathrm{rT}}]^{\mathrm{T}}$. Suppose the initial conditions are such that $\lambda^{\mathrm{r}}(t_0) = \sum_{\ell=1}^{N} \lambda_\ell(t_0)$ and $\xi^{\mathrm{r}}(t_0) = \xi_\ell(t_0), \forall \ell$. The inputs are $u_1^{\mathrm{r}} = \sum_{\ell=1}^{N} u_{1,\ell} = \widehat{\kappa}[p^\star, q^\star]^{\mathrm{T}}$ and $u_2^{\mathrm{r}} = u_{2,\ell}, \forall \ell$. It follows that*

$$\lambda^{\mathrm{r}}(t) = \sum_{\ell=1}^{N} \lambda_\ell(t), \quad \xi^{\mathrm{r}}(t) = \xi_\ell(t), \forall \ell, \quad \forall t \geq t_0. \tag{3.24}$$

Proof. Let x^0 denote the state vector of the inverter with nominal power rating. We also partition $x^0 = [\lambda^{0\mathrm{T}}, \xi^{0\mathrm{T}}]^{\mathrm{T}}$. Since the reduced-order model has power-scaling factor of $\widehat{\kappa}$, it follows that, $\forall t \geq t_0$:

$$\lambda^{\mathrm{r}}(t) = \widehat{\kappa}\lambda^0(t) = \sum_{\ell=1}^{N} \kappa_\ell \lambda^0(t) = \sum_{\ell=1}^{N} \lambda_\ell(t), \tag{3.25}$$

$$\xi^{\mathrm{r}}(t) = \xi^0(t) = \xi_\ell(t), \forall \ell. \tag{3.26}$$

□

3.2.3 Corollary for Arbitrary Reference-power Setpoints

With the parallel aggregation in place, we present a corollary for the case when the reference-power setpoints of the inverters in the parallel system are arbitrary instead of being given by their power-scaling parameters times the nominal setpoints. This model is useful in, e.g., PV systems where the incident irradiation might be different for different inverters (hence resulting in different values for $p^\star$) and where local-voltage control may be implemented by modulating reactive-power injections (hence resulting in different values of $q^\star$). The reduced-order model of such case has the same form as (3.23), albeit with the reference-power setpoints of $u_1^{\mathrm{r}} = \sum_{\ell=1}^{N} u_{1,\ell}$, where $u_{1,\ell} = [p_\ell^\star, q_\ell^\star]$, with $p_\ell^\star$ and $q_\ell^\star$ are the real- and reactive-power setpoints of the ℓ-th inverter. We show analytically the relationships between the states of the reduced-order model and the individual inverters next.

Corollary 3.3 (Aggregation of parallel-connected scaled three-phase inverters with arbitrary reference-power setpoints)**.** *Let us denote x_ℓ as the state vector of the ℓ-th inverter in the parallel system. We partition $x_\ell = [\lambda_\ell^{\mathrm{T}}, v_{\mathrm{f},\ell}^{\mathrm{dqT}}, x_{\mathrm{PLL}}^{\mathrm{T}}]^{\mathrm{T}}$, with $\lambda_\ell = [i_{\mathrm{i},\ell}^{\mathrm{d}}, i_{\mathrm{i},\ell}^{\mathrm{q}}, i_{\mathrm{o},\ell}^{\mathrm{d}}, i_{\mathrm{o},\ell}^{\mathrm{q}}, \gamma_\ell^{\mathrm{d}}, \gamma_\ell^{\mathrm{q}}, p_{\mathrm{avg},\ell}, q_{\mathrm{avg},\ell}, \phi_\ell^{\mathrm{p}}, \phi_\ell^{\mathrm{q}}]^{\mathrm{T}}$, $v_{\mathrm{f},\ell}^{\mathrm{dq}} = [v_{\mathrm{f},\ell}^{\mathrm{d}}, v_{\mathrm{f},\ell}^{\mathrm{q}}]^{\mathrm{T}}$, and $x_{\mathrm{PLL},\ell} = [v_{\mathrm{PLL},\ell}, \phi_{\mathrm{PPL},\ell}, \delta_\ell]^{\mathrm{T}}$. We also partition the state vector of the reduced-order model the same way: $x^{\mathrm{r}} = [\lambda^{\mathrm{rT}}, v_{\mathrm{f}}^{\mathrm{dq,rT}}, x_{\mathrm{PLL}}^{\mathrm{rT}}]^{\mathrm{T}}$. Suppose the initial conditions are such that $\lambda^{\mathrm{r}}(t_0) = \sum_{\ell=1}^{N} \lambda_\ell(t_0)$, $v_{\mathrm{f}}^{\mathrm{dq,r}}(t_0) = \frac{1}{\widehat{\kappa}} \sum_{\ell=1}^{N} \kappa_\ell v_{\mathrm{f},\ell}^{\mathrm{dq}}(t_0)$, and $x_{\mathrm{PLL}}^{\mathrm{r}}(t_0) = x_{\mathrm{PLL},\ell}(t_0), \forall \ell$. The inputs are $u_1^{\mathrm{r}} = \sum_{\ell=1}^{N} u_{1,\ell}$ and $u_2^{\mathrm{r}} = u_{2,\ell}, \forall \ell$. It follows that, $\forall t \geq t_0$:*

$$\lambda^{\mathrm{r}}(t) = \sum_{\ell=1}^{N} \lambda_\ell(t), \quad v_{\mathrm{f}}^{\mathrm{dq,r}}(t) = \frac{1}{\widehat{\kappa}} \sum_{\ell=1}^{N} \kappa_\ell v_{\mathrm{f},\ell}^{\mathrm{dq}}(t), \quad x_{\mathrm{PLL}}^{\mathrm{r}}(t) = x_{\mathrm{PLL},\ell}(t), \forall \ell. \tag{3.27}$$

Proof. The proof is provided in Appendix B.3. □

3.3 Simulation Results

In this section, we simulate a system of 4 parallel-connected inverters alongside the reduced-order equivalent inverter model, as illustrated in Fig. 3.2. For the multi-inverter system, $N = 4$, with power-scaling parameters: $\kappa_1 = \kappa_2 = 1$, $\kappa_3 = 2$, and $\kappa_4 = 3$. The reduced-order inverter model is given initial conditions as prescribed in Theorem 2. The power and RMS voltage ratings are 500 [kW] and 288 [V], respectively, and correspond to a Siemens SINVERT PVS500 inverter [42]. During the time-domain simulation, we

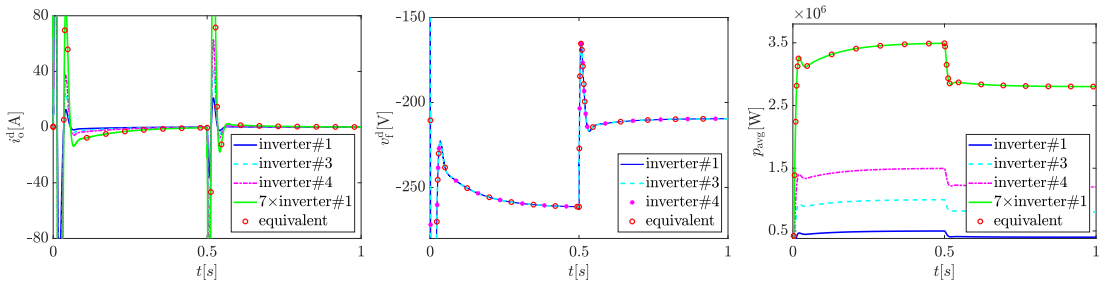

(a) d-axis output current (b) d-axis output voltage (c) Output power

Figure 3.3: Simulation results for three-phase inverter system demonstrating the validity of the scaling and model-reduction procedure.

let $q^\star = 0$ [VAR]. The filter and controller parameters are taken from [27]. We introduce a step change in $p^\star$ from 500 [kW] to 400 [kW] at $t = 0.5$ [s]. Figure 3.3 shows the output current, voltage, and real power dynamics of the individual and equivalent (i.e. reduced-order) inverters. Note that the plots for inverter#2 are omitted since it has the same scaling factor as inverter#1, and therefore their plots are identical. To validate the equivalent inverter and its correspondence to the individual inverters, we also plot the output current and power of the unscaled inverter (i.e., inverter#1) scaled by a factor of 7. We can see that they satisfy the following scaling properties: $i_{\mathrm{o}}^{\mathrm{dr}}(t) = 7i_{\mathrm{o},1}^{\mathrm{d}}(t)$, $v_{\mathrm{f}}^{\mathrm{dr}}(t) = v_{\mathrm{f},1}^{\mathrm{d}}(t)$, and $p_{\mathrm{avg}}^{\mathrm{r}}(t) = 7p_{\mathrm{avg},1}(t)$. The figures also show that the states of the individual inverters follow the scaling properties: $i_{\mathrm{o},3}^{\mathrm{d}}(t) = 2i_{\mathrm{o},1}^{\mathrm{d}}(t)$, $i_{\mathrm{o},4}^{\mathrm{d}}(t) = 3i_{\mathrm{o},1}^{\mathrm{d}}(t)$, $v_{\mathrm{f},1}^{\mathrm{d}}(t) = v_{\mathrm{f},3}^{\mathrm{d}}(t) = v_{\mathrm{f},4}^{\mathrm{d}}(t)$, $p_{\mathrm{avg},3}(t) = 2p_{\mathrm{avg},1}(t)$, and $p_{\mathrm{avg},4}(t) = 3p_{\mathrm{avg},1}(t)$.

Chapter 4

Application: Aggregation of Parallel-connected Grid-tied Three-phase Photovoltaic Inverters

In this chapter, we extend the reduced-order model proposed in Chapter 3 to acknowledge the photovoltaic (PV) array, maximum power point tracking (MPPT) algorithm, and dc-link capacitor dynamics in the model of a PV inverter. PV plants with as many as thousands of inverters are not uncommon [43]. The reduced-order model has similar model complexity as a synchronous machine model, and thus facilitates the accurate representation of PV plants in bulk transmission-scale models with limited computational burden. In this regard, we anticipate applications for the reduced-order model in power quality studies [44], stability analysis for systems with high PV penetration [45–49], and evaluating opportunities for frequency support by PV systems [50]. The aggregate model presented in this chapter differs to other aggregated PV models in the literature [51–53] since it provides a systematic way of scaling the PV and control parameters based on the number of inverters.

The remainder of this chapter is organized as follows. In Section 4.1, we introduce the grid-tied three-phase PV inverter model. In Section 4.2, we derive the reduced-order

model for parallel-connected PV inverters in the homogeneous setting, and describe extensions to the model for different solar irradiance and parameters of the MPPT algorithm. In Section 4.3, we provide comparative numerical simulations of a parallel-connected system and its corresponding reduced-order model.

4.1 Model Description

A block diagram illustrating the PV array, feedback controllers, and output filters in the grid-tied three-phase voltage-source inverter (VSI) is given in Fig. 4.1. The controllers consist of a phase-locked loop (PLL), a maximum power point algorithm, dc-link & power controllers, and a current controller. This PV inverter model (and closely related variants) are fairly common in the literature [9–12]. The PV inverter is assumed to operate at unity power factor. The LCL filter, VSI, PWM, three-phase to dq transformation, PLL, and current controller are identical to those in Chapter 3. We describe the remaining pieces of the model next.

4.1.1 Model of PV Array

Each inverter is connected to an array composed of N_p strings of N_s series-connected modules. We adopt a single-diode model with a parallel output resistance, R_p, for each

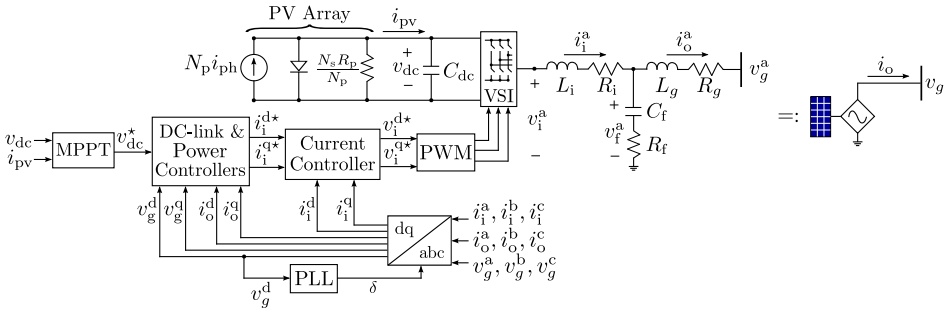

Figure 4.1: Block diagram of the grid-tied three-phase PV inverter (left) and shorthand representation adopted for the same (right). The PV array is represented with a single-diode model. A single leg of the LCL filter corresponding to the a phase is depicted.

module [54–56]. The output current of the PV array is:

$$i_{\rm pv} = N_{\rm p}\left(i_{\rm ph} - i_{\rm rs}\left(\mathrm{e}^{\frac{q\,v_{\rm dc}}{N_{\rm m}KTN_{\rm s}}} - 1\right) - \frac{v_{\rm dc}}{N_{\rm s}R_{\rm p}}\right), \tag{4.1}$$

where $i_{\rm ph}$ is the photocurrent that depends on the solar irradiance, $i_{\rm rs}$ is the reverse saturation current, q is the electron charge, $v_{\rm dc}$ is the voltage across the dc-link capacitor, $N_{\rm m}$ is the number of cells in a module, K is the Boltzmann constant, and T is the surface temperature of the module.

4.1.2 Dc-link Capacitor

The dc-link capacitor, $C_{\rm dc}$, interfaces the PV array to the inverter. It is designed to minimize the current ripple imposed on the PV array. The state of the filter is the energy stored in the capacitor, $e_{\rm dc} := v_{\rm dc}^2$. Assuming lossless operation of the switches in the VSI, the dynamics of $e_{\rm dc}$ are:

$$\dot{e}_{\rm dc} = \frac{1}{C_{\rm dc}}(p_{\rm pv} - p_{\rm i}), \tag{4.2}$$

where $p_{\rm pv}$ and $p_{\rm i}$ denote the power sourced by the PV array and the real power calculated at the terminals of the inverter:

$$p_{\rm pv} = v_{\rm dc} i_{\rm pv}, \tag{4.3}$$

$$p_{\rm i} = \frac{3}{2}(v_{\rm i}^{\rm d} i_{\rm i}^{\rm d} + v_{\rm i}^{\rm q} i_{\rm i}^{\rm q}). \tag{4.4}$$

4.1.3 Maximum Power Point Tracking (MPPT) Algorithm

We assume that the perturb and observe (P&O) algorithm is utilized to track the maximum power point (MPP). The basic premise of this algorithm is to perturb the dc-link voltage reference in a direction to increase the power drawn from the PV array. To facilitate computations with accuracy, a low-pass filter with cut-off frequency, $\omega_{\rm c,pv}$, yields an averaged PV output power, $p_{\rm pv,avg}$, that is utilized in the algorithm:

$$\dot{p}_{\rm pv,avg} = \omega_{\rm c,pv}(p_{\rm pv} - p_{\rm pv,avg}). \tag{4.5}$$

The update for the dc-link voltage reference is given by: [57]

$$v_{\mathrm{dc}}^{\star}(t+\tau) = v_{\mathrm{dc}}^{\star}(t) + \rho \cdot \mathrm{sgn}(\Delta v_{\mathrm{dc}}(t))\mathrm{sgn}(\Delta p_{\mathrm{pv,avg}}(t)), \tag{4.6}$$

where ρ denotes the perturbation size, τ denotes the perturbation period, $\mathrm{sgn}(\cdot)$ denotes the signum function, and

$$\Delta v_{\mathrm{dc}}(t) = v_{\mathrm{dc}}(t) - v_{\mathrm{dc}}(t-\tau), \tag{4.7}$$

$$\Delta p_{\mathrm{pv,avg}}(t) = p_{\mathrm{pv,avg}}(t) - p_{\mathrm{pv,avg}}(t-\tau), \tag{4.8}$$

denote the change in dc-link voltage and corresponding change in averaged PV output power, respectively.

4.1.4 Dc-link & Power Controllers

The controller consists of a dc-link voltage controller and a reactive power controller. The dc-link voltage controller is composed of a PI controller (with PI gains k_{VC}^{p} and k_{VC}^{i}). The reference to the controller is the dc-link energy setpoint, $e_{\mathrm{dc}}^{\star}$, which is equal to the square of dc-link voltage setpoint, $v_{\mathrm{dc}}^{\star}$, i.e., $e_{\mathrm{dc}}^{\star} = v_{\mathrm{dc}}^{\star 2}$. The output is the reference for $i_{\mathrm{i}}^{\mathrm{q}}$:

$$i_{\mathrm{i}}^{\mathrm{q}\star} = -k_{\mathrm{VC}}^{p}(e_{\mathrm{dc}}^{\star} - e_{\mathrm{dc}}) - k_{\mathrm{VC}}^{i}\int (e_{\mathrm{dc}}^{\star} - e_{\mathrm{dc}})\, dt. \tag{4.9}$$

The reactive power controller is composed of a PI controller (with PI gains k_{Q}^{p} and k_{Q}^{i}) and a low-pass filter (with cut-off frequency $\omega_{\mathrm{c,Q}}$). If the inverter operates at unity power factor, the reactive power reference is zero. The output is the reference for $i_{\mathrm{i}}^{\mathrm{d}}$:

$$i_{\mathrm{i}}^{\mathrm{d}\star} = -k_{\mathrm{Q}}^{p} q_{\mathrm{avg}} - k_{\mathrm{Q}}^{i}\int q_{\mathrm{avg}}\, dt, \tag{4.10}$$

where q_{avg} is the output of the low pass filter:

$$\dot{q}_{\mathrm{avg}} = \omega_{\mathrm{c,Q}}(q - q_{\mathrm{avg}}), \tag{4.11}$$

where q is the instantaneous reactive power at the output:

$$q = \frac{3}{2}(v_g^{\mathrm{q}} i_{\mathrm{o}}^{\mathrm{d}} - v_g^{\mathrm{d}} i_{\mathrm{o}}^{\mathrm{q}}). \tag{4.12}$$

We define the following variables to simplify notation subsequently: $\dot{\phi}_{\mathrm{dc}} = e_{\mathrm{dc}}^{\star} - e_{\mathrm{dc}}$, $\dot{\phi}_{\mathrm{q}} = -q_{\mathrm{avg}}$.

4.1.5 State-space Representation

The dynamics of the inverter can be represented in a compact state-space form as follows: $\dot{x} = Ax + g(x, u_1, u_2, u_3)$, where the states and inputs are:

$$x = [i_{\mathrm{i}}^{\mathrm{d}}, i_{\mathrm{i}}^{\mathrm{q}}, i_{\mathrm{o}}^{\mathrm{d}}, i_{\mathrm{o}}^{\mathrm{q}}, v_{\mathrm{f}}^{\mathrm{d}}, v_{\mathrm{f}}^{\mathrm{q}}, e_{\mathrm{dc}}, p_{\mathrm{pv,avg}}, \phi_{\mathrm{dc}}, q_{\mathrm{avg}}, \phi_{\mathrm{q}}, \gamma^{\mathrm{d}}, \gamma^{\mathrm{q}}, v_{\mathrm{PLL}}, \phi_{\mathrm{PLL}}, \delta]^{\mathrm{T}}, \tag{4.13}$$

$$u_1 = v_{\mathrm{dc}}^{\star}, \quad u_2 = [v_g^{\mathrm{a}}, v_g^{\mathrm{b}}, v_g^{\mathrm{c}}]^{\mathrm{T}}, \quad u_3 = i_{\mathrm{ph}}. \tag{4.14}$$

Note that the dc-link voltage setpoint, $v_{\mathrm{dc}}^{\star}$, is obtained from the MPPT algorithm. Entries of $A \in \mathbb{R}^{16\times 16}$ and $g : \mathbb{R}^{16} \times \mathbb{R}^3 \times \mathbb{R} \to \mathbb{R}^{16}$ are in Appendix C.1.

4.2 Reduced-order Aggregated Model

We now derive a reduced-order aggregate model for a collection of N identical inverters with the same PV array configuration, connected in parallel. Following this homogeneous setup, we briefly overview some practicalities for heterogeneous settings.

4.2.1 Aggregation in Homogeneous Settings

In order to derive the aggregate reduced-order model, we scale the following parameters corresponding to the inverter controllers and PV array:

$$\begin{aligned}\left(i_{\mathrm{rs}}, R_{\mathrm{p}}, C_{\mathrm{dc}}, L_{\mathrm{i}}, C_{\mathrm{f}}, L_g, k_{\mathrm{VC}}^p, k_{\mathrm{VC}}^i, k_{\mathrm{CC}}^p, k_{\mathrm{CC}}^i\right) \to (&Ni_{\mathrm{rs}}, \\ &\frac{R_{\mathrm{p}}}{N}, NC_{\mathrm{dc}}, \frac{L_{\mathrm{i}}}{N}, NC_{\mathrm{f}}, \frac{L_g}{N}, Nk_{\mathrm{VC}}^p, Nk_{\mathrm{VC}}^i, \frac{k_{\mathrm{CC}}^p}{N}, \frac{k_{\mathrm{CC}}^i}{N}\Bigg).\end{aligned}$$

Parameters not mentioned above are unchanged. In particular, note that the PLL and reactive power controller parameters, and the frequency of any low pass filter are

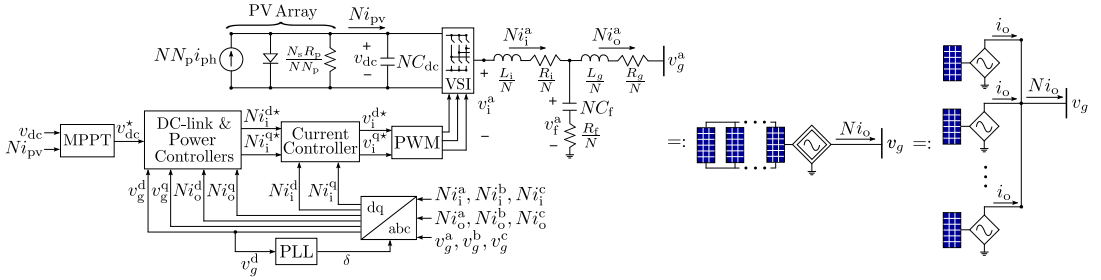

Figure 4.2: Reduced-order aggregated PV inverter model for N parallel-connected inverters (left) and its adopted shorthand (center). This model precisely captures the output current and power injected by the parallel combination of N PV inverters (right). Scaling of parameters corresponding to equivalent PV array and LCL filter acknowledge the parallel interconnection of pertinent circuit elements.

unchanged. With these scaled parameters, the resulting aggregate reduced-order model is illustrated in Fig. 4.2. We draw attention to the fact that this model has the same model order and structure as any individual PV inverter model in the parallel setup. Certain aspects of this model derive straightforwardly from elementary circuit theory. This is particularly obvious for the PV array and the output LCL filter. Given the parallel setup, we can see that the impedance corresponding to the LCL output filter in the reduced-order aggregate model is $1/N$ of that in the individual inverter. Similarly, the equivalent PV array for the aggregation is obtained from a parallel connection of N single-diode models for the individual arrays.

Formally, the dynamical model of the reduced-order equivalent has the following state-space form: $\dot{x}^{\mathrm{r}} = A^{\mathrm{r}}x^{\mathrm{r}} + g^{\mathrm{r}}(x^{\mathrm{r}}, u_1^{\mathrm{r}}, u_2^{\mathrm{r}}, u_3^{\mathrm{r}})$, where the states and the inputs are:

$$\begin{aligned} x^{\mathrm{r}} = [&i_{\mathrm{i}}^{\mathrm{d,r}}, i_{\mathrm{i}}^{\mathrm{q,r}}, i_{\mathrm{o}}^{\mathrm{d,r}}, i_{\mathrm{o}}^{\mathrm{q,r}}, v_{\mathrm{f}}^{\mathrm{d,r}}, v_{\mathrm{f}}^{\mathrm{q,r}}, e_{\mathrm{dc}}^{\mathrm{r}}, p_{\mathrm{pv,avg}}^{\mathrm{r}}, \phi_{\mathrm{dc}}^{\mathrm{r}}, q_{\mathrm{avg}}^{\mathrm{r}}, \phi_{\mathrm{q}}^{\mathrm{r}}, \\ &\gamma^{\mathrm{d,r}}, \gamma^{\mathrm{q,r}}, v_{\mathrm{PLL}}^{\mathrm{r}}, \phi_{\mathrm{PLL}}^{\mathrm{r}}, \delta^{\mathrm{r}}]^{\mathrm{T}}, \end{aligned} \tag{4.15}$$

$$u_1^{\mathrm{r}} = v_{\mathrm{dc}}^{\star,\mathrm{r}}, \quad u_2^{\mathrm{r}} = [v_g^{\mathrm{a}}, v_g^{\mathrm{b}}, v_g^{\mathrm{c}}]^{\mathrm{T}}, \quad u_3^{\mathrm{r}} = N i_{\mathrm{ph}}. \tag{4.16}$$

All signals above with superscript r correspond contextually to their counterparts for the individual inverter model as discussed in Section 4.1. For instance, $v_{\mathrm{dc}}^{\star,\mathrm{r}}$ denotes the dc-link voltage reference for the reduced-order model, generated from the corresponding MPPT algorithm. Inputs also have the same connotation, except notice that u_3^{r} captures N times the photocurrent, i_{ph}. The matrix $A^{\mathrm{r}} \in \mathbb{R}^{16\times16}$ and function $g^{\mathrm{r}} : \mathbb{R}^{16} \times \mathbb{R}^3 \times \mathbb{R} \to$

$\mathbb{R}^{16}$ have the same structure and dimension as A and g.

We now establish the main result of this chapter, whereby the current- and power-related states of the reduced-order aggregate model are noted to be N times those in the individual inverter model, while the voltage- and PLL-related states are the same.

Theorem 4.1 (Aggregation of parallel-connected PV inverters)**.** *Consider the state-space model for the individual PV inverter. Permute x in* (4.13) *as*

$$\widehat{x} = [i_{\mathrm{i}}^{\mathrm{d}}, i_{\mathrm{i}}^{\mathrm{q}}, i_{\mathrm{o}}^{\mathrm{d}}, i_{\mathrm{o}}^{\mathrm{q}}, p_{\mathrm{pv,avg}}, q_{\mathrm{avg}}, \phi_{\mathrm{q}}, \gamma^{\mathrm{d}}, \gamma^{\mathrm{q}}, v_{\mathrm{f}}^{\mathrm{d}}, v_{\mathrm{f}}^{\mathrm{q}}, e_{\mathrm{dc}}, \phi_{\mathrm{dc}}, v_{\mathrm{PLL}}, \phi_{\mathrm{PLL}}, \delta]^{\mathrm{T}}, \tag{4.17}$$

and also permute x^{r} in (4.15) *the same way, denoting the permuted vector by $\widehat{x}^{\mathrm{r}}$. Suppose the initial conditions at time t_0 are such that $\widehat{x}^{\mathrm{r}}(t_0) = \mathrm{diag}(\psi)\widehat{x}(t_0)$, where $\psi := [N\mathbb{1}_9^{\mathrm{T}}, \mathbb{1}_7^{\mathrm{T}}]^{\mathrm{T}}$, and $e_{\mathrm{dc}}^{\mathrm{r}}(t_0) = e_{\mathrm{dc}}(t_0) > 0$. The inputs are $u_1^{\mathrm{r}} = u_1, u_2^{\mathrm{r}} = u_2, u_3^{\mathrm{r}} = Nu_3$. It follows that $\forall t \geq t_0$, $\widehat{x}^{\mathrm{r}}(t) = \mathrm{diag}(\psi)\widehat{x}(t)$. In other words, the states of the reduced-order model and the individual inverter model are related as follows $\forall t \geq t_0$:*

$$\begin{aligned}
&[i_{\mathrm{i}}^{\mathrm{d,r}}, i_{\mathrm{i}}^{\mathrm{q,r}}, i_{\mathrm{o}}^{\mathrm{d,r}}, i_{\mathrm{o}}^{\mathrm{q,r}}, p_{\mathrm{pv,avg}}^{\mathrm{r}}, q_{\mathrm{avg}}^{\mathrm{r}}, \phi_{\mathrm{q}}^{\mathrm{r}}, \gamma^{\mathrm{d,r}}, \gamma^{\mathrm{q,r}}]^{\mathrm{T}} \\
&\quad = N[i_{\mathrm{i}}^{\mathrm{d}}, i_{\mathrm{i}}^{\mathrm{q}}, i_{\mathrm{o}}^{\mathrm{d}}, i_{\mathrm{o}}^{\mathrm{q}}, p_{\mathrm{pv,avg}}, q_{\mathrm{avg}}, \phi_{\mathrm{q}}, \gamma^{\mathrm{d}}, \gamma^{\mathrm{q}}], &(4.18)\\
&[v_{\mathrm{f}}^{\mathrm{d,r}}, v_{\mathrm{f}}^{\mathrm{q,r}}, e_{\mathrm{dc}}^{\mathrm{r}}, \phi_{\mathrm{dc}}^{\mathrm{r}}, v_{\mathrm{PLL}}^{\mathrm{r}}, \phi_{\mathrm{PLL}}^{\mathrm{r}}, \delta^{\mathrm{r}}]^{\mathrm{T}} \\
&\quad = [v_{\mathrm{f}}^{\mathrm{d}}, v_{\mathrm{f}}^{\mathrm{q}}, e_{\mathrm{dc}}, \phi_{\mathrm{dc}}, v_{\mathrm{PLL}}, \phi_{\mathrm{PLL}}, \delta]. &(4.19)
\end{aligned}$$

Proof. We begin by showing the difference in output current of PV array, i.e., $i_{\mathrm{pv}}^{\mathrm{r}} - Ni_{\mathrm{pv}}$, can be written as a function of $(e_{\mathrm{dc}}^{\mathrm{r}} - e_{\mathrm{dc}})$. Let us define $y := i_{\mathrm{pv}}^{\mathrm{r}} - Ni_{\mathrm{pv}}$, given by

$$\begin{aligned}
y := i_{\mathrm{pv}}^{\mathrm{r}} - Ni_{\mathrm{pv}} &= NN_{\mathrm{p}}i_{\mathrm{ph}} - Ni_{\mathrm{rs}}\left(\mathrm{e}^{\frac{q\sqrt{e_{\mathrm{dc}}^{\mathrm{r}}}}{N_{\mathrm{m}}KTN_{\mathrm{s}}}} - 1\right) - \frac{\sqrt{e_{\mathrm{dc}}^{\mathrm{r}}}NN_{\mathrm{p}}}{N_{\mathrm{s}}R_{\mathrm{p}}} \\
&\quad - N\left(N_{\mathrm{p}}i_{\mathrm{ph}} - i_{\mathrm{rs}}\left(\mathrm{e}^{\frac{q\sqrt{e_{\mathrm{dc}}}}{N_{\mathrm{m}}KTN_{\mathrm{s}}}} - 1\right) - \frac{\sqrt{e_{\mathrm{dc}}}N_{\mathrm{p}}}{N_{\mathrm{s}}R_{\mathrm{p}}}\right).
\end{aligned} \tag{4.20}$$

Note that the following identities hold for any $w, z > 0$: [58]

$$w - z = (\sqrt{w} + \sqrt{z})(\sqrt{w} - \sqrt{z}) \Leftrightarrow \sqrt{w} - \sqrt{z} = \frac{w - z}{\sqrt{w} + \sqrt{z}}, \tag{4.21}$$

$$w^n - z^n = (w - z)\sum_{\ell=1}^{n} w^{n-\ell}z^{\ell-1}, \tag{4.22}$$

where n is any nonzero integer. Using the identities above and Taylor series expansion of the exponential function, we can write (4.20) as:

$$
\begin{aligned}
y &= -Ni_{\mathrm{rs}}\left(\mathrm{e}^{\frac{q\sqrt{e_{\mathrm{dc}}^{\mathrm{r}}}}{N_{\mathrm{m}}KTN_{\mathrm{s}}}}-\mathrm{e}^{\frac{q\sqrt{e_{\mathrm{dc}}}}{N_{\mathrm{m}}KTN_{\mathrm{s}}}}\right)-\frac{NN_{\mathrm{p}}}{N_{\mathrm{s}}R_{\mathrm{p}}}\left(\sqrt{e_{\mathrm{dc}}^{\mathrm{r}}}-\sqrt{e_{\mathrm{dc}}}\right)\\
&= -Ni_{\mathrm{rs}}\left(\sum_{k=1}^{\infty}\frac{\left(\frac{q}{N_{\mathrm{m}}KTN_{\mathrm{s}}}\right)^{k}}{k!}\left(\left(\sqrt{e_{\mathrm{dc}}^{\mathrm{r}}}-\sqrt{e_{\mathrm{dc}}}\right)\sum_{\ell=1}^{k}(\sqrt{e_{\mathrm{dc}}^{\mathrm{r}}})^{k-\ell}(\sqrt{e_{\mathrm{dc}}})^{\ell-1}\right)\right)\\
&\quad-\frac{NN_{\mathrm{p}}}{N_{\mathrm{s}}R_{\mathrm{p}}}\left(\sqrt{e_{\mathrm{dc}}^{\mathrm{r}}}-\sqrt{e_{\mathrm{dc}}}\right)\\
&= \left(\sqrt{e_{\mathrm{dc}}^{\mathrm{r}}}-\sqrt{e_{\mathrm{dc}}}\right)\left(-Ni_{\mathrm{rs}}\left(\sum_{k=1}^{\infty}\frac{\left(\frac{q}{N_{\mathrm{m}}KTN_{\mathrm{s}}}\right)^{k}}{k!}\left(\sum_{\ell=1}^{k}(\sqrt{e_{\mathrm{dc}}^{\mathrm{r}}})^{k-\ell}(\sqrt{e_{\mathrm{dc}}})^{\ell-1}\right)\right)-\frac{NN_{\mathrm{p}}}{N_{\mathrm{s}}R_{\mathrm{p}}}\right)\\
&= (e_{\mathrm{dc}}^{\mathrm{r}}-e_{\mathrm{dc}})h(e_{\mathrm{dc}}^{\mathrm{r}},e_{\mathrm{dc}}),
\end{aligned}
\tag{4.23}
$$

where function $h(e_{\mathrm{dc}}^{\mathrm{r}},e_{\mathrm{dc}})$ is given by

$$
\frac{1}{\sqrt{e_{\mathrm{dc}}^{\mathrm{r}}}+\sqrt{e_{\mathrm{dc}}}}\left(-Ni_{\mathrm{rs}}\left(\sum_{k=1}^{\infty}\frac{\left(\frac{q}{N_{\mathrm{m}}KTN_{\mathrm{s}}}\right)^{k}}{k!}\left(\sum_{\ell=1}^{k}(\sqrt{e_{\mathrm{dc}}^{\mathrm{r}}})^{k-\ell}(\sqrt{e_{\mathrm{dc}}})^{\ell-1}\right)\right)-\frac{NN_{\mathrm{p}}}{N_{\mathrm{s}}R_{\mathrm{p}}}\right).
$$

The rest of the proof follows in the same manner as in Theorem 3.1, with the power-scaling parameter picked as $\kappa = N$. □

4.2.2 Aggregation in Heterogeneous Settings

We look into the following heterogeneous settings:

1. Inverters have different perturbation size and frequency for the P&O MPPT algorithm. The dc-link voltage reference for the reduced-order model is updated in the same manner as (4.6), except, with perturbation size, ρ, and period, τ, selected to be the average of the perturbation size and period for the individual PV inverters.

2. Inverters are exposed to different values of incident irradiance. The irradiance for the reduced-order model is the sum of the irradiance values of the individual inverters.

While we are only able to analytically establish dynamic scaling of pertinent states in the homogeneous setting (see Theorem 4.1), the approach suggested above to contend with heterogeneity is empirically established through simulations to yield acceptable performance.

4.3 Simulation Results

We compare results from simulating all the dynamics of a system of $N = 10$ parallel-connected PV inverters and the corresponding reduced-order aggregated model. Parameters are adopted from the Schneider Electric Conext CL125 string inverter [59] (power rating 125 [kW] and voltage rating 600 [V(rms)]) and the First Solar FS-6420 [60] PV module (power rating 420 [W] and open-circuit voltage 218.5 [V]). The PV array interfaced to each inverter consists of $N_{\mathrm{p}} = 60$ strings, with each string comprising $N_{\mathrm{s}} = 5$ series-connected PV modules. Filter and controller parameters are in Table 4.1.

The solar irradiance data for this simulation is sourced from NREL's Oahu Solar Measurement Grid on July 24, 2011, for the time period 09:30:00 to 09:30:10 AM [61]. The data is then interpolated from 1- to 0.1-second step intervals (see Fig. 4.3a). We consider the following cases: #1) For all inverters, the period and perturbation size of the MPPT algorithm are selected to be uniformly distributed between $5 - 10$ [ms] and $50-70$ [mV], respectively. #2) Same setup as #1, but the solar irradiance corresponding

Table 4.1: Controller and Filter Parameters

dc- and ac-side Filters	dc-link & Power Controllers	PLL
$L_{\mathrm{i}} = 23.1$ [μH]	$k^p_{\mathrm{VC}} = 0.0865$ [A/V^2]	$k^p_{\mathrm{PLL}} = 0.735$ [rad/V]
$R_{\mathrm{i}} = 0.016$ [Ω]	$k^i_{\mathrm{VC}} = 0.865$ [A/(V^{2}s)]	$k^i_{\mathrm{PLL}} = 5.88$ [rad/(V $\cdot$ s)]
$C_{\mathrm{f}} = 0.216$ [mF]	$k^p_{\mathrm{Q}} = 0.0059$ [V^{-1}]	$\omega_{\mathrm{c,PLL}} = 7854$ [rad/s]
$R_{\mathrm{f}} = 0.462$ [mΩ]	$k^i_{\mathrm{Q}} = 0.059$ [(V $\cdot$ s)$^{-1}$]	
$L_g = 23.1$ [μH]	$\omega_{\mathrm{c,Q}} = 50.26$ [rad/s]	MPPT
$R_g = 2.77$ [mΩ]		$\omega_{\mathrm{c,pv}} = 50.26$ [rad/s]
$C_{\mathrm{dc}} = 0.1$ [mF]	Current Controller	
	$k^p_{\mathrm{CC}} = 0.6$ [V/A]	
	$k^i_{\mathrm{CC}} = 35$ [V/(A $\cdot$ s)]	

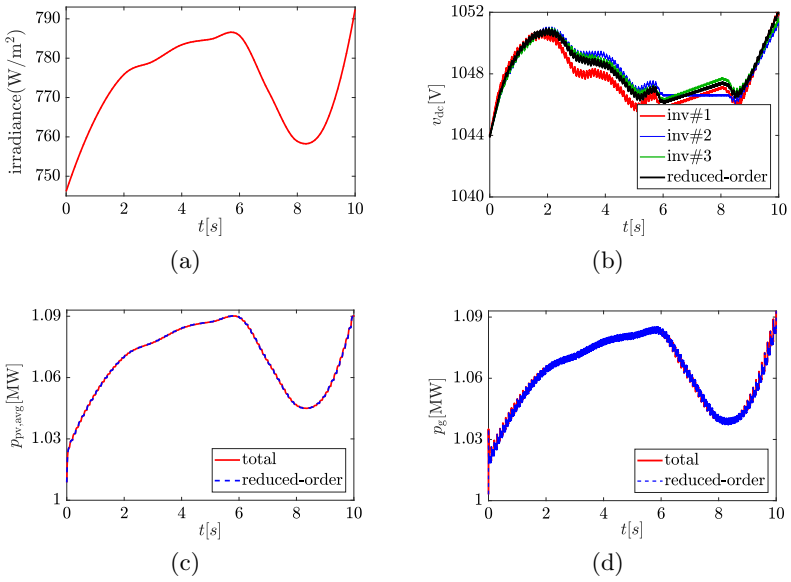

Figure 4.3: (a) Incident solar irradiance. Simulation results for case #1 comparing the multi-inverter system and the corresponding reduced-order model of (b) dc-link voltage, (c) averaged PV power, and (d) injected real power to the grid.

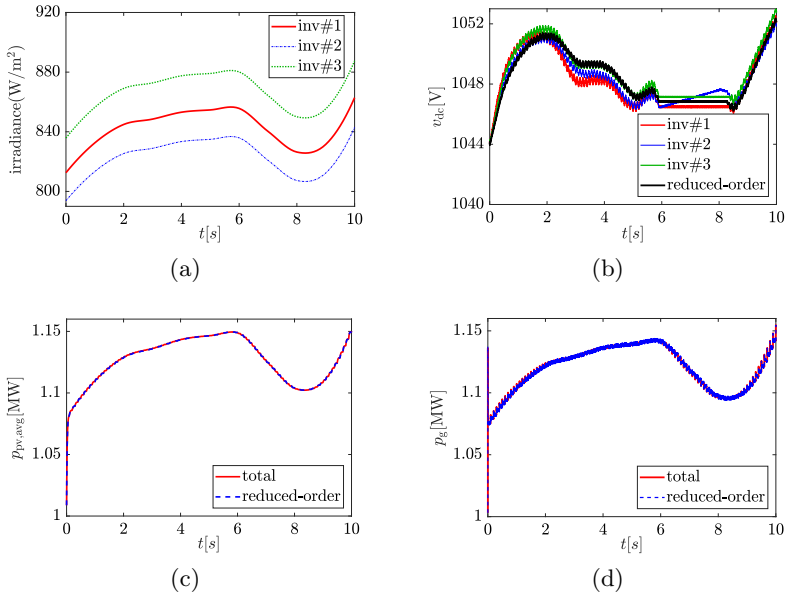

Figure 4.4: (a) Incident solar irradiance for selected inverters. Simulation results for case #2 comparing the multi-inverter system and the corresponding reduced-order model of (b) dc-link voltage, (c) averaged PV power, and (d) injected real power to the grid.

to each inverter varies between ±20% of the nominal value as shown in Fig. 4.4a (for three selected inverters). The simulations were performed on a personal computer with an Intel Core i7-7700HQ processor (2.80GHz CPU with 8GB RAM) using the ODE23 solver in MATLAB.

The results for case #1 are shown in Figs. 4.3b–4.3d. Figure 4.3b shows the dc-link voltage of three inverters (selected arbitrarily) in the parallel system and that of the reduced-order model. Figure 4.3c compares the total averaged PV output power ($p_{\mathrm{pv,avg}}$) of the inverters in the system and the reduced-order model, and Fig. 4.3d plots the total injected real power to the grid of the multi-inverter system and the reduced-order model. Results indicate that despite variations in the operation of the MPPT algorithm in the inverters, the reduced-order model captures the total power of the parallel system closely. The results for case #2 are shown in Figs. 4.4b–4.4d. These figures establish the accuracy of the reduced-order model in spite of differences in the MPPT algorithm *and* solar irradiance. The computation times to simulate dynamics of all the inverters and that required for the reduced-order model for case #1 are 966.8 [s] and 91.2 [s], respectively, and those for case #2 are 1128.9 [s] and 133.0 [s], respectively. This clearly demonstrates the computational benefit of the aggregate model.

Chapter 5

Network-cognizant Model Reduction of Grid-tied Three-phase Inverters

This chapter outlines a model-aggregation procedure for grid-tied three-phase inverters with the goal of capturing the time evolution of real- and reactive-power injections at the distribution-network feeder head while acknowledging power flows between the inverters. The three-phase inverter model is described in details in Chapter 3. In addition to the grid-tied inverters, our model for the distribution network includes impedance loads interconnected to the inverters through lines modeled with Π-equivalent circuits. Individually modeling the dynamics of all inverters, interconnecting lines, and loads to glean insights into the collective behavior of the distribution network, with particular emphasis on the active- and reactive-power injected into the feederhead, is computationally intractable. As a solution, we outline a reduced-order model for the distribution network, where inverters are clustered based on electrical distances from the feederhead and an aggregated model is derived for each cluster.

The aggregation procedure is built on the aggregated model for parallel-connected inverters. We leverage aggregation methods previously used for synchronous generators [18, 21, 22] to transfer all inverters to a single auxiliary bus, and then obtained the aggregated model. The auxiliary bus is connected to the original buses through ideal

transformers to preserve the power flows in the network. The auxiliary-transformer turns ratios are designed such that the voltages of the inverter-facing terminals are approximately the average of the voltages in the original network. To obtain an estimate of these voltages, we leverage linear approximations of the AC power flow equations [62–64].

Recent works in the literature on the single-auxiliary-bus approach for system of inverters are [15, 65]. We improve upon the approach by introducing multiple auxiliary buses and clustering inverters to these buses according to their electrical distance from the grid bus. This strategy is based on the underlying assumption that inverters that are electrically the same distance from the grid bus should be—in theory—dynamically coherent. This assumption is also leveraged in prior work on synchronous-generator coherency [18, 21, 22, 66] and network partitioning [67–70], where, it is recognized that electrically close generators tend to swing together during disturbances. While the classic notion of coherency as it relates to machine angles does not perfectly translate to inverters [71, 72], we find that the electrical-distance-based clustering approach effectively identifies groups of inverters that have similar dynamic behavior during transients. Given its ease of implementation and scalability, we apply the K-means algorithm [73–76] to cluster inverters. With regard to determining the optimal number of clusters, we point to several numerical methods that have been proposed in the literature [77–82] to this end. For the present application, we find that the so-called silhouette analysis method [80–82] provides a good insight into the optimal number of clusters to be introduced. The aggregation method outlined in this chapter can be applied to the other inverter models if aggregated model for elemental parallel connection is known. For instance, Chapter 4 and Appendix A outline the aggregate models for parallel-connected photovoltaic three-phase inverters and single-phase inverters, respectively, [83] for wind turbines, and [37, 84] for grid-forming inverters.

The remainder of this chapter is organized as follows. In Section 5.1, we briefly overview the three-phase grid-connected inverter model and the aggregation results for parallel-connected inverters. In Section 5.2, we describe the distribution feeder model. In Section 5.3, we outline the network-cognizant aggregation approach. We validate the proposed approach with exhaustive numerical simulations for an illustrative feeder network in Section 5.4.

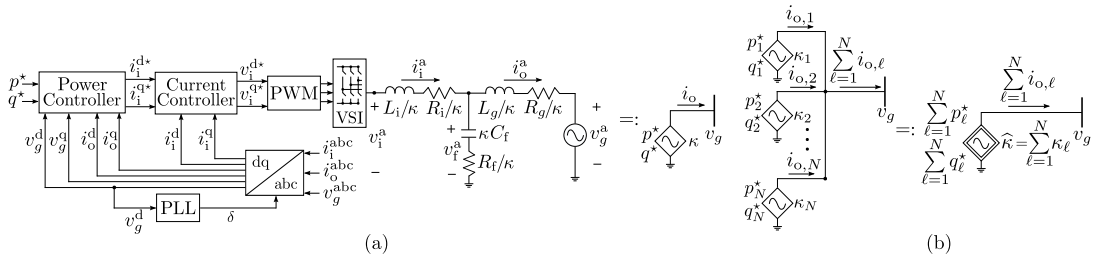

Figure 5.1: (a) Block diagram of grid-tied three-phase inverter (phase a of the output LCL filter is depicted) and adopted shorthand, (b) Parallel connection of N inverters, and the adopted shorthand representation of the reduced-order model. The reduced-order model has the same form as (a) with equivalent power-scaling parameter $\widehat{\kappa} = \sum_{\ell=1}^{N} \kappa_\ell$, real-power setpoint, $\sum_{\ell=1}^{N} p_\ell^\star$, and reactive-power setpoint, $\sum_{\ell=1}^{N} q_\ell^\star$.

5.1 Inverter Model and Parallel Aggregation

This section briefly overviews the model of a single three-phase inverter, and the aggregate model for a parallel collection.

5.1.1 Inverter Model

A block diagram of the inverter model is depicted in Fig. 5.1a. Key elements here are reference frame transformations used to facilitate control, internal controller and filter dynamics, and power-scaling parameters that capture the different power ratings for the inverters.

5.1.1.1 Reference-frame Transformations

Three-phase signals $x^{\mathrm{abc}} = [x^{\mathrm{a}}, x^{\mathrm{b}}, x^{\mathrm{c}}]^{\mathrm{T}}$ are transformed to equivalent DC signals $(x^{\mathrm{d}}, x^{\mathrm{q}})$ using Park's transformation implemented with the PLL angle, δ. The abc-dq block in Fig. 5.1a captures the transformation. In a system of inverters, the controller for each inverter operates on signals in its own dq reference frame. For analytical convenience, inverter outputs and network variables should be represented in the same reference frame. To do so, it is common practice to rely on a global DQ frame with phase denoted by δ_g and frequency ω_g. Given variables in the local dq frame, x^{d} and x^{q}, the corresponding variables in the global reference frame are denoted by x^{D} and x^{Q}, and they are obtained

through:

$$\begin{bmatrix} x^{\mathrm{D}} \\ x^{\mathrm{Q}} \end{bmatrix} = \begin{bmatrix} \cos(\delta_g - \delta) & \sin(\delta_g - \delta) \\ -\sin(\delta_g - \delta) & \cos(\delta_g - \delta) \end{bmatrix} \begin{bmatrix} x^{\mathrm{d}} \\ x^{\mathrm{q}} \end{bmatrix}. \tag{5.1}$$

For subsequent developments, we define $x^{\mathrm{DQ}} := x^{\mathrm{D}} + jx^{\mathrm{Q}}$ and $x^{\mathrm{dq}} := x^{\mathrm{d}} + jx^{\mathrm{q}}$.

5.1.1.2 State-space Model for the Inverter Dynamics

A block diagram of the inverter control architecture is illustrated in Fig. 5.1a. The details on the inverter model are presented in Chapter 3. To capture inverters with different power ratings, recall the *power-scaling parameter*, κ:

$$\kappa = p_{\mathrm{rated}}/p_{\mathrm{base}}, \tag{5.2}$$

with p_{rated} and p_{base} denoting the rated power of the inverter and the system-wide base value, respectively. Inverters with power rating κp_{base} have parameters $L_{\mathrm{i}}, R_{\mathrm{i}}, C_{\mathrm{f}}, R_{\mathrm{f}}$, $L_g, R_g, k^p_{\mathrm{CC}}, k^i_{\mathrm{CC}}$ scaled as $\kappa^{-1}L_{\mathrm{i}}, \kappa^{-1}R_{\mathrm{i}}, \kappa C_{\mathrm{f}}, \kappa^{-1}R_{\mathrm{f}}, \kappa^{-1}L_g, \kappa^{-1}R_g, \kappa^{-1}k^p_{\mathrm{CC}}, \kappa^{-1}k^i_{\mathrm{CC}}$. The reference inputs to the inverter are the real- and reactive-power setpoints (denoted by $p^\star$ and $q^\star$, respectively).

The inverter dynamics can be compactly represented by the following 15th-order model:

$$\dot{x} = Ax + Bu_{\mathrm{s}} + g(x, u_{\mathrm{v}}), \quad y = i_{\mathrm{o}}^{\mathrm{DQ}}, \tag{5.3}$$

with states and inputs:

$$x = [i_{\mathrm{i}}^{\mathrm{d}}, i_{\mathrm{i}}^{\mathrm{q}}, i_{\mathrm{o}}^{\mathrm{d}}, i_{\mathrm{o}}^{\mathrm{q}}, v_{\mathrm{f}}^{\mathrm{d}}, v_{\mathrm{f}}^{\mathrm{q}}, \gamma^{\mathrm{d}}, \gamma^{\mathrm{q}}, p_{\mathrm{avg}}, q_{\mathrm{avg}}, \phi^{\mathrm{p}}, \phi^{\mathrm{q}}, v_{\mathrm{PLL}}, \phi_{\mathrm{PPL}}, \delta]^{\mathrm{T}}, \tag{5.4}$$

$$u_{\mathrm{s}} = [p^\star, q^\star]^{\mathrm{T}}, \quad u_{\mathrm{v}} = v_g^{\mathrm{abc}} := [v_g^{\mathrm{a}}, v_g^{\mathrm{b}}, v_g^{\mathrm{c}}]^{\mathrm{T}}. \tag{5.5}$$

Input u_{s} captures the real- and reactive-power setpoints, and input u_{v} is the voltage sensed at the inverter terminals. The output of the state-space model, $y = i_{\mathrm{o}}^{\mathrm{DQ}} \in \mathbb{C}$ is the L_g-branch current represented in the global DQ reference frame (see Fig. 5.1a).

5.1.2 Reduced-order Model of Parallel-connected Inverters

Consider a collection of N inverters, all with the dynamical model (5.3) connected in parallel to the grid bus. We capture the following types of heterogeneity in inverters:

1. The inverters have different power ratings. The power scaling parameter of the ℓ inverter is denoted by κ_ℓ.

2. The inverters have different reference-power setpoints. The real- and reactive-power setpoints for inverter ℓ are denoted by $p_\ell^\star$ and $q_\ell^\star$, respectively.

We have shown in Collorary 3.3 that the dynamics of this system of inverters can be described by a model with the same structure and order as any individual inverter (see Fig. 5.1a). The aggregated inverter dynamics can be compactly expressed with the following 15th-order state-space model:

$$\dot{\widehat{x}} = \widehat{A}\widehat{x} + \widehat{B}\widehat{u}_{\mathrm{s}} + \widehat{g}(\widehat{x}, \widehat{u}_{\mathrm{v}}), \quad \widehat{y} = \widehat{i}_{\mathrm{o}}^{\mathrm{DQ}}, \tag{5.6}$$

with states and inputs:

$$\widehat{x} = [\widehat{i}_{\mathrm{i}}^{\mathrm{d}}, \widehat{i}_{\mathrm{i}}^{\mathrm{q}}, \widehat{i}_{\mathrm{o}}^{\mathrm{d}}, \widehat{i}_{\mathrm{o}}^{\mathrm{q}}, \widehat{v}_{\mathrm{f}}^{\mathrm{d}}, \widehat{v}_{\mathrm{f}}^{\mathrm{q}}, \widehat{\gamma}^{\mathrm{d}}, \widehat{\gamma}^{\mathrm{q}}, \widehat{p}_{\mathrm{avg}}, \widehat{q}_{\mathrm{avg}}, \widehat{\phi}^{\mathrm{p}}, \widehat{\phi}^{\mathrm{q}}, \widehat{v}_{\mathrm{PLL}}, \widehat{\phi}_{\mathrm{PPL}}, \widehat{\delta}]^{\mathrm{T}}, \tag{5.7}$$

$$\widehat{u}_{\mathrm{s}} = \sum_{\ell=1}^{N} [p_\ell^\star, q_\ell^\star]^{\mathrm{T}}, \quad \widehat{u}_{\mathrm{v}} = v_g^{\mathrm{abc}} = [v_g^{\mathrm{a}}, v_g^{\mathrm{b}}, v_g^{\mathrm{c}}]^{\mathrm{T}}. \tag{5.8}$$

Input $\widehat{u}_{\mathrm{s}}$ captures the net real- and reactive-power setpoints of the inverters in the system, and input $\widehat{u}_{\mathrm{v}}$ is the voltage sensed at the inverter terminals, which in this case, is the grid voltage. The output of the state-space model, $\widehat{y} = \widehat{i}_{\mathrm{o}}^{\mathrm{DQ}} \in \mathbb{C}$ is the output current of the collection of inverters in the global DQ reference frame. The aggregated inverter has power rating of $\widehat{\kappa} p_{\mathrm{base}}$, with $\widehat{\kappa} := \sum_{\ell=1}^{N} \kappa_\ell$ denotes the equivalent power-scaling parameter. The states of the aggregated inverter (5.7) relate to the individual inverter (5.4) as follows $\forall t \geq t_0$:

$$\begin{aligned}
&[\widehat{i}_{\mathrm{i}}^{\mathrm{d}}, \widehat{i}_{\mathrm{i}}^{\mathrm{q}}, \widehat{i}_{\mathrm{o}}^{\mathrm{d}}, \widehat{i}_{\mathrm{o}}^{\mathrm{q}}, \widehat{\gamma}^{\mathrm{d}}, \widehat{\gamma}^{\mathrm{q}}, \widehat{p}_{\mathrm{avg}}, \widehat{q}_{\mathrm{avg}}, \widehat{\phi}^{\mathrm{p}}, \widehat{\phi}^{\mathrm{q}}]^{\mathrm{T}} = \\
&\sum_{\ell=1}^{N} [i_{\mathrm{i},\ell}^{\mathrm{d}}, i_{\mathrm{i},\ell}^{\mathrm{q}}, i_{\mathrm{o},\ell}^{\mathrm{d}}, i_{\mathrm{o},\ell}^{\mathrm{q}}, \gamma_\ell^{\mathrm{d}}, \gamma_\ell^{\mathrm{q}}, p_{\mathrm{avg},\ell}, q_{\mathrm{avg},\ell}, \phi_\ell^{\mathrm{p}}, \phi_\ell^{\mathrm{q}}]^{\mathrm{T}},
\end{aligned}$$

$$[\widehat{v}_{\mathrm{f}}^{\mathrm{d}}, \widehat{v}_{\mathrm{f}}^{\mathrm{q}}]^{\mathrm{T}} = \frac{1}{\widehat{\kappa}} \sum_{\ell=1}^{N} \kappa_\ell [v_{\mathrm{f},\ell}^{\mathrm{d}}, v_{\mathrm{f},\ell}^{\mathrm{q}}]^{\mathrm{T}},$$
$$[\widehat{v}_{\mathrm{PLL}}, \widehat{\phi}_{\mathrm{PPL}}, \widehat{\delta}]^{\mathrm{T}} = [v_{\mathrm{PLL},\ell}, \phi_{\mathrm{PPL},\ell}, \delta_\ell]^{\mathrm{T}}, \forall \ell.$$

5.2 Network Description and Dynamics

In this section, we describe the distribution-network topology and outline its dynamical model.

5.2.1 Distribution-network Topology and Constitution

We study the networked dynamics of inverters connected in a balanced three-phase electrical distribution network with the Π-model adopted for branches in the network [85]. Figure 5.2a illustrates the system: each inverter is pictorially represented with the shorthand established in Fig. 5.1a. The slack bus (representing the secondary of the step-down transformer that connects the distribution network to the bulk system) is denoted by g. The nodes of the electrical network and the grid are collected in the set $\mathcal{N} \cup \{g\}$, inverter buses are denoted by $\mathcal{I} \subseteq \mathcal{N}$, and $\mathcal{Z} = \mathcal{N} \setminus \mathcal{I}$ collects the set of buses with zero current injections. Branches are collected in the set $\mathcal{E} \subseteq \mathcal{N} \cup \{g\} \times \mathcal{N} \cup \{g\}$.

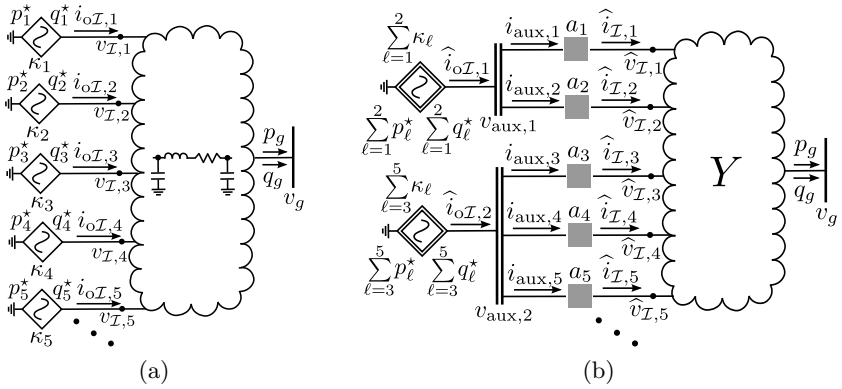

Figure 5.2: Illustrating adopted notation and aggregate model: (a) Network of $|\mathcal{I}|$ inverters with different power ratings and reference-power setpoints (five of which are explicitly illustrated) with Π-equivalent circuits adopted to model interconnecting lines. (b) Reduced-order model of the system with the inverters aggregated into clusters (two of which are explicitly illustrated) determined based on electrical distances from bus g that denotes the transmission-distribution interface.

The edge-incidence matrix of the network, $E \in \mathbb{R}^{(|\mathcal{N}|+1)\times|\mathcal{E}|}$, has entries

$$[E]_{k\ell} := \begin{cases} 1, & \text{if } k \text{ is the source of } \ell\text{-th line,} \\ -1, & \text{if } k \text{ is the sink of } \ell\text{-th line,} \\ 0, & \text{otherwise.} \end{cases} \tag{5.9}$$

Furthermore, we will find it useful to define $F := [\mathrm{I}_{|\mathcal{I}|}, \mathbb{0}^{\mathrm{T}}_{(|\mathcal{N}|+1)\times|\mathcal{I}|}]^{\mathrm{T}}$.

Let $R_{\mathcal{E}} \in \mathbb{R}^{|\mathcal{E}|}$, $L_{\mathcal{E}} \in \mathbb{R}^{|\mathcal{E}|}$, and $C_{\mathcal{E}} \in \mathbb{R}^{|\mathcal{N}|}$ denote the vectors that collect the line resistance, line inductance, and shunt capacitance, respectively. The network admittance matrix, $Y \in \mathbb{C}^{(|\mathcal{N}|+1)\times(|\mathcal{N}|+1)}$, maps the nodal voltages to the current injections, and it is given by:

$$Y := E\mathrm{diag}(R_{\mathcal{E}} + j\omega_g L_{\mathcal{E}})^{-1}E^{\mathrm{T}} + j\omega_g \mathrm{diag}([C_{\mathcal{E}}^{\mathrm{T}}, 0]^{\mathrm{T}}). \tag{5.10}$$

Nodal voltages and current injections in the DQ reference frame are $v^{\mathrm{DQ}} := [(v^{\mathrm{DQ}}_{\mathcal{N}})^{\mathrm{T}}, v^{\mathrm{DQ}}_g]^{\mathrm{T}}$ and $i^{\mathrm{DQ}} := [(i^{\mathrm{DQ}}_{\mathcal{N}})^{\mathrm{T}}, -i^{\mathrm{DQ}}_g]^{\mathrm{T}}$ (the negative sign that precedes i^{DQ}_g is in acknowledgment of its assumed direction as shown in Fig. 5.2a). It follows that $i^{\mathrm{DQ}}_{\mathcal{N}} = [(i^{\mathrm{DQ}}_{\mathcal{I}})^{\mathrm{T}}, \mathbb{0}^{\mathrm{T}}_{|\mathcal{Z}|}]^{\mathrm{T}}$ and $v^{\mathrm{DQ}}_{\mathcal{N}} = [(v^{\mathrm{DQ}}_{\mathcal{I}})^{\mathrm{T}}, (v^{\mathrm{DQ}}_{\mathcal{Z}})^{\mathrm{T}}]^{\mathrm{T}}$. Finally, $i^{\mathrm{DQ}}_{\mathcal{E}} \in \mathbb{C}^{|\mathcal{E}|}$ collects the directed currents of the lines, and $i^{\mathrm{DQ}}_{\mathrm{o}\mathcal{I}} \in \mathbb{C}^{|\mathcal{I}|}$ is the vector that collects output currents of the inverters on the L_g branches. We introduce no additional notation to distinguish between time- and phasor-domain representations of variables. Differences are expected to be contextually clear.

5.2.2 DQ-frame Network Dynamics in the Time Domain

In their original form, and without any model reduction, the dynamics of the distribution feeder include those arising from the interconnecting distribution lines and inverters. With a slight abuse of notation compared to (5.3), the dynamics of all inverters in the system are given by

$$\begin{aligned} \dot{x} &= \mathrm{bdiag}(A_1, \ldots, A_{|\mathcal{I}|})x + [(B_1 u_{\mathrm{s},1})^{\mathrm{T}}, \ldots, (B_{|\mathcal{I}|}u_{\mathrm{s},|\mathcal{I}|})^{\mathrm{T}}]^{\mathrm{T}} + g'(x, u_{\mathrm{v}}), \\ y &= i^{\mathrm{DQ}}_{\mathrm{o}\mathcal{I}}, \end{aligned} \tag{5.11}$$

where $x := [x_1^{\mathrm{T}}, \ldots, x_{|\mathcal{I}|}^{\mathrm{T}}]^{\mathrm{T}} \in \mathbb{R}^{15|\mathcal{I}|}$ collects the states corresponding to all inverters in the system (each $x_\ell \in \mathbb{R}^{15}$ has entries shown in (5.4)), $g' : \mathbb{R}^{15|\mathcal{I}|} \times \mathbb{R}^{3\times|\mathcal{I}|} \to \mathbb{R}^{15|\mathcal{I}|}$ is:

$$g'(x, u_{\mathrm{v}}) = [g_1(x_1, v_{\mathrm{v},1})^{\mathrm{T}}, \ldots, g_{|\mathcal{I}|}(x_{|\mathcal{I}|}, v_{\mathrm{v},|\mathcal{I}|})^{\mathrm{T}}]^{\mathrm{T}},$$

with A_ℓ, B_ℓ, and g_ℓ above defined in the state-space model of an individual inverter as in (5.3). Finally, $u_{\mathrm{s},\ell} = [p_\ell^\star, q_\ell^\star]^{\mathrm{T}}$ captures the real- and reactive-power setpoints of the ℓ-th inverter, and $u_{\mathrm{v}} = v_{\mathcal{I}}^{\mathrm{abc}}$ captures inverter voltages in the abc reference frame. The line-current and bus-voltage dynamics in the network in the DQ-frame are given by

$$\begin{aligned} \mathrm{diag}(L_{\mathcal{E}})\dot{i}_{\mathcal{E}}^{\mathrm{DQ}} &= -\mathrm{diag}(R_{\mathcal{E}} + j\omega_g L_{\mathcal{E}})i_{\mathcal{E}}^{\mathrm{DQ}} + E^{\mathrm{T}} v^{\mathrm{DQ}}, \\ \mathrm{diag}(C_{\mathcal{E}})\dot{v}_{\mathcal{N}}^{\mathrm{DQ}} &= -j\omega_g \mathrm{diag}(C_{\mathcal{E}})v_{\mathcal{N}}^{\mathrm{DQ}} + F_{\mathcal{N}} i_{\mathrm{o}\mathcal{I}}^{\mathrm{DQ}} - E_{\mathcal{N}} i_{\mathcal{E}}^{\mathrm{DQ}}, \end{aligned} \tag{5.12}$$

where, recall that E is the network edge-incidence matrix (5.9), and matrices $F_{\mathcal{N}} \in \mathbb{R}^{|\mathcal{N}|\times|\mathcal{I}|}$ and $E_{\mathcal{N}} \in \mathbb{R}^{|\mathcal{N}|\times|\mathcal{E}|}$ are obtained from F and E by discarding the row that corresponds to the grid bus. The current injected into the grid, i_g, in Fig. 5.2a, is given by $i_g^{\mathrm{DQ}} = -E_g i_{\mathcal{E}}^{\mathrm{DQ}}$, where E_g denotes the row in E corresponding to the grid bus. The real- and reactive-power injections into the grid bus are given by

$$p_g = \frac{3}{2}(v_g^{\mathrm{D}}\, i_g^{\mathrm{D}} + v_g^{\mathrm{Q}}\, i_g^{\mathrm{Q}}), \quad q_g = \frac{3}{2}(v_g^{\mathrm{Q}}\, i_g^{\mathrm{D}} - v_g^{\mathrm{D}}\, i_g^{\mathrm{Q}}). \tag{5.13}$$

With all dynamics explicitly modeled in (5.11), (5.12), the order of the dynamical model one has to simulate to obtain the time-domain evolution of p_g and q_g is $2(|\mathcal{E}| + |\mathcal{N}|) + 15|\mathcal{I}|$.

5.3 Network-cognizant Aggregate Model

In this section, we present the details of the clustering approach and the aggregate dynamical model. The aggregation strategy applies to any connected network topology (meshed, radial) with arbitrary line impedance values.

5.3.1 Auxiliary Network with Aggregated Inverters

To describe the circuit equations that underlie the reduced-order model, consider the network sketched in Fig. 5.2b, where inverters have been clustered (and subsequently aggregated) based on the electrical distances between their terminals and the grid bus in the originating network sketched in Fig. 5.2a. In subsequent developments, this network with clustered and aggregated inverters is referred to as the *auxiliary network*. Let $\widehat{i}_{\mathrm{o}\mathcal{I}}^{\mathrm{DQ}} \in \mathbb{C}^{|\mathcal{C}|}$ denote the vector that collects the output current of the aggregated inverters, $i_{\mathrm{aux}}^{\mathrm{DQ}} \in \mathbb{C}^{|\mathcal{I}|}$ captures the currents from the auxiliary buses into the primary side of the transformers, and $\widehat{i}_{\mathcal{I}}^{\mathrm{DQ}} \in \mathbb{C}^{|\mathcal{I}|}$ captures the currents from the secondary-side of the transformers into the electrical network. Similarly, $\widehat{v}_{\mathcal{I}}^{\mathrm{DQ}} \in \mathbb{C}^{|\mathcal{I}|}$ captures the voltages on the secondary-side of the transformers, and $v_{\mathrm{aux}}^{\mathrm{DQ}} \in \mathbb{C}^{|\mathcal{C}|}$ denotes the voltages on the primary side. See Fig. 5.2b for an illustration of these variables. Denote $\mathcal{I}_c$ as the index set of inverter buses that belong to the c-th cluster. For subsequent developments, we will find matrix $\Phi \in \mathbb{R}^{|\mathcal{I}|\times|\mathcal{C}|}$ with entries:

$$[\Phi]_{kc} := \begin{cases} 1, & \text{if } k \in \mathcal{I}_c, \\ 0, & \text{otherwise,} \end{cases}$$

useful in identifying the clusters that inverters belong to.

5.3.1.1 Clustering of inverters

We use the effective impedance as a measure of the electrical distance. The effective impedance between the grid bus, g, and the ℓ-th inverter bus, denoted by $z_{g\ell}^{\mathrm{eff}} \in \mathbb{C}$, is defined as the potential difference between these two buses when a unit current is injected in bus g and extracted from bus ℓ. It can be computed as [86]:

$$z_{g\ell}^{\mathrm{eff}} = (e_g - e_\ell)^{\mathrm{T}} v = (e_g - e_\ell)^{\mathrm{T}} Y^{\dagger} (e_g - e_\ell), \tag{5.14}$$

where $Y^{\dagger}$ is the pseudoinverse of the network admittance matrix, $e_g \in \mathbb{R}^{|\mathcal{N}|+1}$ and $e_\ell \in \mathbb{R}^{|\mathcal{N}|+1}$ denote the canonical vectors of all zeros except with entry one at the position of index g (i.e., the grid bus) and index ℓ (capturing the inverter at bus $\ell \in \mathcal{I}$), respectively. Let $z^{\mathrm{eff}} \in \mathbb{R}^{|\mathcal{I}|}$ denote the vector that collects all the magnitudes of effective impedances between the grid bus and inverter buses. With this measure of electrical

distance, we utilize the K-means algorithm to group the inverters into $|\mathcal{C}|$ clusters [75,76]. We apply the algorithm to a pre-processed version of z^{eff}, denoted by $z^{\text{eff}}_{\text{scaled}} \in \mathbb{R}^{|\mathcal{I}|}_{\geq 0}$, and defined by:

$$z^{\text{eff}}_{\text{scaled}} := \log\left(z^{\text{eff}} / \min(z^{\text{eff}})\right). \tag{5.15}$$

We scale z^{eff} by the inverse of its smallest entry so that its logarithm is nonnegative. Clustering based on entries of $z^{\text{eff}}_{\text{scaled}}$ is noted empirically to yield better results, i.e., with a higher probability, inverters farther away from the grid bus are clustered together.

5.3.1.2 Determining the optimal number of clusters

One method to measure the quality of clustering is silhouette analysis [80–82]. For a point $a \in \mathcal{C}_\ell$, let $d(a)$ denote the average of the distance between point a and other points inside cluster $\mathcal{C}_\ell$, $\widetilde{d}_k(a, \mathcal{C}_k)$ denote the average of the distance between point a and all other points in cluster $\mathcal{C}_k$, where $k \neq \ell$, and the minimum of all $\widetilde{d}_k(a, \mathcal{C}_k)$ values is denoted by $\widetilde{d}(a)$. The silhouette value of point a, denoted by $s(a)$, is given by: [82]

$$s(a) = \frac{\widetilde{d}(a) - d(a)}{\max(d(a), \widetilde{d}(a))}. \tag{5.16}$$

Note that the range of $s(a)$ is between -1 and 1. Observing (5.16), $s(a)$ has a negative value if $\widetilde{d}(a) < d(a)$, and a value close to 1 if $\widetilde{d}(a) \gg d(a)$. With K-means, the sum of within-cluster distances decreases as the number of clusters increases, therefore, the average silhouette value of all the points tends to approach unity. Without loss of generality, we choose the number of clusters with average silhouette value around 0.8 as the optimal number of clusters for simulations that follow. The silhouette analysis method outlined above is one of many [77–82] that have been proposed in the literature for determining the optimal number of clusters. Empirically, we observe that this yields good results for the considered application.

5.3.1.3 Engineering the Auxiliary Network

The formulation of the auxiliary network (Fig. 5.2b) hinges on the choice of the auxiliary-transformer turns ratios. One option is to pick the nominal auxiliary-bus voltages,

$\overline{v}_{\text{aux}}^{\text{DQ}} \in \mathbb{C}^{|\mathcal{C}|}$ to be the weighted average of the inverter-terminal voltages:

$$\overline{v}_{\text{aux}}^{\text{DQ}} = \text{diag}((\text{diag}(K)\Phi)^{\text{T}}\mathbb{1}_{|\mathcal{I}|})^{-1}(\text{diag}(K)\Phi)^{\text{T}}v_{\mathcal{I}}^{\text{DQ}}, \tag{5.17}$$

where $K := [\kappa_1, \ldots, \kappa_{|\mathcal{I}|}]^{\text{T}}$. Above, $v_{\mathcal{I}}^{\text{DQ}}$ collects the inverter terminal voltages *in the original network* (Fig. 5.2a). This is a key point and deserves emphasis. The choice in (5.17) establishes the link between the original and auxiliary networks. Simulating the dynamics of all constituent elements in the original network to obtain $v_{\mathcal{I}}^{\text{DQ}}$ would be computationally burdensome; instead, we utilize the linear approximation:

$$v_{\mathcal{I}}^{\text{DQ}} \approx v_{\mathcal{I}}^{\star} + V_p P^{\star} + V_q Q^{\star}, \tag{5.18}$$

where $P^{\star} := [p_1^{\star}, \ldots, p_{|\mathcal{I}|}^{\star}]^{\text{T}}$, $Q^{\star} := [q_1^{\star}, \ldots, q_{|\mathcal{I}|}^{\star}]^{\text{T}}$, and $v_{\mathcal{I}}^{\star}$ is the linearization point. We pick $v_{\mathcal{I}}^{\star} = -Y_{\mathcal{I}\mathcal{I}}^{-1}Y_{g\mathcal{I}}^{\text{T}}v_g^{\text{DQ}}$, where $Y_{\mathcal{I}\mathcal{I}}$ and $Y_{g\mathcal{I}}$ are submatrices of the Kron-reduced admittance matrix (formally defined in (5.26)). The voltage $v_{\mathcal{I}}^{\star}$ is the *no-load voltage*, which is the voltage profile in the network with zero power injections at inverter buses [62]. With this choice,

$$\begin{aligned} V_p &= \frac{v_{\text{base}}}{3s_{\text{base}}}(\Gamma + j\Lambda), \\ V_q &= \frac{v_{\text{base}}}{3s_{\text{base}}}(\Lambda - j\Gamma), \end{aligned} \tag{5.19}$$

where matrices Γ, Λ depend on the linearization point and network topology/constitution, and they are given by:

$$\begin{aligned} \Gamma &= R\text{diag}\left(\frac{\cos\angle v_{\mathcal{I}}^{\star}}{|v_{\mathcal{I}}^{\star}|/v_{\text{base}}}\right) - X\text{diag}\left(\frac{\sin\angle v_{\mathcal{I}}^{\star}}{|v_{\mathcal{I}}^{\star}|/v_{\text{base}}}\right), \\ \Lambda &= X\text{diag}\left(\frac{\cos\angle v_{\mathcal{I}}^{\star}}{|v_{\mathcal{I}}^{\star}|/v_{\text{base}}}\right) + R\text{diag}\left(\frac{\sin\angle v_{\mathcal{I}}^{\star}}{|v_{\mathcal{I}}^{\star}|/v_{\text{base}}}\right), \end{aligned} \tag{5.20}$$

with $R := y_{\text{base}}\,\text{Re}\{Y_{\mathcal{I}\mathcal{I}}^{-1}\}$, $X := y_{\text{base}}\,\text{Im}\{Y_{\mathcal{I}\mathcal{I}}^{-1}\}$, and $v_{\text{base}} := |v_g^{\text{DQ}}|$, s_{base} and y_{base} denoting the voltage, power and admittance base values. With the nominal auxiliary-bus voltages specified in (5.17), and the linear approximation of $v_{\mathcal{I}}^{\text{DQ}}$ in (5.18), the

auxiliary-transformers' turns ratios, $n \in \mathbb{C}^{|\mathcal{I}|}$ are:

$$n = \operatorname{diag}\left(\Phi\, \overline{v}_{\text{aux}}^{\text{DQ}}\right)^{-1} v_{\mathcal{I}}^{\text{DQ}}, \tag{5.21}$$

which follows from the fact that $v_{\mathcal{I}}^{\text{DQ}}$ are the voltages on the secondary side, and $\overline{v}_{\text{aux}}^{\text{DQ}}$ are the nominal voltages on the primary side of the transformers.

5.3.2 Dynamics of Auxiliary Network

The dynamics that characterize the auxiliary network are those of the aggregated-inverter models in the $|\mathcal{C}|$ clusters. These, coupled with pertinent algebraic equations that arise from the circuit laws that underlie the auxiliary network yield the real- and reactive-power grid injections. The dynamics of the aggregated inverters in the auxiliary network are:

$$\dot{x}^{\text{r}} = A^{\text{r}} x^{\text{r}} + B^{\text{r}} u_{\text{s}}^{\text{r}} + g^{\text{r}}(x^{\text{r}}, u_{\text{v}}), \quad y^{\text{r}} = \widehat{i}_{\text{o}\mathcal{I}}^{\text{DQ}}, \tag{5.22}$$

where $x^{\text{r}} := [\widehat{x}_1^{\text{T}}, \ldots, \widehat{x}_{|\mathcal{C}|}^{\text{T}}]^{\text{T}} \in \mathbb{R}^{15|\mathcal{C}|}$ collects the states corresponding to all the aggregated inverters in the reduced-order model (each $\widehat{x}_\ell \in \mathbb{R}^{15}$ has entries as shown in (5.7)). The power input $u_{\text{s}}^{\text{r}} = [u_{\text{s},1}^{\text{T}}, \ldots, u_{\text{s},|\mathcal{C}|}^{\text{T}}]^{\text{T}} \in \mathbb{R}^{2|\mathcal{C}|}$, where (with slight abuse of notation) $u_{\text{s},\ell} = \sum_{k \in \mathcal{I}_\ell} [p_k^\star, q_k^\star]^{\text{T}}$, contains the power setpoints of the aggregated inverters; and the voltage input $u_{\text{v}} = v_{\text{aux}}^{\text{abc}}$ (since the inverter terminal voltages are the auxiliary-bus voltages). The model output $y^{\text{r}} = \widehat{i}_{\text{o}\mathcal{I}}^{\text{DQ}} \in \mathbb{C}^{|\mathcal{C}|}$ is the collection of the output currents of the aggregated inverters. Furthermore, $A^{\text{r}} \in \mathbb{R}^{15|\mathcal{C}| \times 15|\mathcal{C}|}$, $B^{\text{r}} \in \mathbb{R}^{15|\mathcal{C}| \times 2|\mathcal{C}|}$, $g^{\text{r}} \in \mathbb{R}^{15|\mathcal{C}|} \times \mathbb{R}^{3 \times |\mathcal{C}|} \to \mathbb{R}^{15|\mathcal{C}|}$ are:

$$\begin{aligned} &A^{\text{r}} = \operatorname{bdiag}(\widehat{A}_1, \ldots, \widehat{A}_{|\mathcal{C}|}),\ B^{\text{r}} = \operatorname{bdiag}(\widehat{B}_1, \ldots, \widehat{B}_{|\mathcal{C}|}), \\ &g^{\text{r}}(x^{\text{r}}, u_{\text{v}}) = \left[\widehat{g}_1(\widehat{x}_1, u_{\text{v},1})^{\text{T}}, \ldots, \widehat{g}_{|\mathcal{C}|}(\widehat{x}_{|\mathcal{C}|}, u_{\text{v},|\mathcal{C}|})^{\text{T}}\right]^{\text{T}}, \end{aligned}$$

where $\widehat{A}_c$, $\widehat{B}_c$, and $\widehat{g}_c$ define the state-space model of the aggregated inverter for $|\mathcal{I}_c|$ parallel-connected inverters in the c-th cluster as in (5.6). To complete the model, we need to specify the terminal voltages of the inverters (which in this case are the voltages of the auxiliary buses $v_{\text{aux}}^{\text{abc}}$ (equivalently $v_{\text{aux}}^{\text{DQ}}$)), as well as the current injected into the

grid for the new model. Kirchhoff's current law at the auxiliary buses is captured by $\widehat{i}_{\mathrm{o}\mathcal{I}}^{\mathrm{DQ}} = \Phi^{\mathrm{T}} i_{\mathrm{aux}}^{\mathrm{DQ}}$. Furthermore, the primary- and secondary-side quantities are related by:

$$\widehat{v}_{\mathcal{I}}^{\mathrm{DQ}} = \mathrm{diag}(n)\Phi\, v_{\mathrm{aux}}^{\mathrm{DQ}}, \quad \widehat{i}_{\mathcal{I}}^{\mathrm{DQ}} = \mathrm{diag}(n^{\mathrm{H}})^{-1} i_{\mathrm{aux}}^{\mathrm{DQ}}, \tag{5.23}$$

with the second equation arising from the conservation of power for an ideal transformer.

With the time-domain model of the network in place, we simplify the network dynamics by modeling them to be in steady-state. Writing (5.12) in phasor form, we get:

$$\widehat{i}_{\mathcal{E}}^{\mathrm{DQ}} = \mathrm{diag}(R_{\mathcal{E}} + j\omega_g L_{\mathcal{E}})^{-1} E^{\mathrm{T}} \widehat{v}^{\mathrm{DQ}}. \tag{5.24}$$

Let $\widehat{i}^{\mathrm{DQ}} \in \mathbb{C}^{|\mathcal{N}|+1}$ denote the vectors that collect the nodal current injections in DQ-frame, defined as follows:

$$\widehat{i}^{\mathrm{DQ}} = E\widehat{i}_{\mathcal{E}}^{\mathrm{DQ}} + j\omega_g \mathrm{diag}([0, C_{\mathcal{E}}^{\mathrm{T}}]^{\mathrm{T}})\widehat{v}^{\mathrm{DQ}}. \tag{5.25}$$

Substituting for $\widehat{i}_{\mathcal{E}}^{\mathrm{DQ}}$ from (5.24) in (5.25), we can write $\widehat{i}^{\mathrm{DQ}} = Y\widehat{v}^{\mathrm{DQ}}$, where Y is the network admittance matrix given in (5.10). Partition $\widehat{i}^{\mathrm{DQ}} = [(\widehat{i}_{\mathcal{I}}^{\mathrm{DQ}})^{\mathrm{T}}, \mathbb{0}_{|\mathcal{Z}|}^{\mathrm{T}}, -\widehat{i}_{g}^{\mathrm{DQ}}]^{\mathrm{T}}$ and $\widehat{v}^{\mathrm{DQ}} = [(\widehat{v}_{\mathcal{I}}^{\mathrm{DQ}})^{\mathrm{T}}, \widehat{v}_{|\mathcal{Z}|}^{\mathrm{T}}, v_{g}^{\mathrm{DQ}}]^{\mathrm{T}}$. Kron reduction of Y eliminates the zero-injection buses and yields:

$$\begin{bmatrix} \widehat{i}_{\mathcal{I}}^{\mathrm{DQ}} \\ -\widehat{i}_{g}^{\mathrm{DQ}} \end{bmatrix} = \begin{bmatrix} Y_{\mathcal{I}\mathcal{I}} & Y_{\mathcal{I}g} \\ Y_{\mathcal{I}g}^{\mathrm{T}} & Y_{gg} \end{bmatrix} \begin{bmatrix} \widehat{v}_{\mathcal{I}}^{\mathrm{DQ}} \\ v_{g}^{\mathrm{DQ}} \end{bmatrix}. \tag{5.26}$$

Substituting $\widehat{v}_{\mathcal{I}}^{\mathrm{DQ}}$ and $\widehat{i}_{\mathcal{I}}^{\mathrm{DQ}}$ from (5.23) to (5.26), we have

$$\mathrm{diag}(n^{\mathrm{H}})^{-1} i_{\mathrm{aux}}^{\mathrm{DQ}} = Y_{\mathcal{I}\mathcal{I}}\, \mathrm{diag}(n)\Phi v_{\mathrm{aux}}^{\mathrm{DQ}} + Y_{\mathcal{I}g} v_{g}^{\mathrm{DQ}}, \tag{5.27}$$

$$-\widehat{i}_{g}^{\mathrm{DQ}} = Y_{\mathcal{I}g}^{\mathrm{T}}\, \mathrm{diag}(n)\Phi v_{\mathrm{aux}}^{\mathrm{DQ}} + Y_{gg} v_{g}^{\mathrm{DQ}}. \tag{5.28}$$

Then, we multiply both sides of (5.27) by $\Phi^{\mathrm{T}}\mathrm{diag}(n^{\mathrm{H}})$ and use $\widehat{i}_{\mathrm{o}\mathcal{I}}^{\mathrm{DQ}} = \Phi^{\mathrm{T}} i_{\mathrm{aux}}^{\mathrm{DQ}}$ to obtain:

$$v_{\mathrm{aux}}^{\mathrm{DQ}} = (\Pi^{\mathrm{H}} Y_{\mathcal{I}\mathcal{I}} \Pi)^{-1} (\widehat{i}_{\mathrm{o}}^{\mathrm{DQ}} - \Pi^{\mathrm{H}} Y_{\mathcal{I}g} v_{g}^{\mathrm{DQ}}), \tag{5.29}$$

where $\Pi := \mathrm{diag}(n)\Phi$. The dynamics of the system with the network represented in

phasors and auxiliary buses introduced to aggregate inverters are given by (5.22) with $u_{\rm v} = v_{\rm aux}^{\rm abc}$ obtained by applying Park's transformation to (5.29). From (5.28) and (5.29), we can write the grid current injection as a function of the output currents of the aggregate inverter model:

$$\widehat{i}_g^{\rm DQ} = -Y_{\mathcal{I}g}^{\rm T}\Pi\left(\Pi^{\rm H}Y_{\mathcal{I}\mathcal{I}}\Pi\right)^{-1}\left(\widehat{i}_{\rm o}^{\rm DQ} - \Pi^{\rm H}Y_{\mathcal{I}g}v_g^{\rm DQ}\right) - Y_{gg}v_g^{\rm DQ}, \tag{5.30}$$

following which, the real- and reactive-power injections into the grid bus g can be straightforwardly computed. The order of the reduced-order model dynamics with $|\mathcal{C}|$ clusters is $15|\mathcal{C}|$. Recall that the order of the original-network dynamics was $2(|\mathcal{E}|+|\mathcal{N}|)+15|\mathcal{I}|$. Since in practice we expect to have less clusters than the number of inverters, i.e., $|\mathcal{C}| << |\mathcal{I}|$, the reduced-order model is indeed computationally less burdensome. We demonstrate this, and the accuracy of the reduced-order model through simulations next.

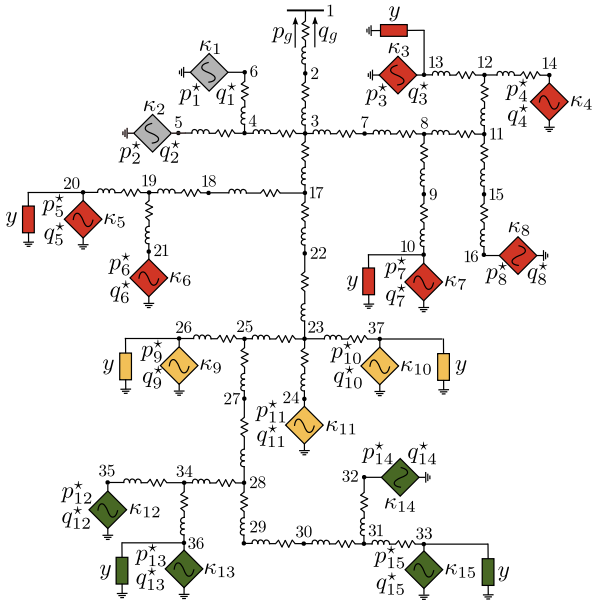

Figure 5.3: IEEE 37-bus feeder system with 15 inverters and 7 loads. Notice that setpoints and ratings of the inverters are all different. Shaded colors represent clusters obtained by applying the electrical-distance clustering algorithm to the network with $C = 4$.

Table 5.1: The z^{eff} value for the inverter buses.

Bus #	5	6	10	13	14	16	20	21
z^{eff}	0.031	0.031	0.047	0.055	0.055	0.055	0.080	0.080
	24	26	32	33	35	36	37	
	0.080	0.088	0.16	0.16	0.14	0.14	0.080	

Table 5.2: Computation time in [s] to simulate the complete time-domain and aggregate models with different number of clusters.

	Time-domain	Aggregation (C-cluster)							
		$C = 1$	2	3	4	5	6	7	8
Case #1	1035.4	1.71	2.56	3.53	3.78	3.93	4.23	4.45	4.82
Case #2	1031.5	1.76	2.45	3.54	3.82	3.95	4.27	4.46	4.81
		$C = 9$	10	11	12	13	14	15	
		4.85	4.87	4.88	4.89	4.91	4.93	4.94	
		4.83	4.86	4.87	4.90	4.93	4.95	4.96	

5.4 Simulation Results

In this section, we validate the model-reduction method with numerical simulation results for a system of 15 inverters connected in a modified IEEE 37-bus network. The network is sketched in Fig. 5.3. The impedance of the lines connecting the buses in $\mathscr{Z}$ is $0.0081 + j0.00027$ [Ω], except the lines: (17,18), (22,23), and (27,28); these have impedances that are 5 times that of the other lines. The impedance of the lines connecting the buses in $\mathscr{Z}$ to $\mathscr{I}$ is $0.0066 + j0.00010$ [Ω]. The shunt capacitors are identical, with capacitance of 1 [μF]. The values of z^{eff} for the inverter buses are listed in Table 5.1. All loads in the system are modeled as resistive loads with identical admittance of 0.05 [Ω^{-1}]. The voltage and frequency of the grid are 288 [V] and $2\pi \times 60$ [rad/s], respectively. The power scaling parameters κ are selected to be uniformly distributed between 1 and 4. Parameters of the unscaled inverter (i.e., $\kappa = 1$) are listed in Table A.1. The simulation is performed on a computer with an Intel Core i7-7700HQ processor @ 2.80GHz CPU and 8GB RAM.

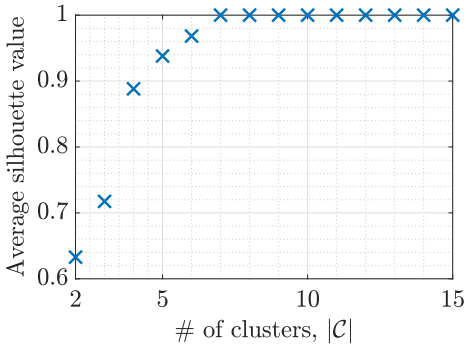

Figure 5.4: The average silhouette value for different number of clusters.

We validate the accuracy of the reduced-order model through the following simulations: case #1: step change in $p^\star$ values from being uniformly distributed between 2-4 [kW] to 4-5 [kW] at $t = 1$ [s], and back to the original values at $t = 1.02$ [s], case #2: step change in $q^\star$ values from 0 [VAR] to being uniformly distributed between 0-1 [kVAR] at $t = 1$ [s], and back to 0 [VAR] at $t = 1.02$ [s]. For both cases, we stop the simulation at $t = 2$ [s]. The running time of the simulations for the complete time-domain model and reduced-order models with 1 to 15 clusters are listed in Table 5.2. Note that the 15-cluster model is the case when all inverter dynamics are retained, and the lines are modeled with phasors. As expected, it takes significantly longer to simulate the full time-domain model, and the reduced-order model with a single cluster has the least simulation time. Figure 5.4 shows the average silhouette value for different number of clusters. We choose 4 as the optimal number of clusters given its average silhouette value is above the reasonable threshold of 0.8. Figures 5.5 and 5.6 show the injected real and reactive power to the grid bus for case #1 and #2 of the following models: A) the time-domain model and the 4-cluster and 15-cluster reduced-order models in Fig. 5.5, and B) the parallel model (i.e., the case when the network is ignored so that all inverters are connected in parallel to the grid bus), the 1-cluster (i.e., without clustering) and 4-cluster reduced-order models in Fig. 5.6. The average errors for the 1-cluster and 4-cluster reduced-order models with respect to the 15-cluster reduced-order model for one AC cycle after each step change in the power setpoints are listed in Table 5.3. The figures show that the reduced-order model with 4 clusters accurately captures the grid injections (indicating that accurate results can be obtained with modeling few clusters)

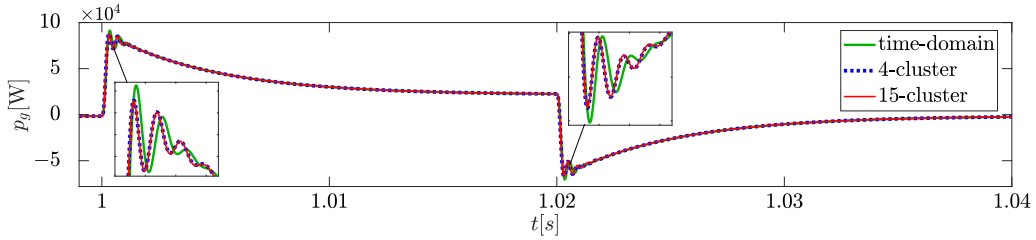

(a) Real power injection to the grid bus

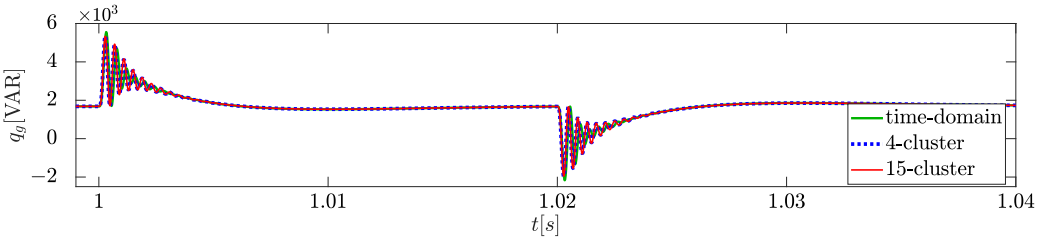

(b) Reactive power injection to the grid bus

Figure 5.5: Simulation results for Case #1: Real-power setpoints $p^\star$ are selected from a uniform distribution between 2-4 [kW] for $t < 1$ [s], 4-5 [kW] for $1 \leq t < 1.02$ [s], and back to the original setpoints for $t \geq 1.02$ [s]. Reactive-power setpoints $q^\star$ are 0 [VAR] for $t \geq 0$ [s].

and it has better transient performance than the 1-cluster reduced-order model while the model where the inverters are simply assumed to be in parallel (by neglecting the distribution network) is associated with errors in steady state and through the transients because the power losses and damping induced by the network are neglected.

Furthermore, we perform simulations with different sets of line impedances for the IEEE 37-bus system. In particular, we consider line impedances with r/x ratios of 0.1, 1, and 5. In these simulations, all inverters have the same power scaling parameters κ as 1, and the same power setpoints with $p^\star$ values having step changes from 3 [kW] to 4 [kW] at $t = 1$ [s] and back to the original values at $t = 1.02$ [s], and $q^\star = 0$ [VAR]. The real power injection to the grid bus for the 1-cluster, 4-cluster, and 15-cluster reduced-order models are shown in Fig. 5.7. The figures show that the 4-cluster model performs well regardless of the r/x ratio of the line impedances, while the performance of the 1-cluster model degrades as the r/x ratio increases (i.e., the network becomes more resistive).

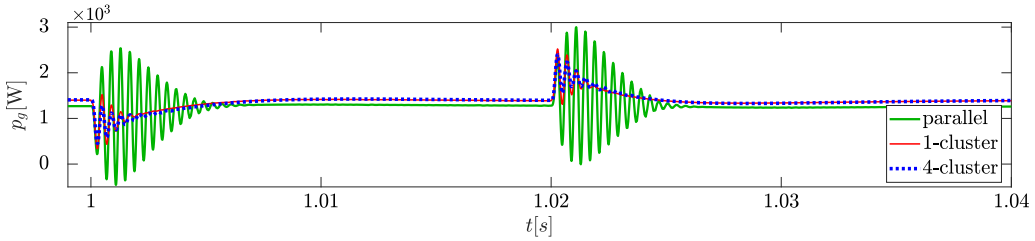

(a) Real power injection to the grid bus

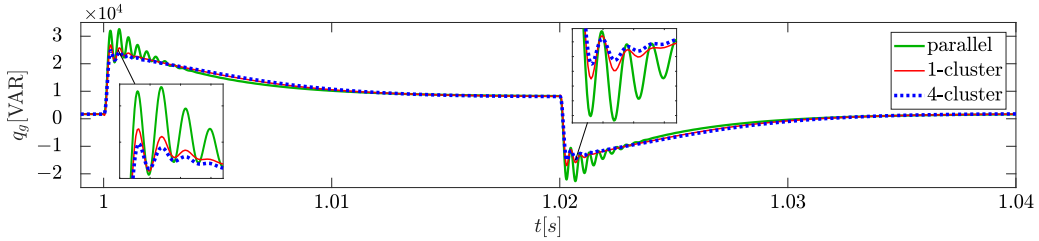

(b) Reactive power injection to the grid bus

Figure 5.6: Simulation results for Case #2: Real-power setpoints $p^\star$ are selected from uniform distribution between 2-4 [kW] for $t \geq 0$s. Reactive-power setpoints $q^\star$ are 0 [VAR] for $t < 1$ [s], uniformly distributed between 0-1 [kVAR] for $1 \leq t < 1.02$ [s], and 0 [VAR] for $t \geq 1.02$ [s].

Table 5.3: Average error of the real and reactive power injection to the grid bus in [%] for one AC cycle after each step change in power setpoints.

		p_g		q_g	
		1st step	2nd step	1st step	2nd step
Case #1	1-cluster	1.58	4.71	0.47	8.4
	4-cluster	0.49	0.47	0.041	0.58
Case #2	1-cluster	0.25	0.24	0.62	9.32
	4-cluster	0.035	0.031	0.064	0.18

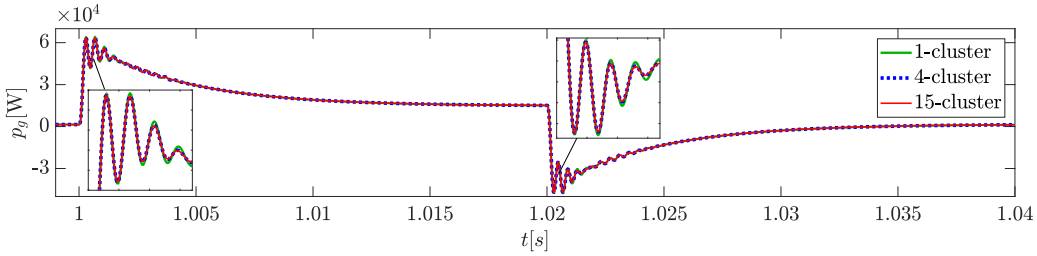

(a) $\frac{r}{x} = 0.1$

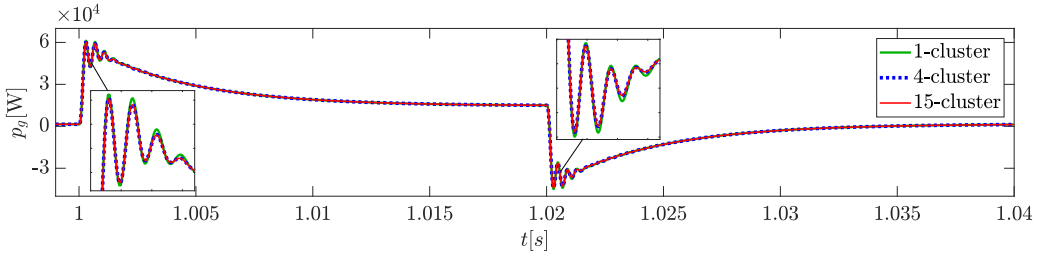

(b) $\frac{r}{x} = 1$

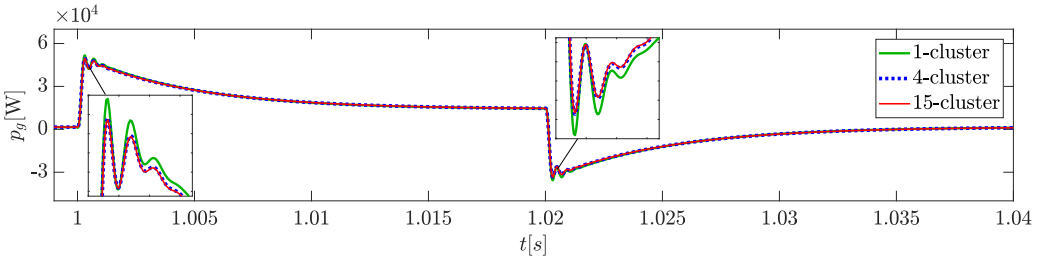

(c) $\frac{r}{x} = 5$

Figure 5.7: Real power injection to the grid bus for various r/x ratio values.

Chapter 6

Conclusion and Future Work

With large numbers of power-electronics inverters being integrated in distribution networks, it is critical to develop computationally affordable models that scale with penetration level and accurately capture the system dynamics. This dissertation developed reduced-order aggregate models for various grid-tied inverter models for parallel configuration and as well as interconnected in a network. In Chapter 3, we laid down the groundwork for this research by deriving a reduced-order structure-preserving model for parallel-connected grid-tied three-phase inverters. In particular, it was shown that N parallel inverters with heterogeneous power ratings can be modeled as a single inverter with an equivalent power rating equal to the sum of the individual inverter ratings. At its foundation, the proposed reduced-order model is built on a set of scaling laws that prescribe how the filter and controller parameters of an individual inverter change with power rating. Ultimately, we showed that N parallel inverters that adhere to such scaling laws can be represented as one equivalent inverter whose output terminal behavior is identical to the original multi-inverter system. In Chapter 4, we extended the reduced-order model for parallel-connected three-phase inverters to acknowledge photovoltaic array, maximum power point tracking algorithm and dc-link capacitor dynamics. Numerical simulations were provided to establish the accuracy of the reduced-order model in capturing the dynamics of inverters during large-signal transients. Direction for future work includes expanding the aggregate models for different types of inverters that are not covered in this dissertation, and developing an accurate method of aggregating inverters with different parameters.

In Chapter 5, we presented a model-reduction method for a collection of inverters connected in an arbitrary electrical network. The foundations of this method were: i) the reduced-order aggregate model for parallel-connected grid-tied inverters, and ii) classical results on aggregation of coherent synchronous generators. This method involves: i) clustering the inverters based on their electrical distance from the grid, ii) transferring the inverters in each group to their respective virtual buses with the aid of ideal transformers and linear approximation of the power-flow equations, and iii) aggregating the inverters in each of the buses to an equivalent inverter using our previous work on the aggregate model for parallel-connected grid-tied three-phase inverters. Numerical simulations established the accuracy and computational benefits of the approach. Future work involves developing a non-heuristic method of determining coherency of the inverters in the network, and accommodating different load models, in particular, constant-power loads, in the aggregation approach.

References

[1] 800,000 Microinverters remotely retrofitted on Oahu in one day. http://spectrum.ieee.org/energywise/green-tech/solar/in-one-day-800000-microinverters-remotely-retrofitted-on-oahu. Accessed: 2020-05-17.

[2] Our plans for the future. https://www.hawaiianelectric.com/clean-energy-hawaii. Accessed: 2020-05-17.

[3] M. Rasheduzzaman, J. A. Mueller, and J. W. Kimball. An accurate small-signal model of inverter- dominated islanded microgrids using *dq* reference frame. *IEEE Journal of Emerging and Selected Topics in Power Electronics*, 2(4):1070–1080, December 2014.

[4] J. A. Mueller, M. Rasheduzzaman, and J. W. Kimball. A model modification process for grid-connected inverters used in islanded microgrids. *IEEE Transactions on Energy Conversion*, 31(1):240–250, March 2016.

[5] M. Prodanovic and T. C. Green. Control and filter design of three-phase inverters for high power quality grid connection. *IEEE Transactions on Power Electronics*, 18(1):373–380, January 2003.

[6] E. Twining and D. G. Holmes. Grid current regulation of a three-phase voltage source inverter with an LCL input filter. *IEEE Transactions on Power Electronics*, 18(3):888–895, May 2003.

[7] N. Pogaku, M. Prodanovic, and T. C. Green. Modeling, analysis and testing of autonomous operation of an inverter-based microgrid. *IEEE Transactions on Power Electronics*, 22(2):613–625, March 2007.

[8] C. A. Plet, M. Graovac, T. C. Green, and R. Iravani. Fault response of grid-connected inverter dominated networks. In *IEEE PES General Meeting*, pages 1–8, July 2010.

[9] Y. Jung, G. Yu, J. Choi, and J. Choi. High-frequency dc link inverter for grid-connected photovoltaic system. In *IEEE 29th Photovoltaic Specialists Conference (PVSC)*, pages 1410–1413, May 2002.

[10] A. Yazdani, A. R. Di Fazio, H. Ghoddami, M. Russo, M. Kazerani, J. Jatskevich, K. Strunz, S. Leva, and J. A. Martinez. Modeling guidelines and a benchmark for power system simulation studies of three-phase single-stage photovoltaic systems. *IEEE Transactions on Power Delivery*, 26(2):1247–1264, April 2011.

[11] T. Kerekes, R. Teodorescu, M. Liserre, C. Klumpner, and M. Sumner. Evaluation of three-phase transformerless photovoltaic inverter topologies. *IEEE Transactions on Power Electronics*, 24(9):2202–2211, September 2009.

[12] H. N. V. Pico and B. B. Johnson. Transient stability assessment of multi-machine multi-converter power systems. *IEEE Transactions on Power Systems*, 34(5):3504–3514, September 2019.

[13] V. Purba, S. V. Dhople, S. Jafarpour, F. Bullo, and B. B. Johnson. Reduced-order structure-preserving model for parallel-connected three-phase grid-tied inverters. In *IEEE 18th Workshop on Control and Modeling for Power Electronics (COMPEL)*, pages 1–7, July 2017.

[14] V. Purba, B. B. Johnson, and S. V. Dhople. Reduced-order aggregate model for parallel-connected grid-tied three-phase photovoltaic inverters. In *IEEE 46th Photovoltaic Specialists Conference (PVSC)*, pages 0724–0729, June 2019.

[15] V. Purba, S. V. Dhople, S. Jafarpour, F. Bullo, and B. B. Johnson. Network-cognizant model reduction of grid-tied three-phase inverters. In *Allerton Conference on Communication, Control, and Computing*, pages 157–164, October 2017.

[16] V. Purba, B. B. Johnson, S. Jafarpour, F. Bullo, and S. V. Dhople. Dynamic aggregation of grid-tied three-phase inverters. *IEEE Transactions on Power Systems*, 35(2):1520–1530, March 2020.

[17] V. Purba, B. B. Johnson, M. Rodriguez, S. Jafarpour, F. Bullo, and S. V. Dhople. Reduced-order aggregate model for parallel-connected single-phase inverters. *IEEE Transactions on Energy Conversion*, 34(2):824–837, June 2019.

[18] J. H. Chow. *Power System Coherency and Model Reduction*. Springer, 2013.

[19] S. D. Pekarek, M. T. Lemanski, and E. A. Walters. On the use of singular perturbations to neglect the dynamic saliency of synchronous machines. *IEEE Transactions on Energy Conversion*, 17(3):385–391, September 2002.

[20] H. You, V. Vittal, and X. Wang. Slow coherency-based islanding. *IEEE Transactions on Power Systems*, 19(1):483–491, February 2004.

[21] M. L. Ourari, L. A. Dessaint, and V.-Q. Do. Dynamic equivalent modeling of large power systems using structure preservation technique. *IEEE Transactions on Power Systems*, 21(3):1284–1295, August 2006.

[22] A. J. Germond and R. Podmore. Dynamic aggregation of generating unit models. *IEEE Transactions on Power Apparatus and Systems*, PAS-97(4):1060–1069, July 1978.

[23] E. Muljadi, S. Pasupulati, A. Ellis, and D. Kosterov. Method of equivalencing for a large wind power plant with multiple turbine representation. In *2008 IEEE Power and Energy Society General Meeting - Conversion and Delivery of Electrical Energy in the 21st Century*, pages 1–9, July 2008.

[24] H. Liu and Z. Chen. Aggregated modelling for wind farms for power system transient stability studies. In *2012 Asia-Pacific Power and Energy Engineering Conference*, pages 1–6, March 2012.

[25] S. Izadkhast, P. Garcia-Gonzalez, P. Frias, L. Ramirez-Elizondo, and P. Bauer. An aggregate model of plug-in electric vehicles including distribution network characteristics for primary frequency control. *IEEE Transactions on Power Systems*, 31(4):2987–2998, July 2016.

[26] J. Zhang and A. Domínguez-García. Evaluation of demand response resource aggregation system capacity under uncertainty. *IEEE Transactions on Smart Grid*, PP(99):1–1, September 2017.

[27] M. Rasheduzzaman, J. A. Mueller, and J. W. Kimball. Reduced-order small-signal model of microgrid systems. *IEEE Transactions on Sustainable Energy*, 6(4):1292–1305, October 2015.

[28] L. Luo and S. V. Dhople. Spatiotemporal model reduction of inverter-based islanded microgrids. *IEEE Transactions on Energy Conversion*, 29(4):823–832, December 2014.

[29] K. Kodra, N. Zhong, and Z. Gajić. Model order reduction of an islanded microgrid using singular perturbations. In *American Control Conference (ACC)*, pages 3650–3655, July 2016.

[30] O. O. Ajala, A. D. Domínguez-García, and P. W. Sauer. A hierarchy of models for inverter-based microgrids. In S. Meyn, T. Samad, S. Glavaski, I. Hiskens, and J. Stoustrup, editors, *Energy Markets and Responsive Grids: Modeling, Control and Optimization*. Springer-Verlag, Berlin, 2017.

[31] A. Dominguez, L. A. Barragan, J. I. Artigas, A. Otin, I. Urriza, and D. Navarro. Reduced-order models of series resonant inverters in induction heating applications. *IEEE Transactions on Power Electronics*, 32(3):2300–2311, March 2017.

[32] N. Femia, G. Spagnuolo, and V. Tucci. State-space models and order reduction for dc-dc switching converters in discontinuous modes. *IEEE Transactions on Power Electronics*, 10(6):640–650, November 1995.

[33] M. and J. Sun. Reduced-order averaged modeling of active-clamp converters. *IEEE Transactions on Power Electronics*, 21(2):487–494, March 2006.

[34] K. Zhang, Z. Shan, and J. Jatskevich. Large- and small-signal average-value modeling of dual-active-bridge dc-dc converter considering power losses. *IEEE Transactions on Power Electronics*, 32(3):1964–1974, March 2017.

[35] G. G. Richards and O. T. Tan. Decomposed, reduced order model for double-cage induction machines. *IEEE Transactions on Energy Conversion*, EC-1(3):87–93, September 1986.

[36] F. D. Rodriguez and O. Wasynczuk. A refined method of deriving reduced order models of induction machines. *IEEE Transactions on Energy Conversion*, EC-2(1):31–37, March 1987.

[37] P. J. Hart, R. H. Lasseter, and T. M. Jahns. Reduced-order harmonic modeling and analysis of droop-controlled distributed generation networks. In *IEEE 7th International Symposium on Power Electronics for Distributed Generation Systems (PEDG)*, pages 1–9, June 2016.

[38] P. J. Hart, R. H. Lasseter, and T. M. Jahns. Enforcing coherency in droop-controlled inverter networks through use of advanced voltage regulation and virtual impedance. In *2017 IEEE Energy Conversion Congress and Exposition (ECCE)*, pages 3367–3374, October 2017.

[39] C. Li, J. Xu, and C. Zhao. A coherency-based equivalence method for mmc inverters using virtual synchronous generator control. *IEEE Transactions on Power Delivery*, 31(3):1369–1378, June 2016.

[40] A. Yazdani and R. Iravani. *Voltage-Sourced Converters in Power Systems*. John Wiley & Sons, Inc., Hoboken, NJ, 2010.

[41] M. K. Kazimierczuk and L. A. Starman. Dynamic performance of PWM DC-DC boost converter with input voltage feedforward control. *IEEE Transactions on Circuits and Systems I: Fundamental Theory and Applications*, 46(12):1473–1481, December 1999.

[42] Siemens SINVERT PVS 500kW power inverter. `https://www.renugen.co.uk/siemens-sinvert-pvs-500kw-power-inverter/`. Accessed: 2020-05-05.

[43] ABB's new 50 kW string inverters power one of the UKs largest solar parks. `http://www.abb.com/ContentPages/Default.aspx?&db=seitp202&c=abbc0eaa1b19a148c1257fd8005bd602`. Accessed: 2020-05-06.

[44] E. C. Aprilia. Modeling of photovoltaic (PV) inverter for power quality studies. Master's thesis, Eindhoven University of Technology, 2012.

[45] S. Eftekharnejad, V. Vittal, G. T. Heydt, B. Keel, and J. Loehr. Impact of increased penetration of photovoltaic generation on power systems. *IEEE Transactions on Power Systems*, 28(2):893–901, May 2013.

[46] Reliability Guideline Power Plant Model Verification for Inverter-Based Resources. `https://www.nerc.com/comm/OC_Reliability_Guidelines_DL/PPMV_for_Inverter-Based_Resources.pdf`. Accessed: 2020-05-11.

[47] A. Ghosh, R. Patel, M. Datta, and L. Meegahapola. Investigation of transient stability of a power network with solar-PV generation: Impact of loading level control strategy. In *2017 IEEE Innovative Smart Grid Technologies - Asia (ISGT-Asia)*, pages 1–6, December 2017.

[48] Y. Lin, B. B. Johnson, V. Gevorgian, V. Purba, and S. V. Dhople. Stability assessment of a system comprising a single machine and inverter with scalable ratings. In *North American Power Symposium (NAPS)*, September 2017.

[49] D. Remon, A. M. Cantarellas, J. M. Mauricio, and P. Rodriguez. Power system stability analysis under increasing penetration of photovoltaic power plants with synchronous power controllers. *IET Renewable Power Generation*, 11(6):733–741, May 2017.

[50] S. S. Guggilam, C. Zhao, E. DallAnese, Y. C. Chen, and S. V. Dhople. Optimizing DER participation in inertial and primary-frequency response. *IEEE Transactions on Power Systems*, 33(5):5194–5205, September 2018.

[51] A. Ghosh. Dynamic modelling of an aggregated solar-PV system for power system transient stability studies. Master's thesis, University of Nottingham, 2018.

[52] D. Remon, A. M. Cantarellas, and P. Rodriguez. Equivalent model of large-scale synchronous photovoltaic power plants. *IEEE Transactions on Industry Applications*, 52(6):5029–5040, November 2016.

[53] H. Meng, X. Ye, M. Yang, X. Song, Z. Su, W. Liu, L. Luo, and H. Zhao. Equivalent modeling and simulation for pv system on dynamic clustering equivalent strategy. In *43rd Annual Conference of the IEEE Industrial Electronics Society (IECON)*, pages 5779–5784, October 2017.

[54] M. G. Villalva, J. R. Gazoli, and E. R. Filho. Comprehensive approach to modeling and simulation of photovoltaic arrays. *IEEE Transactions on Power Electronics*, 24(5):1198–1208, May 2009.

[55] A. Chatterjee, A. Keyhani, and D. Kapoor. Identification of photovoltaic source models. *IEEE Transactions on Energy Conversion*, 26(3):883–889, September 2011.

[56] A. A. A. Radwan and Y. A. I. Mohamed. Power synchronization control for grid-connected current-source inverter-based photovoltaic systems. *IEEE Transactions on Energy Conversion*, 31(3):1023–1036, September 2016.

[57] B. B. Johnson, S. V. Dhople, J. L. Cale, A. O. Hamadeh, and P. T. Krein. Oscillator-based inverter control for islanded three-phase microgrids. *IEEE Journal of Photovoltaics*, 4(1):387–395, January 2014.

[58] M. Spivak. *Calculus 3rd ed.* Publish or Perish, 1994.

[59] Conext CL125 string inverter. `https://solar.schneider-electric.com/product/conext-cl125-string-inverter/`. Accessed: 2020-05-06.

[60] First solar series 6^{TM}. `http://www.firstsolar.com/-/media/First-Solar/Technical-Documents/Series-6-Datasheets/Series-6-Datasheet.ashx`. Accessed: 2020-05-06.

[61] Oahu solar measurement grid (1-year archive): 1-second solar irradiance; oahu, hawaii (data); NREL report no. DA-5500-56506. `http://dx.doi.org/10.5439/1052451`. Accessed: 2020-05-06.

[62] S. V. Dhople, S. S. Guggilam, and Y. C. Chen. Linear approximations to AC power flow in rectangular coordinates. In *Allerton Conference on Communication, Control, and Computing*, pages 211–217, September 2015.

[63] S. Bolognani and F. Dörfler. Fast power system analysis via implicit linearization of the power flow manifold. In *Allerton Conference on Communication, Control, and Computing*, pages 402–409, September 2015.

[64] S. Bolognani and S. Zampieri. On the existence and linear approximation of the power flow solution in power distribution networks. *IEEE Transactions on Power Systems*, 31(1):163–172, January 2016.

[65] Z. Shuai, Y. Peng, X. Liu, Z. Li, J. M. Guerrero, and Z. J. Shen. Dynamic equivalent modeling for multi-microgrid based on structure preservation method. *IEEE Transactions on Smart Grid*, 10(4):3929–3942, July 2019.

[66] L. Ding, Z. Ma, P. Wall, and V. Terzija. Graph spectra based controlled islanding for low inertia power systems. *IEEE Transactions on Power Delivery*, 32(1):302–309, February 2017.

[67] E. Cotilla-Sanchez, P. D. H. Hines, C. Barrows, S. Blumsack, and M. Patel. Multi-attribute partitioning of power networks based on electrical distance. *IEEE Transactions on Power Systems*, 28(4):4979–4987, November 2013.

[68] R. J. Sánchez-García, M. Fennelly, S. Norris, N. Wright, G. Niblo, J. Brodzki, and J. W. Bialek. Hierarchical spectral clustering of power grids. *IEEE Transactions on Power Systems*, 29(5):2229–2237, September 2014.

[69] P. Hines, S. Blumsack, E. C. Sanchez, and C. Barrows. The topological and electrical structure of power grids. In *43rd Hawaii International Conference on System Sciences*, pages 1–10, January 2010.

[70] J. Hu, L. Sankar, and D. J. Mir. Cluster-and-connect: An algorithmic approach to generating synthetic electric power network graphs. In *53rd Annual Allerton Conference on Communication, Control, and Computing*, pages 223–230, September 2015.

[71] A. Ishchenko, J. M. A. Myrzik, and W. L. Kling. Dynamic equivalencing of distribution networks with dispersed generation using Hankel norm approximation. *IET Generation, Transmission Distribution*, 1(5):818–825, September 2007.

[72] F. O. Resende, J. Matevosyan, and J. V. Milanovic. Application of dynamic equivalence techniques to derive aggregated models of active distribution network cells and microgrids. In *2013 IEEE Grenoble Conference*, pages 1–6, June 2013.

[73] J. A. Hartigan and M. A. Wong. Algorithm as 136: A k-means clustering algorithm. *Journal of the Royal Statistical Society. Series C (Applied Statistics)*, 28(1):100–108, 1979.

[74] A. K. Jain and R. C. Dubes. *Algorithms for Clustering Data*. Prentice-Hall, Inc., Upper Saddle River, NJ, USA, 1988.

[75] K. Wagstaff, C. Cardie, S. Rogers, and S. Schrödl. Constrained K-means clustering with background knowledge. In *Proceedings of the 18th International Conference on Machine Learning*, pages 577–584, San Francisco, CA, USA, 2001. Morgan Kaufmann Publishers.

[76] R. Xu and D. Wunsch. Survey of clustering algorithms. *IEEE Transactions on Neural Networks*, 16(3):645–678, May 2005.

[77] G. W. Milligan and M. C. Cooper. An examination of procedures for determining the number of clusters in a data set. *Psychometrika*, 50(2):159–179, June 1985.

[78] R. Tibshirani, G. Walther, and T. Hastie. Estimating the number of clusters in a data set via the gap statistic. *Journal of the Royal Statistical Society: Series B (Statistical Methodology)*, 63(2):411–423, 2001.

[79] C. A. Sugar and G. M. James. Finding the number of clusters in a dataset: An information-theoretic approach. *Journal of the American Statistical Association*, 98(463):750–763, 2003.

[80] P. J. Rousseeuw. Silhouettes: A graphical aid to the interpretation and validation of cluster analysis. *Journal of Computational and Applied Mathematics*, 20:53–65, 1987.

[81] L. Kaufman and P. J. Rousseeuw. *Finding Groups in Data: An Introduction to Cluster Analysis*. John Wiley & Sons, 1990.

[82] A. P. Reynolds, G. Richards, B. de la Iglesia, and V. J. Rayward-Smith. Clustering rules: A comparison of partitioning and hierarchical clustering algorithms. *Journal of Mathematical Modelling and Algorithms*, 5(4):475–504, December 2006.

[83] S. Vijayshankar, V. Purba, P. J. Seiler, and S. V. Dhople. Reduced-order aggregate dynamical model for wind farms. In *American Control Conference (ACC)*, pages 5464–5471, July 2019.

[84] M. M. S. Khan, Y. Lin, B. Johnson, V. Purba, M. Sinha, and S. Dhople. A reduced-order aggregated model for parallel inverter systems with virtual oscillator control. In *IEEE 19th Workshop on Control and Modeling for Power Electronics (COMPEL)*, pages 1–6, June 2018.

[85] P. Kundur, N. J. Balu, and M. G. Lauby. *Power system stability and control*, volume 7. McGraw-hill New York, 1994.

[86] F. Dörfler and F. Bullo. Kron reduction of graphs with applications to electrical networks. *IEEE Transactions on Circuits and Systems I: Regular Papers*, 60(1):150–163, January 2013.

[87] R.-Y. Kim, S.-Y. Choi, and I.-Y. Suh. Instantaneous control of average power for grid tie inverter using single phase d-q rotating frame with all pass filter. In *30th Annual Conference of IEEE Industrial Electronics Society, 2004. IECON 2004*, volume 1, pages 274–279, November 2004.

[88] S. A. Khajehoddin, M. Karimi-Ghartemani, A. Bakhshai, and P. Jain. A power control method with simple structure and fast dynamic response for single-phase grid-connected dg systems. *IEEE Transactions on Power Electronics*, 28(1):221–233, January 2013.

[89] C. Zou, B. Liu, S. Duan, and R. Li. Stationary frame equivalent model of proportional-integral controller in dq synchronous frame. *IEEE Transactions on Power Electronics*, 29(9):4461–4465, September 2014.

[90] M. Sanatkar-Chayjani and M. Monfared. Simple digital current control strategy for single-phase grid-connected converters. *IET Power Electronics*, 8(2):245–254, February 2015.

[91] M. Ebrahimi, S. A. Khajehoddin, and M. Karimi-Ghartemani. Fast and robust single-phase *dq* current controller for smart inverter applications. *IEEE Transactions on Power Electronics*, 31(5):3968–3976, May 2016.

[92] M. Saitou and T. Shimizu. Generalized theory of instantaneous active and reactive powers in single-phase circuits based on hilbert transform. In *33rd Annual IEEE Power Electronics Specialists Conference. Proceedings*, volume 3, pages 1419–1424, June 2002.

[93] M. Ebrahimi, H. R. Karshenas, and M. Hassanzahraee. Comparison of orthogonal quantity generation methods used in single-phase grid-connected inverters. In *IECON 2012 - 38th Annual Conference on IEEE Industrial Electronics Society*, pages 5932–5937, October 2012.

[94] R. Zhang, M. Cardinal, P. Szczesny, and M. Dame. A grid simulator with control of single-phase power converters in D-Q rotating frame. In *33rd Annual IEEE Power Electronics Specialists Conference. Proceedings*, volume 3, pages 1431–1436 vol.3, June 2002.

[95] S. Dasgupta, S. K. Sahoo, and S. K. Panda. Single-phase inverter control techniques for interfacing renewable energy sources with microgridpart i: Parallel-connected inverter topology with active and reactive power flow control along with grid current shaping. *IEEE Transactions on Power Electronics*, 26(3):717–731, March 2011.

Appendix A

Aggregation of Parallel-connected Single-phase Grid-tied Inverters

In this appendix, we examine the ac-timescale dynamics of a single-phase voltage source inverter (VSI) with an output LCL filter. To ensure broad applicability across VSI topologies, we only assume that the switch-averaged voltage across the ac terminals is controllable via pulse width modulation and we neglect switch-level dynamics. The control architecture is composed of an inner current-control loop, an outer power-control loop, and a phase locked loop (PLL) for grid synchronization. This filter and control architecture are prototypical and it ensures broad applicability of the results [87–91]. The state-space model that captures the dynamics of the inverter is composed of 16 states. This appendix significantly builds upon and extends the results for parallel-connected three-phase inverters in Chapter 3. Here, we examine the (admittedly different) filter and controller dynamics for single-phase inverters which will conceivably be more dominant in number in future distribution networks. Furthermore, we provide experimental validation of our approach with a multi-inverter setup composed of three 750 [VA] grid-tied single-phase inverters.

This appendix is organized as follows: In Section A.1, we establish mathematical notation and describe the grid-tied single-phase inverter model. The reduced-order model for a collection of these inverters connected in parallel is derived in Section A.2. We validate the model-reduction method by comparing numerical simulation results

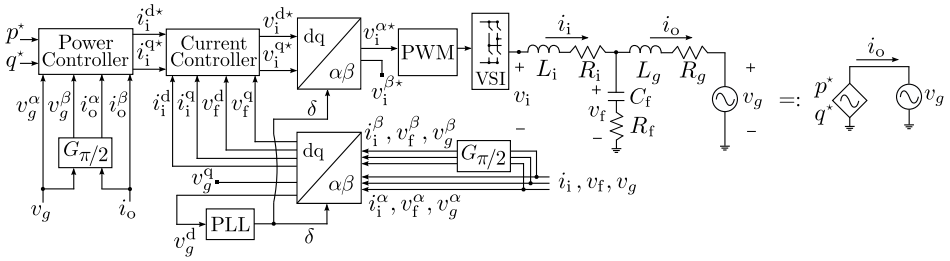

Figure A.1: Block diagram of the single-phase inverter and adopted shorthand.

with results from the experimental prototype in Section A.3.

A.1 Inverter Model

In this section, we describe the single-phase inverter model and develop a standard state-space model representation.

A.1.1 Dynamical Model of Single-phase Inverter

A block diagram of the grid-connected single-phase inverter is illustrated in Fig. A.1. This model represents a prototypical implementation in a single-phase grid-connected setting and captures all relevant ac-side system dynamics. In this appendix, the dynamics of the dc-link and any other converter stages that precede the dc-link are neglected since the focus is at the ac-side of the common coupling. Extensions to include the dc-side dynamics can be done in the same manner as described in Chapter 4 for photovoltaic system. We briefly overview the reference-frame transformations and the dynamics of the filter and controllers next.

A.1.1.1 Reference-frame Transformations

The controllers illustrated in Fig. A.1 are implemented in the dq reference-frame. To enable this, the Hilbert transform [92, 93] (denoted by $G_{\pi/2}$) is first utilized to generate orthogonal signals with quarter-cycle phase lag for each sinusoidal measurement, i.e., it yields signals in the $\alpha\beta$ (stationary) reference-frame [40]. Each signal and its corresponding phase-shifted counterpart is subsequently processed by an $\alpha\beta$ to dq transformation. The dq signals are then used in the PLL and current controller. Note that although the

above formulation utilizes the Hilbert transform as a means of generating quarter-cycle phase-shifted waveforms, these signals can also be realized with a quarter-cycle delay buffer or an all-pass filter with appropriate phase response [93–95]. The remainder of this appendix focuses exclusively on the Hilbert transform without loss of generality.

The transfer function of the Hilbert transform is given by

$$G_{\pi/2}(s) = \frac{\omega_{\text{PLL}} - s}{\omega_{\text{PLL}} + s}, \tag{A.1}$$

where ω_{PLL} is the frequency returned by the PLL. As shown in Fig. A.1, we will consider the measured signal to be the α-component, and the corresponding output of the Hilbert transform as the β component. Next, signals in the $\alpha\beta$ reference frame (x^α, x^β) are transformed to the dq reference-frame $(x^{\text{d}}, x^{\text{q}})$ with the following rotation matrix: [40]

$$\begin{bmatrix} x^{\text{d}} \\ x^{\text{q}} \end{bmatrix} = \begin{bmatrix} \cos\delta & \sin\delta \\ -\sin\delta & \cos\delta \end{bmatrix} \begin{bmatrix} x^\alpha \\ x^\beta \end{bmatrix}, \tag{A.2}$$

where δ is the instantaneous angle generated by the PLL.

A.1.1.2 Controller and Filter Dynamics

The internal controllers in the PLL are identical to those in the three-phase inverter model (see Section 3.1.3.2), with an additional state for v_g^β. The dynamics of v_g^β are obtained by applying (A.1) to v_g:

$$\dot{v}_g^\beta = \omega_{\text{PLL}}(v_g - v_g^\beta) - \dot{v}_g. \tag{A.3}$$

Furthermore, we apply (A.2) to v_g and v_g^β to obtain v_g^{d} which feeds into the v_{PLL} dynamics. Note that we assume the first derivative of v_g, i.e., $\dot{v}_g$, to be well defined.

The LCL filter is composed of inverter-side inductance L_{i}, grid-side inductance, L_g, and filter capacitance, C_{f}. The dynamics introduced by the LCL filter in the $\alpha\beta$ frame are given by

$$\dot{i}_{\text{i}}^\alpha = \frac{1}{L_{\text{i}}}(-R_{\text{i}} i_{\text{i}}^\alpha + v_{\text{i}}^\alpha - v_{\text{f}}^\alpha), \tag{A.4a}$$

$$\dot{i}_{\text{i}}^\beta = \omega_{\text{PLL}}(i_{\text{i}}^\alpha - i_{\text{i}}^\beta) - \dot{i}_{\text{i}}^\alpha, \tag{A.4b}$$

$$\dot{i}_{\mathrm{o}}^{\alpha} = \frac{1}{L_g}(-R_g i_{\mathrm{o}}^{\alpha} + v_{\mathrm{f}}^{\alpha} - v_g), \tag{A.4c}$$

$$\dot{i}_{\mathrm{o}}^{\beta} = \omega_{\mathrm{PLL}}(i_{\mathrm{o}}^{\alpha} - i_{\mathrm{o}}^{\beta}) - \dot{i}_{\mathrm{o}}^{\alpha}, \tag{A.4d}$$

$$\dot{v}_{\mathrm{f}}^{\alpha} = R_{\mathrm{f}}\left(\dot{i}_{\mathrm{i}}^{\alpha} - \dot{i}_{\mathrm{o}}^{\alpha}\right) + \frac{1}{C_{\mathrm{f}}}(i_{\mathrm{i}}^{\alpha} - i_{\mathrm{o}}^{\alpha}), \tag{A.4e}$$

$$\dot{v}_{\mathrm{f}}^{\beta} = \omega_{\mathrm{PLL}}(v_{\mathrm{f}}^{\alpha} - v_{\mathrm{f}}^{\beta}) - \dot{v}_{\mathrm{f}}^{\alpha}, \tag{A.4f}$$

where the α-component dynamics are derived from fundamental circuit laws, and the β-component expressions result from the application of (A.1) to the corresponding α-component dynamics.

The power controller is identical to that in the three-phase inverter model (see Section 3.1.3.4). Note that the instantaneous real- and reactive-power outputs can be calculated directly in the $\alpha\beta$ frame as follows:

$$p = \frac{1}{2}(v_g i_{\mathrm{o}}^{\alpha} + v_g^{\beta} i_{\mathrm{o}}^{\beta}), \tag{A.5a}$$

$$q = \frac{1}{2}(v_g^{\beta} i_{\mathrm{o}}^{\alpha} - v_g i_{\mathrm{o}}^{\beta}), \tag{A.5b}$$

The current controller is also identical to that in the three-phase inverter model (see Section 3.1.3.5), albeit we use different feedforward terms in the outputs:

$$v_{\mathrm{i}}^{\mathrm{d}\star} = v_{\mathrm{f}}^{\mathrm{d}} + k_{\mathrm{CC}}^{p}\left(i_{\mathrm{i}}^{\mathrm{d}\star} - i_{\mathrm{i}}^{\mathrm{d}}\right) + k_{\mathrm{CC}}^{i}\int\left(i_{\mathrm{i}}^{\mathrm{d}\star} - i_{\mathrm{i}}^{\mathrm{d}}\right), \tag{A.6a}$$

$$v_{\mathrm{i}}^{\mathrm{q}\star} = v_{\mathrm{f}}^{\mathrm{q}} + k_{\mathrm{CC}}^{p}\left(i_{\mathrm{i}}^{\mathrm{q}\star} - i_{\mathrm{i}}^{\mathrm{q}}\right) + k_{\mathrm{CC}}^{i}\int\left(i_{\mathrm{i}}^{\mathrm{q}\star} - i_{\mathrm{i}}^{\mathrm{q}}\right). \tag{A.6b}$$

Suppose the VSI is ideal (see Fig. A.1), then the terminal inverter voltage is given by:

$$v_{\mathrm{i}} \approx v_{\mathrm{i}}^{\alpha\star} = v_{\mathrm{i}}^{\mathrm{d}\star}\cos\delta - v_{\mathrm{i}}^{\mathrm{q}\star}\sin\delta, \tag{A.7}$$

where δ is the instantaneous PLL angle.

A.1.2 State-space Representation of Inverter Dynamics

The dynamics of the LCL filter, PLL, power controller, and current controller for an individual inverter are now expressed in state-space form to facilitate analysis:

$$\dot{x} = Ax + B_1 u_1 + B_2 u_2 + g(x, u_1, u_2), \tag{A.8}$$

where the state vector, x, and inputs u_1, u_2 are given by

$$\begin{aligned} x = [&i_{\mathrm{i}}^{\alpha}, i_{\mathrm{i}}^{\beta}, i_{\mathrm{o}}^{\alpha}, i_{\mathrm{o}}^{\beta}, v_{\mathrm{f}}^{\alpha}, v_{\mathrm{f}}^{\beta}, \gamma^{\mathrm{d}}, \gamma^{\mathrm{q}}, p_{\mathrm{avg}}, q_{\mathrm{avg}}, \phi^{\mathrm{p}}, \phi^{\mathrm{q}}, \\ &v_g^{\beta}, v_{\mathrm{PLL}}, \phi_{\mathrm{PPL}}, \delta]^{\mathrm{T}}, \end{aligned} \tag{A.9}$$

$$u_1 = [p^{\star}, q^{\star}]^{\mathrm{T}}, \quad u_2 = [v_g, \dot{v}_g]^{\mathrm{T}}. \tag{A.10}$$

In order to show the entries of matrices $A \in \mathbb{R}^{16\times16}$, $B_1 \in \mathbb{R}^{16\times2}$, and $B_2 \in \mathbb{R}^{16\times2}$, let us partition the state vector as $x = [x_{LCL}^{\mathrm{T}}, x_{\mathrm{CC}}^{\mathrm{T}}, x_{\mathrm{PC}}^{\mathrm{T}}, x_{\mathrm{PLL}}^{\mathrm{T}}]^{\mathrm{T}}$, where $x_{LCL} = [i_{\mathrm{i}}^{\alpha}, i_{\mathrm{i}}^{\beta}, i_{\mathrm{o}}^{\alpha}, i_{\mathrm{o}}^{\beta}, v_{\mathrm{f}}^{\alpha}, v_{\mathrm{f}}^{\beta}]^{\mathrm{T}}$, $x_{\mathrm{CC}} = [\gamma^{\mathrm{d}}, \gamma^{\mathrm{q}}]^{\mathrm{T}}$, $x_{\mathrm{PC}} = [p_{\mathrm{avg}}, q_{\mathrm{avg}}, \phi^{\mathrm{p}}, \phi^{\mathrm{q}}]^{\mathrm{T}}$, and $x_{\mathrm{PLL}} = [v_g^{\beta}, v_{\mathrm{PLL}}, \phi_{\mathrm{PLL}}, \delta]^{\mathrm{T}}$. Then, we can write (A.8) as

$$\begin{aligned} \begin{bmatrix} \dot{x}_{LCL} \\ \dot{x}_{\mathrm{CC}} \\ \dot{x}_{\mathrm{PC}} \\ \dot{x}_{\mathrm{PLL}} \end{bmatrix} &= \begin{bmatrix} A_{LCL} & \mathbb{0}_{6\times2} & \mathbb{0}_{6\times4} & \mathbb{0}_{6\times4} \\ \mathbb{0}_{2\times6} & \mathbb{0}_{2\times2} & A_{\mathrm{CC}} & \mathbb{0}_{2\times4} \\ \mathbb{0}_{4\times6} & \mathbb{0}_{4\times2} & A_{\mathrm{PC}} & \mathbb{0}_{4\times4} \\ \mathbb{0}_{4\times6} & \mathbb{0}_{4\times2} & \mathbb{0}_{4\times4} & A_{\mathrm{PLL}} \end{bmatrix} \begin{bmatrix} x_{LCL} \\ x_{\mathrm{CC}} \\ x_{\mathrm{PC}} \\ x_{\mathrm{PLL}} \end{bmatrix} \\ &\quad + \begin{bmatrix} \mathbb{0}_{6\times2} \\ B_{\mathrm{CC}} \\ B_{\mathrm{PC}} \\ \mathbb{0}_{4\times2} \end{bmatrix} u_1 + \begin{bmatrix} B_{LCL} \\ \mathbb{0}_{2\times2} \\ \mathbb{0}_{4\times2} \\ B_{\mathrm{PLL}} \end{bmatrix} u_2 + g(x, u_1, u_2), \end{aligned} \tag{A.11}$$

where entries of the nonzero sub-matrices A_{LCL}, $A_{\rm CC}$, $A_{\rm PC}$, $A_{\rm PLL}$, $B_{\rm CC}$, $B_{\rm PC}$, B_{LCL}, $B_{\rm PLL}$, and the function $g(x,u_1,u_2):\mathbb{R}^{16}\times\mathbb{R}^2\times\mathbb{R}^2\to\mathbb{R}^{16}$ are spelled out below:

$$A_{LCL}=\begin{bmatrix} -\frac{R_{\rm i}}{L_{\rm i}} & 0 & 0 & 0 & 0 & 0\\ \omega_{\rm nom}+\frac{R_{\rm i}}{L_{\rm i}} & -\omega_{\rm nom} & 0 & 0 & 0 & 0\\ 0 & 0 & -\frac{R_g}{L_g} & 0 & \frac{1}{L_g} & 0\\ 0 & 0 & \omega_{\rm nom}+\frac{R_g}{L_g} & -\omega_{\rm nom} & -\frac{1}{L_g} & 0\\ -R_{\rm f}\frac{R_{\rm i}}{L_{\rm i}}+\frac{1}{C_{\rm f}} & 0 & R_{\rm f}\frac{R_g}{L_g}-\frac{1}{C_{\rm f}} & 0 & -\frac{R_{\rm f}}{L_g} & 0\\ R_{\rm f}\frac{R_{\rm i}}{L_{\rm i}}-\frac{1}{C_{\rm f}} & 0 & -R_{\rm f}\frac{R_g}{L_g}+\frac{1}{C_{\rm f}} & 0 & -\omega_{\rm nom}+\frac{R_{\rm f}}{L_g} & -\omega_{\rm nom}\end{bmatrix},$$

$$A_{\rm CC}=\begin{bmatrix} 0 & -k^p_{\rm PC}\\ -k^p_{\rm PC} & 0\\ 0 & k^i_{\rm PC}\\ k^i_{\rm PC} & 0\end{bmatrix}^{\rm T},\quad A_{\rm PC}=\begin{bmatrix} -\omega_{\rm c,PC} & 0 & 0 & 0\\ 0 & -\omega_{\rm c,PC} & 0 & 0\\ -1 & 0 & 0 & 0\\ 0 & -1 & 0 & 0\end{bmatrix},$$

$$A_{\rm PLL}=\begin{bmatrix} -\omega_{\rm nom} & 0 & 0 & 0\\ 0 & -\omega_{\rm c,PLL} & 0 & 0\\ 0 & -1 & 0 & 0\\ 0 & -k^p_{\rm PLL} & k^i_{\rm PLL} & 0\end{bmatrix},\quad B_{\rm CC}=\begin{bmatrix} 0 & k^p_{\rm PC}\\ k^p_{\rm PC} & 0\end{bmatrix},$$

$$B_{LCL}=\begin{bmatrix} 0 & 0 & 0 & 0 & 0 & 0\\ 0 & 0 & -\frac{1}{L_g} & \frac{1}{L_g} & \frac{R_{\rm f}}{L_g} & -\frac{R_{\rm f}}{L_g}\end{bmatrix}^{\rm T},\quad B_{\rm PC}=\begin{bmatrix} 0 & 0\\ 0 & 0\\ 1 & 0\\ 0 & 1\end{bmatrix},\quad B_{\rm PLL}=\begin{bmatrix} 0 & -1\\ 0 & 0\\ 0 & 0\\ 0 & 0\end{bmatrix},$$

the entries of $g(x,u_1,u_2)$, with g_ℓ denotes the ℓ-th entry of $g(x,u_1,u_2)$, are

$$\begin{aligned} g_1 &= \frac{1}{L_{\rm i}}\left(k^p_{\rm CC}(i^{\rm d\star}_{\rm i}-i^\alpha_{\rm i}\cos\delta-i^\beta_{\rm i}\sin\delta)+k^i_{\rm CC}\gamma^{\rm d}\right)\cos\delta\\ &\quad -\frac{1}{L_{\rm i}}\left(k^p_{\rm CC}(i^{\rm q\star}_{\rm i}+i^\alpha_{\rm i}\sin\delta-i^\beta_{\rm i}\cos\delta)+k^i_{\rm CC}\gamma^{\rm q}\right)\sin\delta,\\ g_2 &= \eta(i^\alpha_{\rm i}-i^\beta_{\rm i})-g_1,\quad g_3=0,\quad g_4=0,\\ g_5 &= R_{\rm f}g_1,\quad g_6=\eta(v^\alpha_{\rm f}-v^\beta_{\rm f})-g_5,\\ g_7 &= -i^\alpha_{\rm i}\cos\delta-i^\beta_{\rm i}\sin\delta,\quad g_8=i^\alpha_{\rm i}\sin\delta-i^\beta_{\rm i}\cos\delta,\\ g_9 &= \frac{\omega_{\rm c,PC}}{2}(v_g i^\alpha_{\rm o}+v^\beta_g i^\beta_{\rm o}),\quad g_{10}=\frac{\omega_{\rm c,PC}}{2}(v^\beta_g i^\alpha_{\rm o}-v_g i^\beta_{\rm o}),\end{aligned}$$

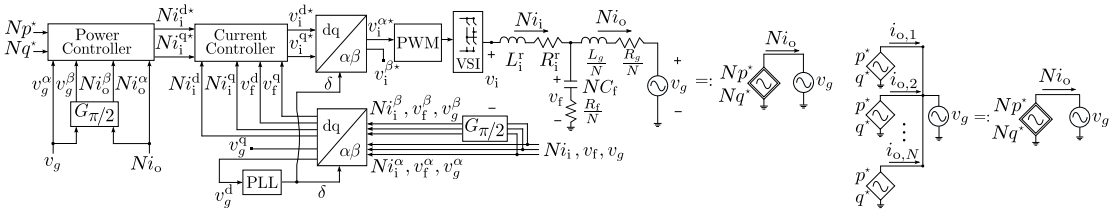

Figure A.2: (a) Reduced-order aggregate single-phase inverter model and adopted shorthand representation. The inverter-side inductance and resistance are related to those in the individual model as $\frac{R_{\mathrm{i}}^{\mathrm{r}}}{L_{\mathrm{i}}^{\mathrm{r}}} = \frac{R_{\mathrm{i}}}{L_{\mathrm{i}}}$. (b) Dynamics of the parallel connection of N single-phase inverters can be captured by the aggregate inverter model in Fig. A.2a.

$$g_{11} = 0, \quad g_{12} = 0, \quad g_{13} = \eta(v_g - v_g^{\beta}),$$
$$g_{14} = \omega_{\mathrm{c,PLL}}(v_g \cos\delta + v_g^{\beta} \sin\delta), \quad g_{15} = 0, \quad g_{16} = \omega_{\mathrm{nom}}.$$

where $\eta := -k_{\mathrm{PLL}}^{p} v_{\mathrm{PLL}} + k_{\mathrm{PLL}}^{i} \phi_{\mathrm{PLL}}$, $i_{\mathrm{i}}^{\mathrm{d}\star} = k_{\mathrm{PC}}^{p}\,(q^{\star} - q_{\mathrm{avg}}) + k_{\mathrm{PC}}^{i} \phi^{\mathrm{q}}$, and $i_{\mathrm{i}}^{\mathrm{q}\star} = k_{\mathrm{PC}}^{p}\,(p^{\star} - p_{\mathrm{avg}}) + k_{\mathrm{PC}}^{i} \phi^{\mathrm{p}}$.

A.2 Aggregation of Parallel-connected Inverters

In this section, we first introduce parametric scalings required to realize the aggregate model for the parallel-connected inverters. Next, we prove that the aggregate model indeed captures all the scalings in pertinent states (currents, voltages, internal-control states) for the uniform setting as well as in cases with heterogeneous power setpoints and ratings.

A.2.1 Parametric Scalings and Structure of Aggregate Model

We consider N identical single-phase inverters (with model described in Section A.1) with the same setpoints, $p^{\star}$ and $q^{\star}$, connected in parallel to a grid bus. We are interested in an aggregated reduced-order model with the same structure and dimension as the model in (A.8):

$$\dot{x}^{\mathrm{r}} = A^{\mathrm{r}} x^{\mathrm{r}} + B_1^{\mathrm{r}} u_1^{\mathrm{r}} + B_2^{\mathrm{r}} u_2^{\mathrm{r}} + g^{\mathrm{r}}(x^{\mathrm{r}}, u_1^{\mathrm{r}}, u_2^{\mathrm{r}}). \tag{A.12}$$

In particular: we desire matrices $A^{\mathrm{r}} \in \mathbb{R}^{16\times 16}$, $B_1^{\mathrm{r}} \in \mathbb{R}^{16\times 2}$, $B_2^{\mathrm{r}} \in \mathbb{R}^{16\times 2}$, and function $g^{\mathrm{r}} : \mathbb{R}^{16} \times \mathbb{R}^2 \times \mathbb{R}^2 \to \mathbb{R}^{16}$ have the same structure and dimension as A, B_1, B_2, and g in (A.8) (implying that the control architecture and output-filter arrangement of the aggregated model are the same as that in an individual inverter); entries of state vector x^{r} and inputs u_1^{r}, u_2^{r} to have the same connotation as states in x and inputs u_1, u_2. In our main result, we demonstrate that *if and only if* the following relationships hold between parameters of the reduced-order and original models:

$$C_{\mathrm{f}}^{\mathrm{r}} = NC_{\mathrm{f}},\ R_{\mathrm{f}}^{\mathrm{r}} = \frac{R_{\mathrm{f}}}{N},\ L_g^{\mathrm{r}} = \frac{L_g}{N},\ R_g^{\mathrm{r}} = \frac{R_g}{N}, \tag{A.13a}$$

$$\frac{R_{\mathrm{i}}^{\mathrm{r}}}{L_{\mathrm{i}}^{\mathrm{r}}} = \frac{R_{\mathrm{i}}}{L_{\mathrm{i}}},\ \frac{k_{\mathrm{CC}}^{p,\mathrm{r}}}{L_{\mathrm{i}}^{\mathrm{r}}} = \frac{k_{\mathrm{CC}}^{p}}{L_{\mathrm{i}}},\ \frac{k_{\mathrm{CC}}^{i,\mathrm{r}}}{L_{\mathrm{i}}^{\mathrm{r}}} = \frac{k_{\mathrm{CC}}^{i}}{L_{\mathrm{i}}}, \tag{A.13b}$$

and the reference power settings of the lumped-parameter aggregate inverter model in Fig. A.2a are N times those of the inverter model in Fig. A.1, the current- and power-related states $i_{\mathrm{i}}^{\alpha,\mathrm{r}}, i_{\mathrm{i}}^{\beta,\mathrm{r}}, i_{\mathrm{f}}^{\alpha,\mathrm{r}}, i_{\mathrm{f}}^{\beta,\mathrm{r}}, \gamma^{\mathrm{d,r}}, \gamma^{\mathrm{q,r}}, p_{\mathrm{avg}}^{\mathrm{r}}, q_{\mathrm{avg}}^{\mathrm{r}}, \phi^{\mathrm{p,r}}, \phi^{\mathrm{q,r}}$ in the reduced-order model are N times the corresponding ones in an individual inverter. Furthermore, the voltage- and PLL-related states in the reduced-order model $v_{\mathrm{f}}^{\alpha,\mathrm{r}}, v_{\mathrm{f}}^{\beta,\mathrm{r}}, v_g^{\beta,\mathrm{r}}, v_{\mathrm{PLL}}^{\mathrm{r}}, \phi_{\mathrm{PPL}}^{\mathrm{r}}, \delta^{\mathrm{r}}$ are the same as those in any inverter in the parallel combination. This is consistent with the electrical behavior of a parallel connection of current (or power) sources.

In establishing the above result, we will have established that the reduced-order aggregate model in Fig. A.2a captures the dynamics of the parallel collection. Put differently, we will mathematically establish the equivalence illustrated in Fig. A.2b.

A.2.2 Validating the Aggregate Model

We now state and prove the main result of this appendix.

Theorem A.1 (Aggregation of parallel-connected identical single-phase inverters)**.** *Consider the dynamical model for the single-phase inverter specified in* (A.8)*. Permute* x *in* (A.9) *as*

$$\begin{aligned}\widehat{x} = [&i_{\mathrm{i}}^{\alpha}, i_{\mathrm{i}}^{\beta}, i_{\mathrm{o}}^{\alpha}, i_{\mathrm{o}}^{\beta}, \gamma^{\mathrm{d}}, \gamma^{\mathrm{q}}, p_{\mathrm{avg}}, q_{\mathrm{avg}}, \phi^{\mathrm{p}}, \phi^{\mathrm{q}}, v_{\mathrm{f}}^{\alpha}, v_{\mathrm{f}}^{\beta},\\ &v_{\mathrm{g}}^{\beta}, v_{\mathrm{PLL}}, \phi_{\mathrm{PPL}}, \delta]^{\mathrm{T}},\end{aligned} \tag{A.14}$$

and also permute x^{r} *(corresponding to the reduced-order model* (A.12)*) the same way, denoting the permuted vector by* $\widehat{x}^{\mathrm{r}}$*. Denote* $\widehat{x}(t)$ *to be the solution to the permuted version of* (A.8) *with initial condition* $\widehat{x}(t_0)$ *and inputs* u_1, u_2*; and* $\widehat{x}^{\mathrm{r}}(t)$ *to be the solution to the permuted version of* (A.12) *with initial condition* $\widehat{x}^{\mathrm{r}}(t_0)$ *and inputs* $u_1^{\mathrm{r}}, u_2^{\mathrm{r}}$*. Suppose initial conditions are such that* $\widehat{x}^{\mathrm{r}}(t_0) = \mathrm{diag}(\Psi)\widehat{x}(t_0)$*, where the* scaling vector*,* $\Psi := [N\mathbb{1}_{10}^{\mathrm{T}}, \mathbb{1}_6^{\mathrm{T}}]^{\mathrm{T}}$*, and the inputs are:* $u_1^{\mathrm{r}} = Nu_1, u_2^{\mathrm{r}} = u_2$ *(see* (A.10)*). The states of the reduced-order model and the individual inverter are related as:*

$$\widehat{x}^{\mathrm{r}}(t) = \mathrm{diag}(\Psi)\widehat{x}(t), \quad \forall t \geq t_0, \tag{A.15}$$

if and only if their parameters are related as (A.13a)–(A.13b)*.*

In particular, given the definition of the scaling vector, Ψ, (A.15) establishes the following relationships between states of the reduced-order model and those in the individual inverter model $\forall t \geq t_0$:

$$\begin{aligned}
&[i_{\mathrm{i}}^{\alpha,\mathrm{r}}, i_{\mathrm{i}}^{\beta,\mathrm{r}}, i_{\mathrm{o}}^{\alpha,\mathrm{r}}, i_{\mathrm{o}}^{\beta,\mathrm{r}}, \gamma^{\mathrm{d,r}}, \gamma^{\mathrm{q,r}}, p_{\mathrm{avg}}^{\mathrm{r}}, q_{\mathrm{avg}}^{\mathrm{r}}, \phi^{\mathrm{p,r}}, \phi^{\mathrm{q,r}}]^{\mathrm{T}} \\
&\qquad = N[i_{\mathrm{i}}^{\alpha}, i_{\mathrm{i}}^{\beta}, i_{\mathrm{o}}^{\alpha}, i_{\mathrm{o}}^{\beta}, \gamma^{\mathrm{d}}, \gamma^{\mathrm{q}}, p_{\mathrm{avg}}, q_{\mathrm{avg}}, \phi^{\mathrm{p}}, \phi^{\mathrm{q}}]^{\mathrm{T}}, &\text{(A.16a)} \\
&[v_{\mathrm{f}}^{\alpha,\mathrm{r}}, v_{\mathrm{f}}^{\beta,\mathrm{r}}, v_{g}^{\beta,\mathrm{r}}, v_{\mathrm{PLL}}^{\mathrm{r}}, \phi_{\mathrm{PPL}}^{\mathrm{r}}, \delta^{\mathrm{r}}]^{\mathrm{T}} \\
&\qquad = [v_{\mathrm{f}}^{\alpha}, v_{\mathrm{f}}^{\beta}, v_{g}^{\beta}, v_{\mathrm{PLL}}, \phi_{\mathrm{PPL}}, \delta]^{\mathrm{T}}. &\text{(A.16b)}
\end{aligned}$$

Proof. Let us define $z := \widehat{x}^{\mathrm{r}} - \mathrm{diag}(\Psi)\widehat{x}$. The dynamics of z are given by

$$\begin{aligned}
\dot{z} = \dot{\widehat{x}}^{\mathrm{r}} - \mathrm{diag}(\Psi)\dot{\widehat{x}} &= \widehat{A}^{\mathrm{r}}\widehat{x}^{\mathrm{r}} + \widehat{B}_1^{\mathrm{r}}u_1^{\mathrm{r}} + \widehat{B}_2^{\mathrm{r}}u_2^{\mathrm{r}} + \widehat{g}(\widehat{x}^{\mathrm{r}}, u_1^{\mathrm{r}}, u_2^{\mathrm{r}}) \\
&\quad - \mathrm{diag}(\Psi)\widehat{A}\widehat{x} - \mathrm{diag}(\Psi)\widehat{B}_1u_1 - \mathrm{diag}(\Psi)\widehat{B}_2u_2 \\
&\quad - \mathrm{diag}(\Psi)\widehat{g}(\widehat{x}, u_1, u_2),
\end{aligned} \tag{A.17}$$

where matrices $\widehat{A}$, $\widehat{B}_1$, $\widehat{B}_2$, $\widehat{A}^{\mathrm{r}}$, $\widehat{B}_1^{\mathrm{r}}$, $\widehat{B}_2^{\mathrm{r}}$ and functions $\widehat{g}(\widehat{x}, u_1, u_2)$, $\widehat{g}(\widehat{x}^{\mathrm{r}}, u_1^{\mathrm{r}}, u_2^{\mathrm{r}})$ are appropriately permuted versions of corresponding matrices and functions in (A.8) and (A.12). We will now show that $\dot{z} = \mathbb{0}_{16}, \forall t \geq t_0$ when $z(t_0) = \widehat{x}^{\mathrm{r}}(t_0) - \mathrm{diag}(\Psi)\widehat{x}(t_0) = \mathbb{0}_{16}$. This would further imply that $z(t) = \widehat{x}^{\mathrm{r}}(t) - \mathrm{diag}(\Psi)\widehat{x}(t) = \mathbb{0}_{16}\ \forall t \geq t_0$, as claimed in the statement of the Theorem.

Partition $\widehat{x} = [\widehat{x}_1^{\mathrm{T}}, \widehat{x}_2^{\mathrm{T}}]^{\mathrm{T}}$, where $\widehat{x}_1 = [i_{\mathrm{i}}^{\alpha}, i_{\mathrm{i}}^{\beta}, i_{\mathrm{o}}^{\alpha}, i_{\mathrm{o}}^{\beta}, \gamma^{\mathrm{d}}, \gamma^{\mathrm{q}}, p_{\mathrm{avg}}, q_{\mathrm{avg}}, \phi^{\mathrm{p}}, \phi^{\mathrm{q}}]^{\mathrm{T}}$ and $\widehat{x}_2 =$

$[v_{\mathrm{f}}^{\alpha}, v_{\mathrm{f}}^{\beta}, v_{g}^{\beta},\, v_{\mathrm{PLL}}, \phi_{\mathrm{PPL}}, \delta]^{\mathrm{T}}$, and we also partition $\widehat{x}^{\mathrm{r}}$ the same way. Then, we partition the appropriately permuted versions of (A.8) and (A.12) as

$$\begin{bmatrix}\dot{\widehat{x}}_1\\ \dot{\widehat{x}}_2\end{bmatrix} = \begin{bmatrix}\widehat{A}_{11} & \widehat{A}_{12}\\ \widehat{A}_{21} & \widehat{A}_{22}\end{bmatrix}\begin{bmatrix}\widehat{x}_1\\ \widehat{x}_2\end{bmatrix} + \begin{bmatrix}\widehat{B}_{11}\\ \widehat{B}_{12}\end{bmatrix} u_1 + \begin{bmatrix}\widehat{B}_{21}\\ \widehat{B}_{22}\end{bmatrix} u_2 + \widehat{g}(\widehat{x}, u_1, u_2), \tag{A.18}$$

$$\begin{bmatrix}\dot{\widehat{x}}_1^{\mathrm{r}}\\ \dot{\widehat{x}}_2^{\mathrm{r}}\end{bmatrix} = \begin{bmatrix}\widehat{A}_{11}^{\mathrm{r}} & \widehat{A}_{12}^{\mathrm{r}}\\ \widehat{A}_{21}^{\mathrm{r}} & \widehat{A}_{22}^{\mathrm{r}}\end{bmatrix}\begin{bmatrix}\widehat{x}_1^{\mathrm{r}}\\ \widehat{x}_2^{\mathrm{r}}\end{bmatrix} + \begin{bmatrix}\widehat{B}_{11}^{\mathrm{r}}\\ \widehat{B}_{12}^{\mathrm{r}}\end{bmatrix} u_1^{\mathrm{r}} + \begin{bmatrix}\widehat{B}_{21}^{\mathrm{r}}\\ \widehat{B}_{22}^{\mathrm{r}}\end{bmatrix} u_2^{\mathrm{r}} + \widehat{g}^{\mathrm{r}}(\widehat{x}^{\mathrm{r}}, u_1^{\mathrm{r}}, u_2^{\mathrm{r}}). \tag{A.19}$$

From the definition of matrices A_{LCL}, A_{CC}, A_{PC}, A_{PLL}, B_{CC}, B_{PC}, B_{LCL}, B_{PLL}, and the parametric scalings established in (A.13a)–(A.13b), we note the following:

$$\begin{aligned}&\widehat{A}_{11}^{\mathrm{r}} = \widehat{A}_{11},\ \widehat{A}_{12}^{\mathrm{r}} = N\widehat{A}_{12},\ \widehat{A}_{21}^{\mathrm{r}} = \frac{1}{N}\widehat{A}_{21},\ \widehat{A}_{22}^{\mathrm{r}} = \widehat{A}_{22},\\ &\widehat{B}_{11}^{\mathrm{r}} = \widehat{B}_{11},\ \widehat{B}_{12}^{\mathrm{r}} = \frac{1}{N}\widehat{B}_{12},\ \widehat{B}_{21}^{\mathrm{r}} = N\widehat{B}_{21},\ \widehat{B}_{22}^{\mathrm{r}} = \widehat{B}_{22}.\end{aligned} \tag{A.20}$$

Then, we have

$$\mathrm{diag}(\Psi)\widehat{A} = \begin{bmatrix}N\widehat{A}_{11} & N\widehat{A}_{12}\\ \widehat{A}_{21} & \widehat{A}_{22}\end{bmatrix} = \begin{bmatrix}N\widehat{A}_{11}^{\mathrm{r}} & \widehat{A}_{12}^{\mathrm{r}}\\ N\widehat{A}_{21}^{\mathrm{r}} & \widehat{A}_{22}^{\mathrm{r}}\end{bmatrix} = \widehat{A}^{\mathrm{r}}\mathrm{diag}(\Psi), \tag{A.21}$$

$$\mathrm{diag}(\Psi)\widehat{B}_1 = \begin{bmatrix}N\widehat{B}_{11}\\ \widehat{B}_{12}\end{bmatrix} = \begin{bmatrix}N\widehat{B}_{11}^{\mathrm{r}}\\ N\widehat{B}_{12}^{\mathrm{r}}\end{bmatrix} = N\widehat{B}_1^{\mathrm{r}}, \tag{A.22}$$

$$\mathrm{diag}(\Psi)\widehat{B}_2 = \begin{bmatrix}N\widehat{B}_{21}\\ \widehat{B}_{22}\end{bmatrix} = \begin{bmatrix}\widehat{B}_{21}^{\mathrm{r}}\\ \widehat{B}_{22}^{\mathrm{r}}\end{bmatrix} = \widehat{B}_2^{\mathrm{r}}. \tag{A.23}$$

The next step is to show that $\widehat{g}^{\mathrm{r}}(\mathrm{diag}(\Psi)\widehat{x}, u_1^{\mathrm{r}}, u_2^{\mathrm{r}}) = \mathrm{diag}(\Psi)\widehat{g}(\widehat{x}, u_1, u_2)$. Let $\widehat{g}_\ell(\widehat{x})$ and $\widehat{g}_\ell^{\mathrm{r}}(\mathrm{diag}(\Psi)\widehat{x})$ denote the ℓ-th entry of $\widehat{g}(\widehat{x}, u_1, u_2)$ and $\widehat{g}^{\mathrm{r}}(\mathrm{diag}(\Psi)\widehat{x}, u_1^{\mathrm{r}}, u_2^{\mathrm{r}})$, respectively. The nonzero entries of $\widehat{g}^{\mathrm{r}}(\mathrm{diag}(\Psi)\widehat{x}, u_1^{\mathrm{r}}, u_2^{\mathrm{r}})$ are related to the corresponding entries of $\widehat{g}(\widehat{x}, u_1, u_2)$ through:

$$\begin{aligned}&\widehat{g}_1^{\mathrm{r}}(\mathrm{diag}(\Psi)\widehat{x}) = \frac{N}{L_{\mathrm{i}}}\left[\left(\frac{k_{\mathrm{CC}}^p}{N}\left(k_{\mathrm{PC}}^p(Nq^\star - Nq_{\mathrm{avg}}) + k_{\mathrm{PC}}^i N\phi^{\mathrm{q}} - Ni_{\mathrm{i}}^{\mathrm{d}}\right) + \frac{k_{\mathrm{CC}}^i}{N}N\gamma^{\mathrm{d}}\right)\cos\delta\right.\\ &\left. - \left(\frac{k_{\mathrm{CC}}^p}{N}\left(k_{\mathrm{PC}}^p(Np^\star - Np_{\mathrm{avg}}) + k_{\mathrm{PC}}^i N\phi^{\mathrm{p}} - Ni_{\mathrm{i}}^{\mathrm{q}}\right) + \frac{k_{\mathrm{CC}}^i}{N}N\gamma^{\mathrm{q}}\right)\sin\delta\right] = N\widehat{g}_1(\widehat{x}),\\ &\widehat{g}_2^{\mathrm{r}}(\mathrm{diag}(\Psi)\widehat{x}) = \eta(Ni_{\mathrm{i}}^{\alpha} - Ni_{\mathrm{i}}^{\beta}) - \widehat{g}_1^{\mathrm{r}}(\mathrm{diag}(\Psi)\widehat{x}) = N\widehat{g}_2(\widehat{x}),\end{aligned}$$

$$
\begin{aligned}
\widehat{g}_5^{\mathrm{r}}(\mathrm{diag}(\Psi)\widehat{x}) &= -Ni_{\mathrm{i}}^{\alpha}\cos\delta - Ni_{\mathrm{i}}^{\beta}\sin\delta = N\widehat{g}_5(\widehat{x}),\\
\widehat{g}_6^{\mathrm{r}}(\mathrm{diag}(\Psi)\widehat{x}) &= Ni_{\mathrm{i}}^{\alpha}\sin\delta - Ni_{\mathrm{i}}^{\beta}\cos\delta = N\widehat{g}_6(\widehat{x}),\\
\widehat{g}_7^{\mathrm{r}}(\mathrm{diag}(\Psi)\widehat{x}) &= \frac{\omega_{\mathrm{c,PC}}}{2}(v_g Ni_{\mathrm{o}}^{\alpha} + v_g^{\beta} Ni_{\mathrm{o}}^{\beta}) = N\widehat{g}_7(\widehat{x}),\\
\widehat{g}_8^{\mathrm{r}}(\mathrm{diag}(\Psi)\widehat{x}) &= \frac{\omega_{\mathrm{c,PC}}}{2}(v_g^{\beta} Ni_{\mathrm{o}}^{\alpha} - v_g Ni_{\mathrm{o}}^{\beta}) = N\widehat{g}_8(\widehat{x}),\\
\widehat{g}_{11}^{\mathrm{r}}(\mathrm{diag}(\Psi)\widehat{x}) &= \frac{R_{\mathrm{f}}}{N}\widehat{g}_1^{\mathrm{r}}(\mathrm{diag}(\Psi)\widehat{x}) = R_{\mathrm{f}}\widehat{g}_1(\widehat{x}) = \widehat{g}_{11}(\widehat{x}),\\
\widehat{g}_{12}^{\mathrm{r}}(\mathrm{diag}(\Psi)\widehat{x}) &= \eta(v_{\mathrm{f}}^{\alpha} - v_{\mathrm{f}}^{\beta}) - \widehat{g}_{11}^{\mathrm{r}}(\mathrm{diag}(\Psi)\widehat{x}) = \widehat{g}_{12}(\widehat{x}),\\
\widehat{g}_{13}^{\mathrm{r}}(\mathrm{diag}(\Psi)\widehat{x}) &= \eta(v_g - v_g^{\beta}) = \widehat{g}_{13}(\widehat{x}),\\
\widehat{g}_{14}^{\mathrm{r}}(\mathrm{diag}(\Psi)\widehat{x}) &= \omega_{\mathrm{c,PLL}}(v_g\cos\delta + v_g^{\beta}\sin\delta) = \widehat{g}_{14}(\widehat{x}),\\
\widehat{g}_{16}^{\mathrm{r}}(\mathrm{diag}(\Psi)\widehat{x}) &= \omega_{\mathrm{nom}} = \widehat{g}_{16}(\widehat{x}),
\end{aligned}
$$

with $\eta := -k_{\mathrm{PLL}}^{p} v_{\mathrm{PLL}} + k_{\mathrm{PLL}}^{i}\phi_{\mathrm{PLL}}$. Therefore we have

$$
\mathrm{diag}(\Psi)\widehat{g}(\widehat{x}, u_1, u_2) = \widehat{g}^{\mathrm{r}}(\mathrm{diag}(\Psi)\widehat{x}, u_1^{\mathrm{r}}, u_2^{\mathrm{r}}). \tag{A.24}
$$

Notice that the PLL dynamics are decoupled from the remainder of the states in the state-space model. Therefore, the parameters of the PLL in the individual and reduced-order models are the same, and we can conclude that:

$$
v_g^{\beta,\mathrm{r}} = v_g^{\beta}, \quad v_{\mathrm{PLL}}^{\mathrm{r}} = v_{\mathrm{PLL}}, \quad \phi_{\mathrm{PLL}}^{\mathrm{r}} = \phi_{\mathrm{PLL}}, \quad \delta^{\mathrm{r}} = \delta. \tag{A.25}
$$

Now, consider the function $h(\widehat{x}^{\mathrm{r}}, u_1^{\mathrm{r}}, u_2^{\mathrm{r}}) : \mathbb{R}^{16}\times\mathbb{R}^2\times\mathbb{R}^2 \to \mathbb{R}^{16}$, which is defined to have the same structure as $\widehat{g}^{\mathrm{r}}(\widehat{x}^{\mathrm{r}}, u_1^{\mathrm{r}}, u_2^{\mathrm{r}})$ except that its 13th, 14th, and 16th entries are 0. Then, the following holds

$$
\widehat{g}^{\mathrm{r}}(\widehat{x}^{\mathrm{r}}, u_1^{\mathrm{r}}, u_2^{\mathrm{r}}) - \widehat{g}^{\mathrm{r}}(\mathrm{diag}(\Psi)\widehat{x}, u_1^{\mathrm{r}}, u_2^{\mathrm{r}}) = h((\widehat{x}^{\mathrm{r}} - \mathrm{diag}\,(\Psi)\widehat{x}), \mathbb{0}_2, u_2^{\mathrm{r}})\,. \tag{A.26}
$$

Using identities (A.21)–(A.26) in (A.17), we have

$$
\begin{aligned}
\dot{z} &= \widehat{A}^{\mathrm{r}}(\widehat{x}^{\mathrm{r}} - \mathrm{diag}(\Psi)\widehat{x}) + h((\widehat{x}^{\mathrm{r}} - \mathrm{diag}\,(\Psi)\widehat{x}), \mathbb{0}_2, u_2^{\mathrm{r}})\\
&= \widehat{A}^{\mathrm{r}} z + h(z, \mathbb{0}_2, u_2^{\mathrm{r}}).
\end{aligned} \tag{A.27}
$$

If we initialize $z(t_0) = \mathbb{0}_{16}$, we have $z(t) = \mathbb{0}_{16}, \forall t \geq t_0$, due to the fact that $h(\mathbb{0}_{16}, \mathbb{0}_2, u_2^{\mathrm{r}}) = \mathbb{0}_{16}$. By the definition of $z(t)$, we have $\widehat{x}^{\mathrm{r}}(t) = \mathrm{diag}(\Psi)\widehat{x}(t), \forall t \geq t_0$.

For the other direction, given that $z(t) = \widehat{x}^{\mathrm{r}} - \mathrm{diag}(\Psi)\widehat{x} = \mathbb{0}_{16}$, $\forall t \geq t_0$, $u_1^{\mathrm{r}} = Nu_1$, and $u_2^{\mathrm{r}} = u_2$, (A.17) can be written as

$$\begin{aligned}\mathbb{0}_{16} = (\widehat{A}^{\mathrm{r}}\mathrm{diag}(\Psi) - \mathrm{diag}(\Psi)\widehat{A})\widehat{x} + (N\widehat{B}_1^{\mathrm{r}} - \mathrm{diag}(\Psi)\widehat{B}_1)u_1 + (\widehat{B}_2^{\mathrm{r}} - \mathrm{diag}(\Psi)\widehat{B}_2)u_2 \\ + \widehat{g}^{\mathrm{r}}(\mathrm{diag}(\Psi)\widehat{x}, Nu_1, u_2) - \mathrm{diag}(\Psi)\widehat{g}(\widehat{x}, u_1, u_2). \qquad \text{(A.28)}\end{aligned}$$

The equality above is satisfied when the following identities hold:

$$\widehat{A}^{\mathrm{r}}\mathrm{diag}(\Psi) = \mathrm{diag}(\Psi)\widehat{A}, \quad N\widehat{B}_1^{\mathrm{r}} = \mathrm{diag}(\Psi)\widehat{B}_1, \quad \widehat{B}_2^{\mathrm{r}} = \mathrm{diag}(\Psi)\widehat{B}_2, \qquad \text{(A.29)}$$

$$\widehat{g}^{\mathrm{r}}(\mathrm{diag}(\Psi)\widehat{x}, Nu_1, u_2) = \mathrm{diag}(\Psi)\widehat{g}(\widehat{x}, u_1, u_2). \qquad \text{(A.30)}$$

It emerges that R_{i}, L_{i}, k_{CC}^p, and k_{CC}^i always appear in the identities above as fractions: $\frac{R_{\mathrm{i}}}{L_{\mathrm{i}}}$, $\frac{k_{\mathrm{CC}}^p}{L_{\mathrm{i}}}$, and $\frac{k_{\mathrm{CC}}^i}{L_{\mathrm{i}}}$. Therefore, these parameters relate to those in the reduced-order model through (A.13b). The remainder of the parameters can be determined straightforwardly from (A.29) and (A.30); they are given uniquely by (A.13a), including the unchanged parameters (i.e., those which are not mentioned in (A.13a) and (A.13b)). This concludes the proof. □

A.2.3 Corollaries for Heterogeneous Settings

We now present two corollaries. In the first, we examine inverters with different reference-power setpoints for both active and reactive power. In this particular case, the relationships between the states of the reduced-order model and those of the individual inverters $\ell = 1, \ldots, N$ are as follows $\forall t \geq t_0$:

$$\begin{aligned}&[i_{\mathrm{i}}^{\alpha,\mathrm{r}}, i_{\mathrm{i}}^{\beta,\mathrm{r}}, i_{\mathrm{o}}^{\alpha,\mathrm{r}}, i_{\mathrm{o}}^{\beta,\mathrm{r}}, \gamma^{\mathrm{d,r}}, \gamma^{\mathrm{q,r}}, p_{\mathrm{avg}}^{\mathrm{r}}, q_{\mathrm{avg}}^{\mathrm{r}}, \phi^{\mathrm{p,r}}, \phi^{\mathrm{q,r}}]^{\mathrm{T}} \\ &= \sum_{\ell=1}^{N}[i_{\mathrm{i},\ell}^{\alpha}, i_{\mathrm{i},\ell}^{\beta}, i_{\mathrm{g},\ell}^{\alpha}, i_{\mathrm{g},\ell}^{\beta}, \gamma_{\ell}^{\mathrm{d}}, \gamma_{\ell}^{\mathrm{q}}, p_{\mathrm{avg},\ell}, q_{\mathrm{avg},\ell}, \phi_{\ell}^{\mathrm{p}}, \phi_{\ell}^{\mathrm{q}}]^{\mathrm{T}}, \\ &[v_{\mathrm{f}}^{\alpha,\mathrm{r}}, v_{\mathrm{f}}^{\beta,\mathrm{r}}]^{\mathrm{T}} = \frac{1}{N}\sum_{\ell=1}^{N}[v_{\mathrm{f},\ell}^{\alpha}, v_{\mathrm{f},\ell}^{\beta}]^{\mathrm{T}},\end{aligned}$$

$$[v_g^{\beta,\mathrm{r}}, v_{\mathrm{PLL}}^{\mathrm{r}}, \phi_{\mathrm{PPL}}^{\mathrm{r}}, \delta^{\mathrm{r}}]^{\mathrm{T}} = [v_{g,\ell}^{\beta}, v_{\mathrm{PLL},\ell}, \phi_{\mathrm{PPL},\ell}, \delta_\ell]^{\mathrm{T}}, \forall \ell.$$

In the second corollary, we examine inverters with different power ratings, and derive an aggregate model with currents that scale systematically. Recall the notion of *power-scaling parameter* κ_ℓ for the ℓ-th inverter introduced in Chapter 3 as:

$$\kappa_\ell = \frac{p_{\mathrm{rated},\ell}}{p_{\mathrm{base}}}, \tag{A.32}$$

where $p_{\mathrm{rated},\ell}$ and p_{base} denote the rated power of the ℓ-th inverter in the parallel system and system-wide base value, respectively. Without loss of generality, we assume that the inverter model in Fig. A.1 has a power rating equal to the base value. Also recall the notion of *equivalent power-scaling parameter*:

$$\widehat{\kappa} := \sum_{\ell=1}^{N} \kappa_\ell. \tag{A.33}$$

The states of the reduced-order model relate to those in the individual inverters $\ell = 1, \ldots, N$ and the *unscaled* inverter (i.e., inverter model with rating equal to the base value) as follows $\forall t \geq t_0$:

$$\begin{aligned}
&[i_{\mathrm{i}}^{\alpha,\mathrm{r}}, i_{\mathrm{i}}^{\beta,\mathrm{r}}, i_{\mathrm{o}}^{\alpha,\mathrm{r}}, i_{\mathrm{o}}^{\beta,\mathrm{r}}, \gamma^{\mathrm{d},\mathrm{r}}, \gamma^{\mathrm{q},\mathrm{r}}, p_{\mathrm{avg}}^{\mathrm{r}}, q_{\mathrm{avg}}^{\mathrm{r}}, \phi^{\mathrm{p},\mathrm{r}}, \phi^{\mathrm{q},\mathrm{r}}]^{\mathrm{T}} \\
&= \sum_{\ell=1}^{N} [i_{\mathrm{i},\ell}^{\alpha}, i_{\mathrm{i},\ell}^{\beta}, i_{\mathrm{g},\ell}^{\alpha}, i_{\mathrm{g},\ell}^{\beta}, \gamma_\ell^{\mathrm{d}}, \gamma_\ell^{\mathrm{q}}, p_{\mathrm{avg},\ell}, q_{\mathrm{avg},\ell}, \phi_\ell^{\mathrm{p}}, \phi_\ell^{\mathrm{q}}]^{\mathrm{T}} \\
&= \widehat{\kappa} [i_{\mathrm{i}}^{\alpha}, i_{\mathrm{i}}^{\beta}, i_{\mathrm{g}}^{\alpha}, i_{\mathrm{g}}^{\beta}, \gamma^{\mathrm{d}}, \gamma^{\mathrm{q}}, p_{\mathrm{avg}}, q_{\mathrm{avg}}, \phi^{\mathrm{p}}, \phi^{\mathrm{q}}]^{\mathrm{T}}, \\
&[v_{\mathrm{f}}^{\alpha,\mathrm{r}}, v_{\mathrm{f}}^{\beta,\mathrm{r}}, v_g^{\beta,\mathrm{r}}, v_{\mathrm{PLL}}^{\mathrm{r}}, \phi_{\mathrm{PPL}}^{\mathrm{r}}, \delta^{\mathrm{r}}]^{\mathrm{T}} \\
&= [v_{\mathrm{f},\ell}^{\alpha}, v_{\mathrm{f},\ell}^{\beta}, v_{g,\ell}^{\beta}, v_{\mathrm{PLL},\ell}, \phi_{\mathrm{PPL},\ell}, \delta_\ell]^{\mathrm{T}}, \forall \ell \\
&= [v_{\mathrm{f}}^{\alpha}, v_{\mathrm{f}}^{\beta}, v_g^{\beta}, v_{\mathrm{PLL}} \phi_{\mathrm{PPL}}, \delta]^{\mathrm{T}}.
\end{aligned}$$

Formal results establishing these two aspects follow next.

Corollary A.2 (Aggregation of parallel-connected identical single-phase inverters with different reference-power setpoints)**.** *Let us denote x_ℓ, $p_\ell^\star$, and $q_\ell^\star$ as the state vector,*

real-, and reactive-power setpoints of the ℓ-th inverter in the parallel system. Permute x_ℓ the same way as in (A.14)*, denoting the permuted vector as $\widehat{x}_\ell$. Partition $\widehat{x}_\ell = [\lambda_\ell^{\mathrm{T}}, v_{\mathrm{f},\ell}^{\alpha\beta\mathrm{T}}, x_{\mathrm{PLL},\ell}^{\mathrm{T}}]^{\mathrm{T}}$, where $\lambda_\ell = [i_{\mathrm{i},\ell}^{\alpha}, i_{\mathrm{i},\ell}^{\beta}, i_{\mathrm{g},\ell}^{\alpha}, i_{\mathrm{g},\ell}^{\beta}, \gamma_\ell^{\mathrm{d}}, \gamma_\ell^{\mathrm{q}}, p_{\mathrm{avg},\ell}, q_{\mathrm{avg},\ell}, \phi_\ell^{\mathrm{p}}, \phi_\ell^{\mathrm{q}}]^{\mathrm{T}}$, $v_{\mathrm{f},\ell}^{\alpha\beta} = [v_{\mathrm{f},\ell}^{\alpha}, v_{\mathrm{f},\ell}^{\beta}]^{\mathrm{T}}$, and $x_{\mathrm{PLL}} = [v_{g,\ell}^{\beta}, v_{\mathrm{PLL},\ell}, \phi_{\mathrm{PPL},\ell}, \delta_\ell]^{\mathrm{T}}$. We also permute and partition x^{r} the same way, denoting the permuted vector as $\widehat{x}^{\mathrm{r}} = [\lambda^{\mathrm{rT}}, v_{\mathrm{f}}^{\alpha\beta,\mathrm{rT}}, x_{\mathrm{PLL}}^{\mathrm{rT}}]^{\mathrm{T}}$. Suppose the initial conditions are such that $\lambda^{\mathrm{r}}(t_0) = \sum_{\ell=1}^{N} \lambda_\ell(t_0)$, $v_{\mathrm{f}}^{\alpha\beta,\mathrm{r}}(t_0) = \frac{1}{N}\sum_{\ell=1}^{N} v_{\mathrm{f},\ell}^{\alpha\beta}(t_0)$, and $x_{\mathrm{PLL}}^{\mathrm{r}}(t_0) = x_{\mathrm{PLL},\ell}(t_0), \forall \ell$, and the inputs are:*

$$u_1^{\mathrm{r}} = \sum_{\ell=1}^{N} u_{1,\ell}, \quad u_2^{\mathrm{r}} = u_2. \tag{A.35}$$

It follows that, $\forall t \geq t_0$:

$$\begin{gathered} \lambda^{\mathrm{r}}(t) = \sum_{\ell=1}^{N} \lambda_\ell(t), \quad v_{\mathrm{f}}^{\alpha\beta,\mathrm{r}}(t) = \frac{1}{N}\sum_{\ell=1}^{N} v_{\mathrm{f},\ell}^{\alpha\beta}(t), \\ x_{\mathrm{PLL}}^{\mathrm{r}}(t) = x_{\mathrm{PLL},\ell}(t), \forall \ell, \end{gathered} \tag{A.36}$$

if and only if the parameters of the reduced-order are related to the individual inverters through (A.13a)–(A.13b)*.*

Proof. We begin by noting that the PLL dynamics are decoupled, and the its parameters in the individual and reduced-order models are the same, therefore $\forall t \geq t_0$, $x_{\mathrm{PLL}}^{\mathrm{r}}(t) = x_{\mathrm{PLL},\ell}(t)\ \forall \ell$ if we initialize $x_{\mathrm{PLL}}^{\mathrm{r}}(t_0) = x_{\mathrm{PLL},\ell}(t_0)\ \forall \ell$. Next, partition the permuted versions of (A.8) and (A.12), excluding the PLL dynamics, as

$$\begin{bmatrix} \dot{\lambda}_\ell \\ \dot{v}_{\mathrm{f},\ell}^{\alpha\beta} \end{bmatrix} = \begin{bmatrix} \widehat{A}_{11} & \widehat{A}_{12} \\ \widehat{A}_{21} & \widehat{A}_{22} \end{bmatrix} \begin{bmatrix} \lambda_\ell \\ v_{\mathrm{f},\ell}^{\alpha\beta} \end{bmatrix} + \begin{bmatrix} \widehat{B}_{11} \\ \widehat{B}_{12} \end{bmatrix} u_{1,\ell} + \begin{bmatrix} \widehat{B}_{21} \\ \widehat{B}_{22} \end{bmatrix} u_2 + \begin{bmatrix} \widehat{g}_1(\widehat{x}_\ell, u_{1,\ell}, u_2) \\ \widehat{g}_2(\widehat{x}_\ell, u_{1,\ell}, u_2) \end{bmatrix}, \tag{A.37}$$

$$\begin{bmatrix} \dot{\lambda}^{\mathrm{r}} \\ \dot{v}_{\mathrm{f}}^{\alpha\beta,\mathrm{r}} \end{bmatrix} = \begin{bmatrix} \widehat{A}_{11}^{\mathrm{r}} & \widehat{A}_{12}^{\mathrm{r}} \\ \widehat{A}_{21}^{\mathrm{r}} & \widehat{A}_{22}^{\mathrm{r}} \end{bmatrix} \begin{bmatrix} \lambda^{\mathrm{r}} \\ v_{\mathrm{f}}^{\alpha\beta,\mathrm{r}} \end{bmatrix} + \begin{bmatrix} \widehat{B}_{11}^{\mathrm{r}} \\ \widehat{B}_{12}^{\mathrm{r}} \end{bmatrix} u_1^{\mathrm{r}} + \begin{bmatrix} \widehat{B}_{21}^{\mathrm{r}} \\ \widehat{B}_{22}^{\mathrm{r}} \end{bmatrix} u_2^{\mathrm{r}} + \begin{bmatrix} \widehat{g}_1^{\mathrm{r}}(\widehat{x}^{\mathrm{r}}, u_1^{\mathrm{r}}, u_2^{\mathrm{r}}) \\ \widehat{g}_2^{\mathrm{r}}(\widehat{x}^{\mathrm{r}}, u_1^{\mathrm{r}}, u_2^{\mathrm{r}}) \end{bmatrix}, \tag{A.38}$$

where $\widehat{g}_1 : \mathbb{R}^{16} \times \mathbb{R}^2 \times \mathbb{R}^2 \to \mathbb{R}^{10}$ and $\widehat{g}_2 : \mathbb{R}^{16} \times \mathbb{R}^2 \times \mathbb{R}^2 \to \mathbb{R}^2$ are the nonlinear parts of the dynamics of λ_ℓ and $v_{\mathrm{f},\ell}^{\alpha\beta}$, respectively (similarly for $\widehat{g}_1^{\mathrm{r}}$ and $\widehat{g}_2^{\mathrm{r}}$). We bring to note a slight abuse of notation in terms of the submatrices in (A.37) and (A.38) and those in (A.18) and (A.19). Furthermore, the submatrices in (A.37) and (A.38) also follow

the relationships in (A.20). Define $z_1 := \lambda^{\mathrm{r}} - \sum_{\ell=1}^{N} \lambda_\ell$ and $z_2 := N v_{\mathrm{f}}^{\alpha\beta,\mathrm{r}} - \sum_{\ell=1}^{N} v_{\mathrm{f},\ell}^{\alpha\beta}$. The dynamics of z_1 and z_2 are:

$$\begin{aligned}\dot{z}_1 = \dot{\lambda}^{\mathrm{r}} - \sum_{\ell=1}^{N} \dot{\lambda}_\ell &= \widehat{A}_{11}^{\mathrm{r}} \lambda^{\mathrm{r}} + \widehat{A}_{12}^{\mathrm{r}} v_{\mathrm{f}}^{\alpha\beta,\mathrm{r}} + \widehat{B}_{11}^{\mathrm{r}} u_1^{\mathrm{r}} + \widehat{B}_{21}^{\mathrm{r}} u_2^{\mathrm{r}} + \widehat{g}_1^{\mathrm{r}}(\widehat{x}^{\mathrm{r}}, u_1^{\mathrm{r}}, u_2^{\mathrm{r}}) \\ &\quad - \sum_{\ell=1}^{N} \left(\widehat{A}_{11} \lambda_\ell + \widehat{A}_{12} v_{\mathrm{f},\ell}^{\alpha\beta,\mathrm{r}} + \widehat{B}_{11} u_{1,\ell} + \widehat{B}_{21} u_2 + \widehat{g}_1(\widehat{x}_\ell, u_{1,\ell}, u_2^{\mathrm{r}}) \right), \end{aligned} \tag{A.39}$$

$$\begin{aligned}\dot{z}_2 = N \dot{v}_{\mathrm{f}}^{\alpha\beta,\mathrm{r}} - \sum_{\ell=1}^{N} \dot{v}_{\mathrm{f},\ell}^{\alpha\beta} &= N \left(\widehat{A}_{21}^{\mathrm{r}} \lambda^{\mathrm{r}} + \widehat{A}_{21}^{\mathrm{r}} v_{\mathrm{f}}^{\alpha\beta,\mathrm{r}} + \widehat{B}_{12}^{\mathrm{r}} u_1^{\mathrm{r}} + \widehat{B}_{22}^{\mathrm{r}} u_2^{\mathrm{r}} + \widehat{g}_2^{\mathrm{r}}(\widehat{x}^{\mathrm{r}}, u_1^{\mathrm{r}}, u_2^{\mathrm{r}}) \right) \\ &\quad - \sum_{\ell=1}^{N} \left(\widehat{A}_{21} \lambda_\ell + \widehat{A}_{22} v_{\mathrm{f},\ell}^{\alpha\beta,\mathrm{r}} + \widehat{B}_{12} u_{1,\ell} + \widehat{B}_{22} u_2 + \widehat{g}_2(\widehat{x}_\ell, u_{1,\ell}, u_2^{\mathrm{r}}) \right). \end{aligned} \tag{A.40}$$

Next, we will show that

$$\widehat{g}_1^{\mathrm{r}}(\widehat{x}^{\mathrm{r}}, u_1^{\mathrm{r}}, u_2^{\mathrm{r}}) - \sum_{\ell=1}^{N} \widehat{g}_1(\widehat{x}_\ell, u_{1,\ell}, u_2) = \widehat{g}_1(\chi, \mathbb{0}_2, u_2), \tag{A.41}$$

$$N\widehat{g}_2^{\mathrm{r}}(\widehat{x}^{\mathrm{r}}, u_1^{\mathrm{r}}, u_2^{\mathrm{r}}) - \sum_{\ell=1}^{N} \widehat{g}_2(\widehat{x}_\ell, u_{1,\ell}, u_2) = \widehat{g}_2(\chi, \mathbb{0}_2, u_2), \tag{A.42}$$

where $\chi := [z_1^{\mathrm{T}}, z_2^{\mathrm{T}}, x_{\mathrm{PLL}}^{\mathrm{rT}}]^{\mathrm{T}}$. Let $\widehat{g}_{1,k}(\widehat{x}_\ell)$, $\widehat{g}_{2,k}(\widehat{x}_\ell)$, $\widehat{g}_{1,k}^{\mathrm{r}}(\widehat{x}^{\mathrm{r}})$, and $\widehat{g}_{2,k}^{\mathrm{r}}(\widehat{x}^{\mathrm{r}})$ denote the k-th entries of $\widehat{g}_1(\widehat{x}_\ell, u_{1,\ell}, u_2)$, $\widehat{g}_2(\widehat{x}_\ell, u_{1,\ell}, u_2)$, $\widehat{g}_1^{\mathrm{r}}(\widehat{x}^{\mathrm{r}}, u_1^{\mathrm{r}}, u_2^{\mathrm{r}})$, and $\widehat{g}_2^{\mathrm{r}}(\widehat{x}^{\mathrm{r}}, u_1^{\mathrm{r}}, u_2^{\mathrm{r}})$, respectively. Then, we have

$$\begin{aligned}&\widehat{g}_{1,1}^{\mathrm{r}}(\widehat{x}^{\mathrm{r}}) - \sum_{\ell=1}^{N} \widehat{g}_{1,1}(\widehat{x}_\ell) = \frac{N}{L_{\mathrm{i}}} \left[\left(\frac{k_{\mathrm{CC}}^p}{N} \left(k_{\mathrm{PC}}^p (\sum_{\ell=1}^{N} q_\ell^\star - q_{\mathrm{avg}}^{\mathrm{r}}) + k_{\mathrm{PC}}^i \phi^{\mathrm{q,r}} - i_{\mathrm{i}}^{\mathrm{d,r}} \right) \right.\right. \\ &\left.\left. + \frac{k_{\mathrm{CC}}^i}{N} \gamma^{\mathrm{d,r}} \right) \cos\delta^{\mathrm{r}} - \left(\frac{k_{\mathrm{CC}}^p}{N} \left(k_{\mathrm{PC}}^p (\sum_{\ell=1}^{N} p_\ell^\star - p_{\mathrm{avg}}^{\mathrm{r}}) + k_{\mathrm{PC}}^i \phi^{\mathrm{p}} - i_{\mathrm{i}}^{\mathrm{q,r}} \right) - \frac{k_{\mathrm{CC}}^i}{N} \gamma^{\mathrm{q,r}} \right) \sin\delta^r \right] \\ &- \sum_{\ell=1}^{N} \left(\left(\frac{k_{\mathrm{CC}}^p}{L_{\mathrm{i}}} \left(k_{\mathrm{PC}}^p (q_\ell^\star - q_{\mathrm{avg},\ell}) + k_{\mathrm{PC}}^i \phi_\ell^{\mathrm{q}} - i_{\mathrm{i},\ell}^{\mathrm{d}} \right) + \frac{k_{\mathrm{CC}}^i}{L_{\mathrm{i}}} \gamma_\ell^{\mathrm{d}} \right) \cos\delta_\ell \right. \\ &\left. + \frac{k_{\mathrm{CC}}^p}{L_{\mathrm{i}}} \left(\left(k_{\mathrm{PC}}^p (p_\ell^\star - p_{\mathrm{avg},\ell}) + k_{\mathrm{PC}}^i \phi^{\mathrm{p}} - i_{\mathrm{i}}^{\mathrm{q,r}} \right) - \frac{k_{\mathrm{CC}}^i}{N} \gamma^{\mathrm{q,r}} \right) \sin\delta_\ell \right) \\ &= \left(\frac{k_{\mathrm{CC}}^p}{L_{\mathrm{i}}} \left(k_{\mathrm{PC}}^p (0 - (q_{\mathrm{avg}}^{\mathrm{r}} - \sum_{\ell=1}^{N} q_{\mathrm{avg},\ell})) + k_{\mathrm{PC}}^i (\phi^{\mathrm{q,r}} - \sum_{\ell=1}^{N} \phi_\ell^{\mathrm{q}}) - (i_{\mathrm{i}}^{\mathrm{d,r}} - \sum_{\ell=1}^{N} i_{\mathrm{i},\ell}^{\mathrm{d}}) \right) \right. \end{aligned}$$

$$+\frac{k^i_{\mathrm{CC}}}{L_{\mathrm{i}}}(\gamma^{\mathrm{d,r}}-\sum_{\ell=1}^{N}\gamma^{\mathrm{d}}_{\ell})\Big)\cos\delta^{\mathrm{r}}+\Big(\frac{k^p_{\mathrm{CC}}}{L_{\mathrm{i}}}\Big(k^p_{\mathrm{PC}}(0-(p^{\mathrm{r}}_{\mathrm{avg}}-\sum_{\ell=1}^{N}p_{\mathrm{avg},\ell}))+k^i_{\mathrm{PC}}(\phi^{\mathrm{p},r}$$
$$-\sum_{\ell=1}^{N}\phi^{\mathrm{p}}_{\ell})-(i^{\mathrm{q,r}}_{\mathrm{i}}-\sum_{\ell=1}^{N}i^{\mathrm{q}}_{\mathrm{i},\ell})\Big)+\frac{k^i_{\mathrm{CC}}}{L_{\mathrm{i}}}(\gamma^{\mathrm{q,r}}-\sum_{\ell=1}^{N}\gamma^{\mathrm{q}}_{\ell})\Big)\sin\delta^{\mathrm{r}}$$
$$=\widehat{g}_{1,1}(\chi,\mathbb{0}_2,u_2), \tag{A.43}$$

$$\widehat{g}^{\mathrm{r}}_{1,2}(\widehat{x}^{\mathrm{r}})-\sum_{\ell=1}^{N}\widehat{g}_{1,2}(\widehat{x}_\ell)=(-k^p_{\mathrm{PLL}}v^{\mathrm{r}}_{\mathrm{PLL}}+k^i_{\mathrm{PLL}}\phi^{\mathrm{r}}_{\mathrm{PLL}})(i^{\alpha,\mathrm{r}}_{\mathrm{i}}-i^{\beta,\mathrm{r}}_{\mathrm{i}})-\widehat{g}^{\mathrm{r}}_{1,1}(\widehat{x}^{\mathrm{r}})$$
$$-\sum_{\ell=1}^{N}\Big((-k^p_{\mathrm{PLL}}v_{\mathrm{PLL},\ell}+k^i_{\mathrm{PLL}}\phi_{\mathrm{PLL},\ell})(i^{\alpha}_{\mathrm{i},\ell}-i^{\beta}_{\mathrm{i},\ell})-\widehat{g}_{1,1}(\widehat{x}_\ell)\Big)$$
$$=(-k^p_{\mathrm{PLL}}v^{\mathrm{r}}_{\mathrm{PLL}}+k^i_{\mathrm{PLL}}\phi^{\mathrm{r}}_{\mathrm{PLL}})\Big((i^{\alpha,\mathrm{r}}_{\mathrm{i}}-\sum_{\ell=1}^{N}i^{\alpha}_{\mathrm{i},\ell})+(i^{\beta,\mathrm{r}}_{\mathrm{i}}-\sum_{\ell=1}^{N}i^{\beta}_{\mathrm{i},\ell})\Big)-\Big(\widehat{g}^{\mathrm{r}}_{1,1}(\widehat{x}^{\mathrm{r}})$$
$$-\sum_{\ell=1}^{N}\widehat{g}_{1,1}(\widehat{x}_\ell)\Big)=\widehat{g}_{1,2}(\chi,\mathbb{0}_2,u_2), \tag{A.44}$$

$$\widehat{g}^{\mathrm{r}}_{1,3}(\widehat{x}^{\mathrm{r}})-\sum_{\ell=1}^{N}\widehat{g}_{1,3}(\widehat{x}_\ell)=0=\widehat{g}_{1,3}(\chi,\mathbb{0}_2,u_2), \tag{A.45}$$

$$\widehat{g}^{\mathrm{r}}_{1,4}(\widehat{x}^{\mathrm{r}})-\sum_{\ell=1}^{N}\widehat{g}_{1,4}(\widehat{x}_\ell)=0=\widehat{g}_{1,4}(\chi,\mathbb{0}_2,u_2), \tag{A.46}$$

$$\widehat{g}^{\mathrm{r}}_{1,5}(\widehat{x}^{\mathrm{r}})-\sum_{\ell=1}^{N}\widehat{g}_{1,5}(\widehat{x}_\ell)=-i^{\alpha,\mathrm{r}}_{\mathrm{i}}\cos\delta^{\mathrm{r}}-i^{\beta,\mathrm{r}}_{\mathrm{i}}\sin\delta^{\mathrm{r}}-\sum_{\ell=1}^{N}\Big(-i^{\alpha}_{\mathrm{i},\ell}\cos\delta_\ell-i^{\beta}_{\mathrm{i},\ell}\sin\delta_\ell\Big)$$
$$=-(i^{\alpha,\mathrm{r}}_{\mathrm{i}}-\sum_{\ell=1}^{N}i^{\alpha}_{\mathrm{i},\ell})\cos\delta^{\mathrm{r}}-(i^{\beta,\mathrm{r}}_{\mathrm{i}}-\sum_{\ell=1}^{N}i^{\beta}_{\mathrm{i},\ell})\sin\delta^{\mathrm{r}}=\widehat{g}_{1,5}(\chi,\mathbb{0}_2,u_2), \tag{A.47}$$

$$\widehat{g}^{\mathrm{r}}_{1,6}(\widehat{x}^{\mathrm{r}})-\sum_{\ell=1}^{N}\widehat{g}_{1,6}(\widehat{x}_\ell)=i^{\alpha,\mathrm{r}}_{\mathrm{i}}\sin\delta^{\mathrm{r}}-i^{\beta,\mathrm{r}}_{\mathrm{i}}\cos\delta^{\mathrm{r}}-\sum_{\ell=1}^{N}\Big(i^{\alpha}_{\mathrm{i},\ell}\sin\delta_\ell-i^{\beta}_{\mathrm{i},\ell}\cos\delta_\ell\Big)$$
$$=(i^{\alpha,\mathrm{r}}_{\mathrm{i}}-\sum_{\ell=1}^{N}i^{\alpha}_{\mathrm{i},\ell})\sin\delta^{\mathrm{r}}-(i^{\beta,\mathrm{r}}_{\mathrm{i}}-\sum_{\ell=1}^{N}i^{\beta}_{\mathrm{i},\ell})\cos\delta^{\mathrm{r}}=\widehat{g}_{1,6}(\chi,\mathbb{0}_2,u_2), \tag{A.48}$$

$$\widehat{g}^{\mathrm{r}}_{1,7}(\widehat{x}^{\mathrm{r}})-\sum_{\ell=1}^{N}\widehat{g}_{1,7}(\widehat{x}_\ell)=\frac{\omega_{\mathrm{c,PC}}}{2}(v_g i^{\alpha,\mathrm{r}}_{\mathrm{o}}+v^{\beta,\mathrm{r}}_{g}i^{\beta,\mathrm{r}}_{\mathrm{o}})-\sum_{\ell=1}^{N}\frac{\omega_{\mathrm{c,PC}}}{2}\Big(v_g i^{\alpha}_{\mathrm{g},\ell}+v^{\beta}_{\mathrm{g},\ell}i^{\beta}_{\mathrm{g},\ell}\Big)$$
$$=\frac{\omega_{\mathrm{c,PC}}}{2}\Big(v_g(i^{\alpha,\mathrm{r}}_{\mathrm{o}}-\sum_{\ell=1}^{N}i^{\alpha}_{\mathrm{g},\ell})+v^{\beta,\mathrm{r}}_{g}(i^{\beta,\mathrm{r}}_{\mathrm{o}}-\sum_{\ell=1}^{N}i^{\beta}_{\mathrm{g},\ell})\Big)=\widehat{g}_{1,7}(\chi,\mathbb{0}_2,u_2), \tag{A.49}$$

$$\widehat{g}^{\mathrm{r}}_{1,8}(\widehat{x}^{\mathrm{r}}) - \sum_{\ell=1}^{N} \widehat{g}_{1,8}(\widehat{x}_\ell) = \frac{\omega_{\mathrm{c,PC}}}{2}(v_g^{\beta,\mathrm{r}} i_{\mathrm{o}}^{\alpha,\mathrm{r}} - v_g i_{\mathrm{o}}^{\beta,\mathrm{r}}) - \sum_{\ell=1}^{N} \frac{\omega_{\mathrm{c,PC}}}{2} \left(v_{\mathrm{g},\ell}^{\beta} i_{\mathrm{g},\ell}^{\alpha} - v_g i_{\mathrm{g},\ell}^{\beta} \right)$$

$$= \frac{\omega_{\mathrm{c,PC}}}{2} \Big(v_g^{\beta,\mathrm{r}} (i_{\mathrm{o}}^{\alpha,\mathrm{r}} - \sum_{\ell=1}^{N} i_{\mathrm{g},\ell}^{\alpha}) - v_g (i_{\mathrm{o}}^{\beta,\mathrm{r}} - \sum_{\ell=1}^{N} i_{\mathrm{g},\ell}^{\beta}) \Big) = \widehat{g}_{1,8}(\chi, \mathbb{0}_2, u_2), \tag{A.50}$$

$$\widehat{g}^{\mathrm{r}}_{1,9}(\widehat{x}^{\mathrm{r}}) - \sum_{\ell=1}^{N} \widehat{g}_{1,9}(\widehat{x}_\ell) = 0 = \widehat{g}_{1,9}(\chi, \mathbb{0}_2, u_2), \tag{A.51}$$

$$\widehat{g}^{\mathrm{r}}_{1,10}(\widehat{x}^{\mathrm{r}}) - \sum_{\ell=1}^{N} \widehat{g}_{1,10}(\widehat{x}_\ell) = 0 = \widehat{g}_{1,10}(\chi, \mathbb{0}_2, u_2), \tag{A.52}$$

$$N\widehat{g}^{\mathrm{r}}_{2,1}(\widehat{x}^{\mathrm{r}}) - \sum_{\ell=1}^{N} \widehat{g}_{2,1}(\widehat{x}_\ell) = N\frac{R_{\mathrm{f}}}{N}\widehat{g}^{\mathrm{r}}_{1,1}(\widehat{x}^{\mathrm{r}}) - R_{\mathrm{f}} \sum_{\ell=1}^{N} \widehat{g}_{1,1}(\widehat{x}_\ell)$$

$$= R_{\mathrm{f}}(\widehat{g}^{\mathrm{r}}_{1,1}(\widehat{x}^{\mathrm{r}}) - \sum_{\ell=1}^{N} \widehat{g}_{1,1}(\widehat{x}_\ell)) = \widehat{g}_{2,1}(\chi, \mathbb{0}_2, u_2), \tag{A.53}$$

$$N\widehat{g}^{\mathrm{r}}_{2,2}(\widehat{x}^{\mathrm{r}}) - \sum_{\ell=1}^{N} \widehat{g}_{2,2}(\widehat{x}_\ell) = N(-k^p_{\mathrm{PLL}} v^{\mathrm{r}}_{\mathrm{PLL}} + k^i_{\mathrm{PLL}} \phi^{\mathrm{r}}_{\mathrm{PLL}})(v_{\mathrm{f}}^{\alpha,\mathrm{r}} - v_{\mathrm{f}}^{\beta,\mathrm{r}}) - N\widehat{g}^{\mathrm{r}}_{2,1}(\widehat{x}^{\mathrm{r}})$$

$$- \sum_{\ell=1}^{N} \Big((-k^p_{\mathrm{PLL}} v_{\mathrm{PLL},\ell} + k^i_{\mathrm{PLL}} \phi_{\mathrm{PLL},\ell})(v_{\mathrm{f},\ell}^{\alpha} - v_{\mathrm{f},\ell}^{\beta}) - \widehat{g}_{2,1}(\widehat{x}_\ell) \Big)$$

$$= (-k^p_{\mathrm{PLL}} v^{\mathrm{r}}_{\mathrm{PLL}} + k^i_{\mathrm{PLL}} \phi^{\mathrm{r}}_{\mathrm{PLL}}) \Big((N v_{\mathrm{f}}^{\alpha,\mathrm{r}} - \sum_{\ell=1}^{N} v_{\mathrm{f},\ell}^{\alpha}) - (N v_{\mathrm{f}}^{\beta,\mathrm{r}} - \sum_{\ell=1}^{N} v_{\mathrm{f},\ell}^{\beta}) \Big)$$

$$- (N\widehat{g}^{\mathrm{r}}_{2,1}(\widehat{x}^{\mathrm{r}}) - \sum_{\ell=1}^{N} \widehat{g}_{2,1}(\widehat{x}_\ell)) = \widehat{g}_{2,2}(\chi, \mathbb{0}_2, u_2). \tag{A.54}$$

Therefore, (A.41) and (A.42) hold. Using identities (A.20), (A.41) and (A.42), we can write the dynamics of z_1 and z_2 as

$$\dot{z}_1 = A_{11} z_1 + A_{12} z_2 + \widehat{g}_1(\chi, \mathbb{0}_2, u_2), \tag{A.55}$$

$$\dot{z}_2 = A_{21} z_1 + A_{22} z_2 + \widehat{g}_2(\chi, \mathbb{0}_2, u_2). \tag{A.56}$$

If we initialize $z_1(t_0) = \mathbb{0}_{10}$ and $z_2(t_0) = \mathbb{0}_2$, we have $z_1(t) = \mathbb{0}_{10}, z_2(t) = \mathbb{0}_2, \forall t \geq t_0$ since $g_1(\chi, \mathbb{0}_2, u_2) = \mathbb{0}_{10}$ and $g_2(\chi, \mathbb{0}_2, u_2) = \mathbb{0}_2$ when $z_1 = \mathbb{0}_{10}$ and $z_2 = \mathbb{0}_2$. By the definition of z_1 and z_2, we have $\lambda^{\mathrm{r}}(t) = \sum_{\ell=1}^{N} \lambda_\ell(t), v_{\mathrm{f}}^{\alpha\beta,\mathrm{r}}(t) = \frac{1}{N} \sum_{\ell=1}^{N} v_{\mathrm{f},\ell}^{\alpha\beta}(t), \forall t \geq t_0$.

For the other direction, given that $\forall t \geq t_0$: $z_1(t) = \lambda^{\mathrm{T}}(t) - \sum_{\ell=1}^{N} \lambda_\ell(t) = \mathbb{0}_{10}, z_2(t) =$

$Nv_{\rm f}^{\alpha\beta,{\rm r}}(t)-\sum_{\ell=1}^{N}v_{{\rm f},\ell}^{\alpha\beta}(t)=\mathbb{0}_2, x_{\rm PLL}^{\rm r}(t)=x_{{\rm PLL},\ell}(t),\forall\ell$, (A.39) and (A.40) can be written as

$$\begin{aligned}\mathbb{0}_{10}&=(\widehat{A}_{11}^{\rm r}-\widehat{A}_{11})\lambda^{\rm r}+(\widehat{A}_{12}^{\rm r}-N\widehat{A}_{12})v_{\rm f}^{\alpha\beta,{\rm r}}+(\widehat{B}_{11}^{\rm r}-\widehat{B}_{11})u_1^{\rm r}\\&\quad+(\widehat{B}_{21}^{\rm r}-N\widehat{B}_{21})u_2^{\rm r}+\widehat{g}_1^{\rm r}(\widehat{x}^{\rm r},u_1^{\rm r},u_2^{\rm r})-\sum_{\ell=1}^{N}\widehat{g}_1(\widehat{x}_\ell,u_{1,\ell},u_2^{\rm r}),\\\mathbb{0}_2&=(N\widehat{A}_{21}^{\rm r}-\widehat{A}_{21})\lambda^{\rm r}+(N\widehat{A}_{22}^{\rm r}-N\widehat{A}_{22})v_{\rm f}^{\alpha\beta,{\rm r}}+(N\widehat{B}_{21}^{\rm r}-\widehat{B}_{21})u_1^{\rm r}\\&\quad+(N\widehat{B}_{22}^{\rm r}-N\widehat{B}_{22})u_2^{\rm r}+N\widehat{g}_2^{\rm r}(\widehat{x}^{\rm r},u_1^{\rm r},u_2^{\rm r})-\sum_{\ell=1}^{N}\widehat{g}_2(\widehat{x}_\ell,u_{1,\ell},u_2^{\rm r}).\end{aligned}$$

These equalities are satisfied when the following identities hold:

$$\begin{aligned}&\widehat{A}_{11}^{\rm r}=\widehat{A}_{11},\ \widehat{A}_{12}^{\rm r}=N\widehat{A}_{12},\ \widehat{A}_{21}^{\rm r}=\frac{1}{N}\widehat{A}_{21},\ \widehat{A}_{22}^{\rm r}=\widehat{A}_{22},\\&\widehat{B}_{11}^{\rm r}=\widehat{B}_{11},\ \widehat{B}_{21}^{\rm r}=N\widehat{B}_{21},\ \widehat{B}_{12}^{\rm r}=\frac{1}{N}\widehat{B}_{12},\ \widehat{B}_{22}^{\rm r}=\widehat{B}_{22},\end{aligned}\tag{A.57}$$

$$\widehat{g}_1^{\rm r}(\widehat{x}^{\rm r},u_1^{\rm r},u_2^{\rm r})=\sum_{\ell=1}^{N}\widehat{g}_1(\widehat{x}_\ell,u_{1,\ell},u_2),\tag{A.58}$$

$$N\widehat{g}_2^{\rm r}(\widehat{x}^{\rm r},u_1^{\rm r},u_2^{\rm r})=\sum_{\ell=1}^{N}\widehat{g}_2(\widehat{x}_\ell,u_{1,\ell},u_2).\tag{A.59}$$

It is straightforward to see that (A.13a) and the unscaled parameters are the only set of parameters that satisfy (A.57). For the rest of parameters, i.e., $R_{\rm i}$, $L_{\rm i}$, $k_{\rm CC}^p$, and $k_{\rm CC}^i$, it can be derived that they always appear in (A.57)–(A.59) as fractions of $\frac{R_{\rm i}}{L_{\rm i}}$, $\frac{k_{\rm CC}^p}{L_{\rm i}}$, and $\frac{k_{\rm CC}^i}{L_{\rm i}}$. Therefore, they are related to those in the reduced-order model through (A.13b). This concludes the proof. □

Corollary A.3 (Aggregation of parallel-connected single-phase inverters with heterogeneous power ratings)**.** *The parameters of each inverter are related to the unscaled inverter through*

$$C_{{\rm f},\ell}=\kappa_\ell C_{\rm f},\ R_{{\rm f},\ell}=\frac{R_{\rm f}}{\kappa_\ell},\ L_{g,\ell}=\frac{L_g}{\kappa_\ell},\ R_{g,\ell}=\frac{R_g}{\kappa_\ell},\tag{A.60a}$$

$$\frac{R_{{\rm i},\ell}}{L_{{\rm i},\ell}}=\frac{R_{\rm i}}{L_{\rm i}},\ \frac{k_{{\rm CC},\ell}^p}{L_{{\rm i},\ell}}=\frac{k_{\rm CC}^p}{L_{\rm i}},\ \frac{k_{{\rm CC},\ell}^i}{L_{{\rm i},\ell}}=\frac{k_{\rm CC}^i}{L_{\rm i}},\tag{A.60b}$$

and parameters not mentioned are unchanged. Suppose the reference-power setpoints for each inverter are $p_\ell^\star = \kappa_\ell p^\star$ *and* $q_\ell^\star = \kappa_\ell q^\star$*. The parameters of the reduced-order model are related to the unscaled inverter through*

$$C_{\mathrm{f}}^{\mathrm{r}} = \widehat{\kappa} C_{\mathrm{f}},\ R_{\mathrm{f}}^{\mathrm{r}} = \frac{R_{\mathrm{f}}}{\widehat{\kappa}},\ L_g^{\mathrm{r}} = \frac{L_g}{\widehat{\kappa}},\ R_g^{\mathrm{r}} = \frac{R_g}{\widehat{\kappa}}, \tag{A.61a}$$

$$\frac{R_{\mathrm{i}}^{\mathrm{r}}}{L_{\mathrm{i}}^{\mathrm{r}}} = \frac{R_{\mathrm{i}}}{L_{\mathrm{i}}},\ \frac{k_{\mathrm{CC}}^{p,\mathrm{r}}}{L_{\mathrm{i}}^{\mathrm{r}}} = \frac{k_{\mathrm{CC}}^{p}}{L_{\mathrm{i}}},\ \frac{k_{\mathrm{CC}}^{i,\mathrm{r}}}{L_{\mathrm{i}}^{\mathrm{r}}} = \frac{k_{\mathrm{CC}}^{i}}{L_{\mathrm{i}}}. \tag{A.61b}$$

Parameters not mentioned are unchanged. Let x*,* x_ℓ*,* x^{r} *denote the state vectors of the unscaled inverter model,* ℓ*-th inverter of the parallel system, and the reduced-order model, respectively. Permute the state vectors the same way as* (A.14)*, denoting the permuted vectors as* $\widehat{x}$*,* $\widehat{x}_\ell$*,* $\widehat{x}^{\mathrm{r}}$*. Partition the permuted state vector* $\widehat{x} = [\lambda^{\mathrm{T}}, \psi^{\mathrm{T}}]^{\mathrm{T}}$*, where* $\lambda = [i_{\mathrm{i}}^{\alpha}, i_{\mathrm{i}}^{\beta}, i_{\mathrm{g}}^{\alpha}, i_{\mathrm{g}}^{\beta}, \gamma^{\mathrm{d}}, \gamma^{\mathrm{q}}, p_{\mathrm{avg}}, q_{\mathrm{avg}}, \phi^{\mathrm{p}}, \phi^{\mathrm{q}}]^{\mathrm{T}}$ *and* $\psi = [v_{\mathrm{f}}^{\alpha}, v_{\mathrm{f}}^{\beta}, v_g^{\beta}, v_{\mathrm{PLL}}, \phi_{\mathrm{PLL}}, \delta]^{\mathrm{T}}$*. We also partition* $\widehat{x}_\ell$ *and* $\widehat{x}^{\mathrm{r}}$ *the same way:* $\widehat{x}_\ell = [\lambda_\ell^{\mathrm{T}}, \psi_\ell^{\mathrm{T}}]^{\mathrm{T}}$*,* $\widehat{x}^{\mathrm{r}} = [\lambda^{\mathrm{rT}}, \psi^{\mathrm{rT}}]^{\mathrm{T}}$*. Suppose the initial conditions are such that* $\lambda^{\mathrm{r}}(t_0) = \sum_{\ell=1}^{N} \lambda_\ell(t_0) = \widehat{\kappa}\lambda(t_0)$*,* $\psi^{\mathrm{r}}(t_0) = \psi_\ell(t_0) = \psi(t_0), \forall \ell$*, and the inputs are:*

$$u_1^{\mathrm{r}} = \sum_{\ell=1}^{N} u_{1,\ell} = \widehat{\kappa} u_1, \quad u_2^{\mathrm{r}} = u_{2,\ell} = u_2, \forall \ell. \tag{A.62}$$

It follows that for $t \geq t_0$*:*

$$\lambda^{\mathrm{r}}(t) = \sum_{\ell=1}^{N} \lambda_\ell(t) = \widehat{\kappa}\lambda(t),\ \psi^{\mathrm{r}}(t) = \psi_\ell(t) = \psi(t), \forall \ell, \tag{A.63}$$

if and only if the parameters of the reduced-order model are related to the unscaled inverter through (A.61a)–(A.61b)*.*

Proof. Each of the inverters in the parallel system can be viewed as the aggregate of κ_ℓ inverters, while keeping in mind that κ_ℓ is not necessarily an integer. The rest of this proof is straightforward from Theorem A.1. □

A.3 Experimental Validation & Simulation Results

In this section, we outline results from an experimental prototype and an exhaustive simulation study to demonstrate various aspects of the reduced-order model. The purpose and scope of the experiments is to demonstrate the validity and establish the accuracy of the reduced-order model (under uniform and symmetric settings) and this is done by comparing the net current injected by the parallel system of inverters in hardware to the output current of the aggregated reduced-order model. The experiments also establish robustness of the reduced-order model to parametric variations that are indeed inescapable in any hardware setup. Following the experimental results, we also include an exhaustive simulation study that: validates the reduced-order model derived for hetereogeneous settings (Corollaries A.2 and A.3), investigates robustness of the reduced-order model to variations in filter parameters, and demonstrates the computational benefits of the reduced-order model.

A.3.1 Hardware Setup

To validate the reduced-order model, our collaborators at the National Renewable Energy Laboratory (NREL) built an experimental system comprised of three identical 750 [VA] single-phase inverters connected in parallel across a stiff voltage source. The hardware setup is illustrated in Fig. A.3(a). It consists of three distinct inverters each with a dedicated power stage and a TI F28335 DSP controller. Each inverter utilizes the control structure shown in Fig. A.1. Controllers are discretized with a step size of $1/(15 \times 10^3)$ [s] and unipolar sine-triangle PWM is utilized with a switching frequency of 30 [kHz]. The single-phase 60 [Hz], 120 [V] RMS ac system voltage (i.e., the grid point of interconnection) is realized with an Ametek MX-45 grid simulator. Subsequently, measurements obtained from the multi-inverter system are compared to a software simulation of a single aggregated inverter model (see Figs. A.2a and A.3b). The simulation of the aggregated inverter, as given in Fig. A.3b, was carried in MATLAB with the ODE45 solver, performed on a computer with Intel Core i7-7700HQ processor @ 2.80GHz CPU and 8GB RAM. The parameters of the experimental setup are summarized in Table A.1. Simulation parameters used in the aggregated inverter model are obtained from these, and the scalings reported in (A.13a)–(A.13b).

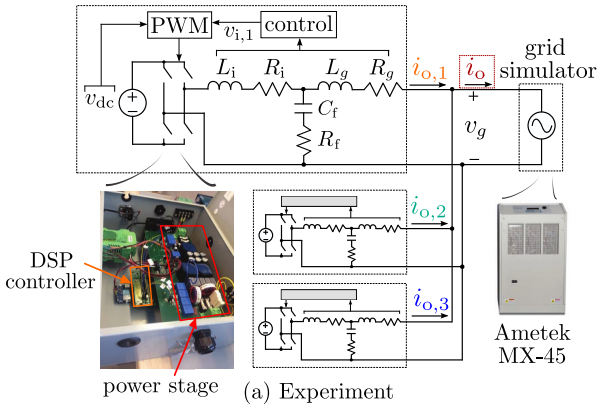

(a) Experiment

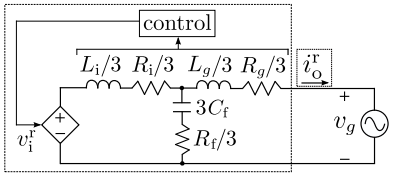

(b) Simulation

Figure A.3: (a) Experimental setup consisting of three parallel-connected single-phase inverters rated at 750 [VA]. The system of three inverters are given real- and reactive-power step commands to generate the results in Fig. A.4 (Currents plotted in Fig. A.4 are shown in dashed boxes, marked with the same color scheme above.) (b) The reduced-order aggregated model where the multi-inverter system is represented as one equivalent inverter.

Table A.1: Inverter LCL-filter and controller parameters.

LCL filter	Current Controller	PLL
$L_i = 1.0$ [mH]	$k^p_{CC} = 6$ [V/A]	$k^p_{PLL} = 1.25$ [rad/(V · s)]
$R_i = 0.7$ [Ω]	$k^i_{CC} = 350$ [V/(A · s)]	$k^i_{PLL} = 10$ [rad/(V · s^2)]
$C_f = 24$ [μF]		$\omega_{c,PLL} = 2\pi \times 200$ [rad/s]
$R_f = 0.02$ [Ω]	Power Controller	
$L_g = 0.2$ [mH]	$k^p_{PC} = 0.01$ [A/VA]	
$R_g = 0.12$ [Ω]	$k^i_{PC} = 0.1$ [A/(VA · s)]	
	$\omega_{c,PC} = 50.26$ [rad/s]	

A.3.2 Validation of Reduced-order Model

To validate the proposed reduced-order model, we compared the measured and simulated dynamic responses under a comprehensive set of step changes in both real and reactive power. The real-power steps are representative of, e.g., sudden irradiance transients that

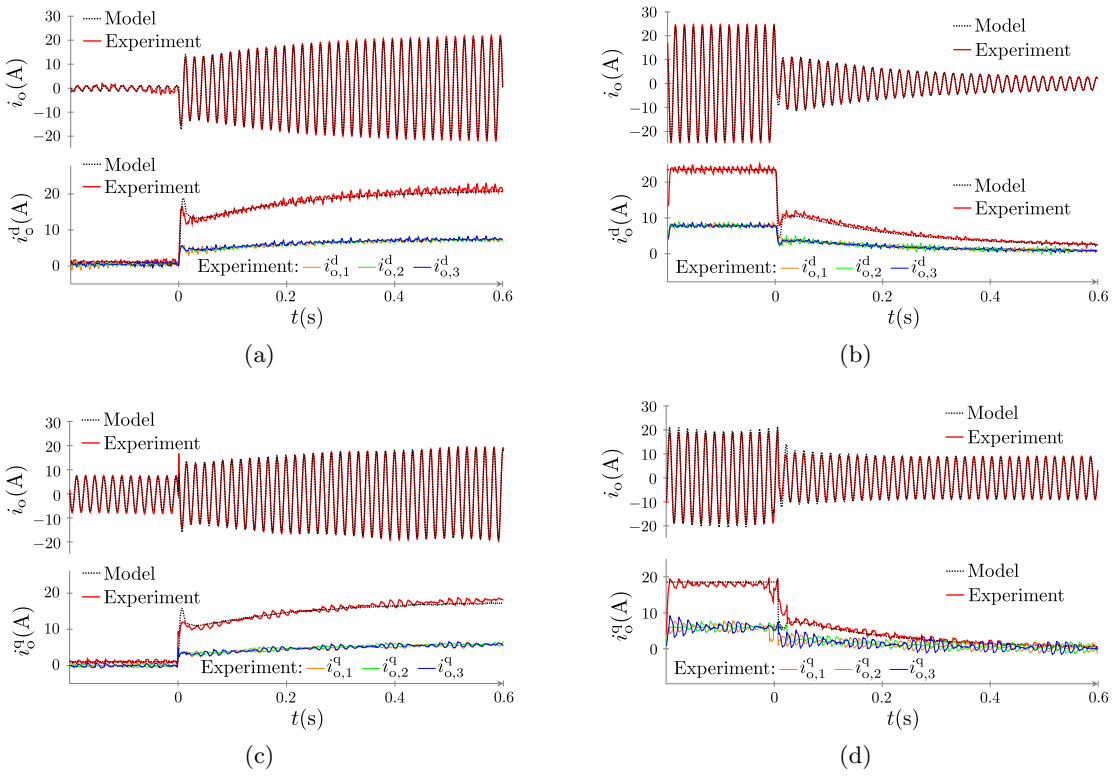

Figure A.4: Comparison of experimentally measured and simulated waveforms: (a) Real-power step up $p^\star$: 30 [W] $\rightarrow$ 600 [W] with fixed $q^\star = 0$ [VAR], (b) Real-power step down $p^\star$: 700 [W] $\rightarrow$ 50 [W] with fixed $q^\star = 0$ [VAR], (c) Reactive-power step up $q^\star$: 0 [VAR] $\rightarrow$ 500 [VAR] with fixed $p^\star = 200$ [W], (d) Reactive-power step down $q^\star$: 500 [VAR] $\rightarrow$ 0 [W] with fixed $p^\star = 250$ [W].

a microinverter system might contend with. The reactive-power steps are representative of, e.g., ancillary services that grid-connected inverters may provide. Results are plotted in Fig. A.4. The plot pair in each subfigure illustrates:

1. The measured net sinusoidal current injected into the grid by the parallel inverters overlaid with the simulated current from the aggregated-inverter model. The measurement point and corresponding point in the reduced-order model are marked prominently in Fig. A.3.

2. Pertinent d- or q-axis current waveforms measured at each inverter output in addition to measured and simulated net current injection.

It is worth emphasizing that we focus just on the *net* current at the point of grid

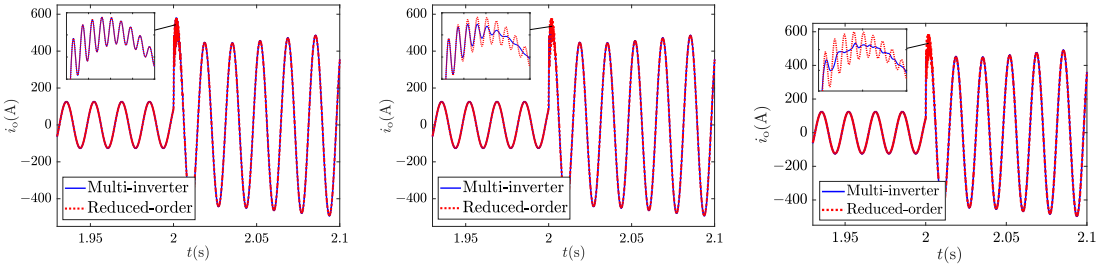

(a) Case #1 (b) Case #2 (c) Case #3

Figure A.5: Simulation results comparing the injected current for a system of 100 parallel-connected inverters with all inverter dynamics simulated superimposed to results from the reduced-order model for the following cases: (a) heterogeneous power ratings with power-scaling parameters (κ) vary between 0.5 and 5, (b) identical power ratings with $\kappa = 1$ and LCL-filter parameters vary between $\pm 10\%$ of their nominal values,(c) same setup as (b), but with variation of $\pm 80\%$.

interconnection and compare that with the current suggested by the aggregate model. The match between these through a variety of large-signal changes—as suggested in Fig. A.4—validates the accuracy of the aggregate model. Furthermore, note that in this case, the parallel collection of inverters are collectively described by a 48-state model, while the simulations are performed with the reduced-order 16-state model.

A.3.3 Simulation Results

Next, we establish the accuracy and computational benefits of the proposed reduced-order model (for a system of 100 parallel-connected inverters) in heterogeneous settings with numerical simulation results. The parameters of the inverter with nominal power rating are listed in Table A.1. We consider the following cases: #1) Inverters have heterogeneous power ratings with power-scaling parameters κ selected to be uniformly distributed between 0.5 and 5. #2) All inverters have ratings that match the nominal power ratings, but their LCL-filter parameters vary between $\pm 10\%$ of their nominal values. #3) Same setup as #2, but the LCL-filter parameters of the inverters vary between $\pm 80\%$ of their nominal values. For all cases, the real- and reactive-power setpoints of the inverters are assumed to be uniformly distributed between $0 - 200$ [W] and $0 - 100$ [VAR], respectively, and we perform a step change to both setpoints, with the values again selected to be uniformly distributed between $400 - 600$ [W] and

$300 - 500$ [VAR], respectively. The step change is introduced at $t = 2$ [s], and we stop the simulations at $t = 4$ [s]. We note that case #2 and #3 have the same reduced-order model. The parameter scalings of the reduced-order models for case #1 and #2 (#3) are given by (A.61a)–(A.61b) and (A.13a)–(A.13b), respectively. The net current injection of the multi-inverter system and the reduced-order models for case #1, #2, and #3 are shown in Fig. A.5. We can clearly see in Fig. A.5a that for case#1, the output current of the reduced-order model is exactly the same as the net current injection of the parallel system—this validates Corollaries A.2 and A.3. Furthermore, Fig. A.5b shows that the reduced-order model is quite robust with respect to the parametric variations in the LCL filter parameters with discrepancies obvious in high-frequency content. For larger variation ($\pm 80\%$), Fig. A.5c shows that the reduced-order model captures the dynamics of the multi-inverter system, albeit with degraded accuracy during the transient. Finally, the computation time for the 1600-th order multi-inverter system simulation for cases #1, #2, and #3 are 58.23 [s], 66.97 [s], and 145.08 [s], respectively, and of the reduced-order 16-th order aggregate model are 1.89 [s], 1.62 [s], and 1.62 [s], respectively. This clearly establishes the computational benefits of the proposed model.

Appendix B

Three-phase Inverter Model Particulars

B.1 Steady-state Operation of PLL

The three-phase grid voltage is expressed as $v_g^{\mathrm{a}} = V_g \sin\delta_g, v_g^{\mathrm{b}} = V_g \sin(\delta_g - 2\pi/3), v_g^{\mathrm{c}} = V_g \sin(\delta_g + 2\pi/3)$, where V_g and δ_g are the voltage amplitude and the angle of the phase-a voltage, respectively. The d-axis component of v_g is obtained by applying the Park's transformation (3.2) to the three-phase voltage as follows:

$$\begin{aligned} v_g^{\mathrm{d}} &= \frac{2}{3}\begin{bmatrix}\cos\delta & \cos(\delta - \frac{2\pi}{3}) & \cos(\delta + \frac{2\pi}{3})\end{bmatrix}\begin{bmatrix} V_g \sin\delta_g \\ V_g \sin(\delta_g - 2\pi/3) \\ V_g \sin(\delta_g + 2\pi/3)\end{bmatrix} \\ &= V_g \sin(\delta_g - \delta). \end{aligned}$$

From above, it follows that when $v_g^{\mathrm{d}} = 0$, $\delta = \delta_g$.

B.2 Entries of State-space Matrices of Three-phase Inverter

In order to show the entries of matrices A, B, and function $g(x, u_2)$ compactly, let us permute the state vector as $\widehat{x} := [i_{\mathrm{i}}^{\mathrm{d}}, i_{\mathrm{i}}^{\mathrm{q}}, i_{\mathrm{o}}^{\mathrm{d}}, i_{\mathrm{o}}^{\mathrm{q}}, v_{\mathrm{f}}^{\mathrm{d}}, v_{\mathrm{f}}^{\mathrm{q}}, \gamma^{\mathrm{d}}, \gamma^{\mathrm{q}}, p_{\mathrm{avg}}, q_{\mathrm{avg}}, \phi^{\mathrm{p}}, \phi^{\mathrm{q}}, v_{\mathrm{PLL}}, \phi_{\mathrm{PPL}}, \delta]^{\mathrm{T}}$,

and the permuted dynamics are given by

$$\dot{\widehat{x}} = \widehat{A}\widehat{x} + \widehat{B}u_1 + \widehat{g}(\widehat{x}, u_2), \tag{B.1}$$

Suppose we partition the permuted state vector as $\widehat{x} = [x_{LCL}^{\mathrm{T}}, x_{\mathrm{CC}}^{\mathrm{T}}, x_{\mathrm{PC}}^{\mathrm{T}}, x_{\mathrm{PLL}}^{\mathrm{T}}]^{\mathrm{T}}$, where $x_{LCL} = [i_{\mathrm{i}}^{\mathrm{d}}, i_{\mathrm{i}}^{\mathrm{q}}, i_{\mathrm{o}}^{\mathrm{d}}, i_{\mathrm{o}}^{\mathrm{q}}, v_{\mathrm{f}}^{\mathrm{d}}, v_{\mathrm{f}}^{\mathrm{q}}]^{\mathrm{T}}$, $x_{\mathrm{CC}} = [\gamma^{\mathrm{d}}, \gamma^{\mathrm{q}}]^{\mathrm{T}}$, $x_{\mathrm{PC}} = [p_{\mathrm{avg}}, q_{\mathrm{avg}}, \phi^{\mathrm{p}}, \phi^{\mathrm{q}}]^{\mathrm{T}}$, and $x_{\mathrm{PLL}} = [v_{\mathrm{PLL}}, \phi_{\mathrm{PLL}}, \delta]^{\mathrm{T}}$. Then, we can write (B.1) as

$$\begin{bmatrix} \dot{x}_{LCL} \\ \dot{x}_{\mathrm{CC}} \\ \dot{x}_{\mathrm{PC}} \\ \dot{x}_{\mathrm{PLL}} \end{bmatrix} = \begin{bmatrix} A_{LCL} & A_{LCL}^{\mathrm{CC}} & A_{LCL}^{\mathrm{PC}} & \mathbb{0}_{6\times 3} \\ A_{\mathrm{CC}}^{LCL} & \mathbb{0}_{2\times 2} & A_{\mathrm{CC}}^{\mathrm{PC}} & \mathbb{0}_{2\times 3} \\ \mathbb{0}_{4\times 6} & \mathbb{0}_{4\times 2} & A_{\mathrm{PC}} & \mathbb{0}_{4\times 3} \\ \mathbb{0}_{4\times 6} & \mathbb{0}_{4\times 2} & \mathbb{0}_{4\times 4} & A_{\mathrm{PLL}} \end{bmatrix} \begin{bmatrix} x_{LCL} \\ x_{\mathrm{CC}} \\ x_{\mathrm{PC}} \\ x_{\mathrm{PLL}} \end{bmatrix} + \begin{bmatrix} B_{LCL} \\ B_{\mathrm{CC}} \\ B_{\mathrm{PC}} \\ \mathbb{0}_{3\times 2} \end{bmatrix} u_1 + \widehat{g}(\widehat{x}, u_2),$$

where the nonzero submatrices A_{LCL}, A_{LCL}^{CC}, A_{LCL}^{PC}, A_{CC}^{LCL}, $A_{\mathrm{CC}}^{\mathrm{PC}}$, A_{PC}, A_{PLL}, B_{LCL}, B_{CC}, and B_{PC} are given by

$$A_{LCL} = \begin{bmatrix} -\frac{k_{\mathrm{CC}}^p + R_{\mathrm{i}}}{L_{\mathrm{i}}} & 0 & 0 & 0 & 0 & 0 \\ 0 & -\frac{k_{\mathrm{CC}}^p + R_{\mathrm{i}}}{L_{\mathrm{i}}} & 0 & 0 & 0 & 0 \\ 0 & 0 & -\frac{R_g}{L_g} & \omega_{\mathrm{nom}} & \frac{1}{L_g} & 0 \\ 0 & 0 & -\omega_{\mathrm{nom}} & -\frac{R_g}{L_g} & 0 & \frac{1}{L_g} \\ -R_{\mathrm{f}}\frac{k_{\mathrm{CC}}^p + R_{\mathrm{i}}}{L_{\mathrm{i}}} + \frac{1}{C_{\mathrm{f}}} & -\omega_{\mathrm{nom}} R_{\mathrm{f}} & R_{\mathrm{f}}\frac{R_g}{L_g} - \frac{1}{C_{\mathrm{f}}} & 0 & -R_{\mathrm{f}}(\frac{1}{L_g} + \frac{1}{L_{\mathrm{i}}}) & \omega_{\mathrm{nom}} \\ \omega_{\mathrm{nom}} R_{\mathrm{f}} & -R_{\mathrm{f}}\frac{k_{\mathrm{CC}}^p + R_{\mathrm{i}}}{L_{\mathrm{i}}} + \frac{1}{C_{\mathrm{f}}} & 0 & R_{\mathrm{f}}\frac{R_g}{L_g} - \frac{1}{C_{\mathrm{f}}} & -\omega_{\mathrm{nom}} & -R_{\mathrm{f}}(\frac{1}{L_g} + \frac{1}{L_{\mathrm{i}}}) \end{bmatrix},$$

$$A_{LCL}^{\mathrm{CC}} = \begin{bmatrix} \frac{k_{\mathrm{CC}}^i}{L_{\mathrm{i}}} & 0 \\ 0 & \frac{k_{\mathrm{CC}}^i}{L_{\mathrm{i}}} \\ 0 & 0 \\ 0 & 0 \\ \frac{R_{\mathrm{f}}}{L_{\mathrm{i}}} k_{\mathrm{CC}}^i & 0 \\ 0 & \frac{R_{\mathrm{f}}}{L_{\mathrm{i}}} k_{\mathrm{CC}}^i \end{bmatrix}, \; A_{LCL}^{\mathrm{PC}} = \begin{bmatrix} 0 & -\frac{k_{\mathrm{CC}}^p}{L_{\mathrm{i}}} k_{\mathrm{PC}}^p & 0 & \frac{k_{\mathrm{CC}}^p}{L_{\mathrm{i}}} k_{\mathrm{PC}}^i \\ -\frac{k_{\mathrm{CC}}^p}{L_{\mathrm{i}}} k_{\mathrm{PC}}^p & 0 & \frac{k_{\mathrm{CC}}^p}{L_{\mathrm{i}}} k_{\mathrm{PC}}^i & 0 \\ 0 & 0 & 0 & 0 \\ 0 & 0 & 0 & 0 \\ 0 & -\frac{k_{\mathrm{CC}}^p}{L_{\mathrm{i}}} k_{\mathrm{PC}}^p R_{\mathrm{f}} & 0 & \frac{k_{\mathrm{CC}}^i}{L_{\mathrm{i}}} k_{\mathrm{PC}}^p R_{\mathrm{f}} \\ -\frac{k_{\mathrm{CC}}^p}{L_{\mathrm{i}}} k_{\mathrm{PC}}^p R_{\mathrm{f}} & 0 & \frac{k_{\mathrm{CC}}^i}{L_{\mathrm{i}}} k_{\mathrm{PC}}^p R_{\mathrm{f}} & 0 \end{bmatrix},$$

$$A_{\mathrm{CC}}^{LCL} = \begin{bmatrix} -1 & 0 & 0 & 0 & 0 & 0 \\ 0 & -1 & 0 & 0 & 0 & 0 \end{bmatrix}, \quad A_{\mathrm{CC}}^{\mathrm{PC}} = \begin{bmatrix} 0 & -k_{\mathrm{PC}}^p & 0 & k_{\mathrm{PC}}^i \\ -k_{\mathrm{PC}}^p & 0 & k_{\mathrm{PC}}^i & \end{bmatrix},$$

$$A_{\mathrm{PC}} = \begin{bmatrix} -\omega_{\mathrm{c,PC}} & 0 & 0 & 0 \\ 0 & -\omega_{\mathrm{c,PC}} & 0 & 0 \\ -1 & 0 & 0 & 0 \\ 0 & -1 & 0 & 0 \end{bmatrix}, \quad A_{\mathrm{PLL}} = \begin{bmatrix} -\omega_{\mathrm{c,PLL}} & 0 & 0 \\ -1 & 0 & 0 \\ -k_{\mathrm{PLL}}^p & k_{\mathrm{PLL}}^i & 0 \end{bmatrix},$$

$$B_{LCL} = \begin{bmatrix} 0 & \frac{k_{\mathrm{CC}}^p}{L_{\mathrm{i}}} k_{\mathrm{PC}}^p \\ \frac{k_{\mathrm{CC}}^p}{L_{\mathrm{i}}} k_{\mathrm{PC}}^p & 0 \\ 0 & 0 \\ 0 & 0 \\ 0 & \frac{k_{\mathrm{CC}}^p}{L_{\mathrm{i}}} k_{\mathrm{PC}}^p R_{\mathrm{f}} \\ \frac{k_{\mathrm{CC}}^p}{L_{\mathrm{i}}} k_{\mathrm{PC}}^p R_{\mathrm{f}} & 0 \end{bmatrix}, \quad B_{\mathrm{CC}} = \begin{bmatrix} 0 & k_{\mathrm{PC}}^p \\ k_{\mathrm{PC}}^p & 0 \end{bmatrix}, \quad B_{\mathrm{PC}} = \begin{bmatrix} 0 & 0 \\ 0 & 0 \\ 1 & 0 \\ 0 & 1 \end{bmatrix}.$$

Let $\widehat{g}_\ell(\widehat{x}, u_2)$ denote the ℓ-th entry of $\widehat{g}(\widehat{x}, u_2)$. The nonzero entries of $\widehat{g}(\widehat{x}, u_2)$ are:

$$\begin{aligned}
\widehat{g}_3(\widehat{x}, u_2) &= (-k_{\mathrm{PLL}}^p v_{\mathrm{PLL}} + k_{\mathrm{PLL}}^i \phi_{\mathrm{PLL}}) i_{\mathrm{o}}^{\mathrm{q}} - \frac{1}{L_g} v_g^{\mathrm{d}}(\widehat{x}, u_2), \\
\widehat{g}_4(\widehat{x}, u_2) &= (k_{\mathrm{PLL}}^p v_{\mathrm{PLL}} - k_{\mathrm{PLL}}^i \phi_{\mathrm{PLL}}) i_{\mathrm{o}}^{\mathrm{d}} - \frac{1}{L_g} v_g^{\mathrm{q}}(\widehat{x}, u_2), \\
\widehat{g}_5(\widehat{x}, u_2) &= (-k_{\mathrm{PLL}}^p v_{\mathrm{PLL}} + k_{\mathrm{PLL}}^i \phi_{\mathrm{PLL}})(-R_{\mathrm{f}} i_{\mathrm{i}}^{\mathrm{q}} + v_{\mathrm{f}}^{\mathrm{q}}) + \frac{R_{\mathrm{f}}}{L_g} v_g^{\mathrm{d}}(\widehat{x}, u_2), \\
\widehat{g}_6(\widehat{x}, u_2) &= (k_{\mathrm{PLL}}^p v_{\mathrm{PLL}} - k_{\mathrm{PLL}}^i \phi_{\mathrm{PLL}})(-R_{\mathrm{f}} i_{\mathrm{i}}^{\mathrm{d}} + v_{\mathrm{f}}^{\mathrm{d}}) + \frac{R_{\mathrm{f}}}{L_g} v_g^{\mathrm{q}}(\widehat{x}, u_2), \\
\widehat{g}_9(\widehat{x}, u_2) &= \frac{3}{2} \omega_{\mathrm{c,PC}} \left(v_g^{\mathrm{d}}(\widehat{x}, u_2) i_{\mathrm{o}}^{\mathrm{d}} + v_g^{\mathrm{q}}(\widehat{x}, u_2) i_{\mathrm{o}}^{\mathrm{q}} \right), \\
\widehat{g}_{10}(\widehat{x}, u_2) &= \frac{3}{2} \omega_{\mathrm{c,PC}} \left(v_g^{\mathrm{q}}(\widehat{x}, u_2) i_{\mathrm{o}}^{\mathrm{d}} - v_g^{\mathrm{d}}(\widehat{x}, u_2) i_{\mathrm{o}}^{\mathrm{q}} \right), \\
\widehat{g}_{13}(\widehat{x}, u_2) &= \omega_{\mathrm{c,PLL}} v_g^{\mathrm{d}}(\widehat{x}, u_2),
\end{aligned}$$

$$\widehat{g}_{15}(\widehat{x}, u_2) = \omega_{\text{nom}},$$

where $v_g^{\text{d}}(\widehat{x}, u_2)$ and $v_g^{\text{q}}(\widehat{x}, u_2)$ are given by

$$v_g^{\text{d}}(\widehat{x}, u_2) = \frac{2}{3}\left(\cos(\delta)v_g^{\text{a}} + \cos(\delta - \frac{2\pi}{3})v_g^{\text{b}} + \cos(\delta + \frac{2\pi}{3})v_g^{\text{c}}\right),$$
$$v_g^{\text{q}}(\widehat{x}, u_2) = -\frac{2}{3}\left(\sin(\delta)v_g^{\text{a}} + \sin(\delta - \frac{2\pi}{3})v_g^{\text{b}} + \sin(\delta + \frac{2\pi}{3})v_g^{\text{c}}\right).$$

B.3 Proof of Corollary 3.3

Note that the PLL dynamics are decoupled from the rest of internal states and their parameters are the same in the reduced-order and individual models, therefore $x_{\text{PLL}}^{\text{r}}(t) = x_{\text{PLL},\ell}(t), \forall \ell$ for $t \geq t_0$ if we initialize $x_{\text{PLL}}^{\text{r}}(t_0) = x_{\text{PLL},\ell}(t_0), \forall \ell$. Next, we partition the dynamics of the individual inverter and the reduced-order model excluding the PLL dynamics as follows:

$$\begin{bmatrix} \dot{\lambda}_\ell \\ \dot{v}_{\text{f},\ell}^{\text{dq}} \end{bmatrix} = \begin{bmatrix} A_{11,\ell} & A_{12,\ell} \\ A_{21,\ell} & A_{22,\ell} \end{bmatrix} \begin{bmatrix} \lambda_\ell \\ v_{\text{f},\ell}^{\text{dq}} \end{bmatrix} + \begin{bmatrix} B_{1,\ell} \\ B_{2,\ell} \end{bmatrix} u_{1,\ell} + \begin{bmatrix} g_{1,\ell}(x_\ell, u_2) \\ g_{2,\ell}(x_\ell, u_2), \end{bmatrix} \tag{B.2}$$

$$\begin{bmatrix} \dot{\lambda}^{\text{r}} \\ \dot{v}_{\text{f}}^{\text{dq,r}} \end{bmatrix} = \begin{bmatrix} A_{11}^{\text{r}} & A_{12}^{\text{r}} \\ A_{21}^{\text{r}} & A_{22}^{\text{r}} \end{bmatrix} \begin{bmatrix} \lambda^{\text{r}} \\ v_{\text{f}}^{\text{dq,r}} \end{bmatrix} + \begin{bmatrix} B_1^{\text{r}} \\ B_2^{\text{r}} \end{bmatrix} u_1^{\text{r}} + \begin{bmatrix} g_1^{\text{r}}(x^{\text{r}}, u_2^{\text{r}}) \\ g_2^{\text{r}}(x^{\text{r}}, u_2^{\text{r}}) \end{bmatrix}. \tag{B.3}$$

We also consider the dynamics of the inverter with nominal power rating, whose states denoted by x^0, as follows:

$$\begin{bmatrix} \dot{\lambda}^0 \\ \dot{v}_o^{\text{dq},0} \end{bmatrix} = \begin{bmatrix} A_{11}^0 & A_{12}^0 \\ A_{21}^0 & A_{22}^0 \end{bmatrix} \begin{bmatrix} \lambda^0 \\ v_o^{\text{dq},0} \end{bmatrix} + \begin{bmatrix} B_1^0 \\ B_2^0 \end{bmatrix} u_1^0 + \begin{bmatrix} g_1^0(x^0, u_2^0) \\ g_2^0(x^0, u_2^0) \end{bmatrix}. \tag{B.4}$$

The submatrices in (B.2) and (B.3) are related to those in (B.4) above as follows:

$$A_{11,\ell} = A_{11}^0,\ A_{12,\ell} = \kappa_\ell A_{12}^0,\ A_{21,\ell} = \frac{1}{\kappa_\ell}A_{21}^0,\ A_{22,\ell} = A_{22}^0,\ B_{1,\ell} = B_1^0,\ B_{2,\ell} = \frac{1}{\kappa_\ell}B_2^0, \tag{B.5}$$

$$A_{11}^{\mathrm{r}} = A_{11}^{0},\ A_{12}^{\mathrm{r}} = \widehat{\kappa} A_{12}^{0} = \sum_{\ell=1}^{N} \kappa_\ell A_{12}^{0},\ A_{21}^{\mathrm{r}} = \frac{1}{\widehat{\kappa}} A_{21}^{0},\ A_{22}^{\mathrm{r}} = A_{22}^{0},\ B_{1}^{\mathrm{r}} = B_{1}^{0},\ B_{2}^{\mathrm{r}} = \frac{1}{\widehat{\kappa}} B_{2}^{0}. \tag{B.6}$$

We define $z_1 := \lambda^{\mathrm{r}} - \sum_{\ell=1}^{N} \lambda_\ell$ and $z_2 = \widehat{\kappa} v_{\mathrm{f}}^{\mathrm{dq,r}} - \sum_{\ell=1}^{N} \kappa_\ell v_{\mathrm{f},\ell}^{\mathrm{dq}}$. The dynamics of z_1 and z_2 are:

$$\begin{aligned} \dot{z}_1 = \dot{\lambda}^{\mathrm{r}} - \sum_{\ell=1}^{N} \dot{\lambda}_\ell &= A_{11}^{\mathrm{r}} \lambda^{\mathrm{r}} + A_{12}^{\mathrm{r}} v_{\mathrm{f}}^{\mathrm{dq,r}} + B_1^{\mathrm{r}} u_1^{\mathrm{r}} + g_1^{\mathrm{r}}(x^{\mathrm{r}}, u_2^{\mathrm{r}}) \\ &\quad - \sum_{\ell=1}^{N} (A_{11,\ell} \lambda_\ell + A_{12,\ell} v_{\mathrm{f},\ell}^{\mathrm{dq}} + B_{1,\ell} u_{1,\ell} + g_{1,\ell}(x_\ell, u_2)) \end{aligned} \tag{B.7}$$

$$\begin{aligned} \dot{z}_2 = \widehat{\kappa} \dot{v}_{\mathrm{f}}^{\mathrm{dq,r}} - \sum_{\ell=1}^{N} \kappa_\ell \dot{v}_{\mathrm{f},\ell}^{\mathrm{dq}} &= \widehat{\kappa} (A_{21}^{\mathrm{r}} \lambda^{\mathrm{r}} + A_{22}^{\mathrm{r}} v_{\mathrm{f}}^{\mathrm{dq,r}} + B_2^{\mathrm{r}} u_1^{\mathrm{r}} + g_2^{\mathrm{r}}(x^{\mathrm{r}}, u_2^{\mathrm{r}})) \\ &\quad - \sum_{\ell=1}^{N} \kappa_\ell (A_{21,\ell} \lambda_\ell + A_{22,\ell} v_{\mathrm{f},\ell}^{\mathrm{dq}} + B_{2,\ell} u_{1,\ell} + g_{2,\ell}(x_\ell, u_2)). \end{aligned} \tag{B.8}$$

Using identities in (B.5) and (B.6), the dynamics above can be written as follows:

$$\dot{z}_1 = A_{11}^{0} z_1 + A_{12}^{0} z_2 + g_1^{\mathrm{r}}(x^{\mathrm{r}}, u_2^{\mathrm{r}}) - \sum_{\ell=1}^{N} g_{1,\ell}(x_\ell, u_2), \tag{B.9}$$

$$\dot{z}_2 = A_{21}^{0} z_1 + A_{22}^{0} z_2 + \widehat{\kappa} g_2^{\mathrm{r}}(x^{\mathrm{r}}, u_2^{\mathrm{r}}) - \sum_{\ell=1}^{N} \kappa_\ell g_{2,\ell}(x_\ell, u_2). \tag{B.10}$$

Let $g_{1,k}^{\mathrm{r}}$ and $g_{1,\ell,k}$ $g_{1,k}^{0}$ denote the k-th entry of $g_1^{\mathrm{r}}(x^{\mathrm{r}}, u_2^{\mathrm{r}})$ and $g_{1,\ell}(x_\ell, u_2)$, respectively, and $g_{2,k}^{\mathrm{r}}$ and $g_{2,\ell,k}$ denote the k-th entry of $g_2^{\mathrm{r}}(x^{\mathrm{r}}, u_2^{\mathrm{r}})$ and $g_{2,\ell}(x_\ell, u_2)$. We also denote the k-th entry of z_1 and z_2 as $z_{1,k}$ and $z_{2,k}$. The entries of $g_1^{\mathrm{r}}(x^{\mathrm{r}}, u_2^{\mathrm{r}}) - \sum_{\ell=1}^{N} g_{1,\ell}(x_\ell, u_2)$ are:

$$g_{1,1}^{\mathrm{r}} - \sum_{\ell=1}^{N} g_{1,\ell,1} = 0, \quad g_{1,2}^{\mathrm{r}} - \sum_{\ell=1}^{N} g_{1,\ell,2} = 0, \tag{B.11}$$

$$g_{1,3}^{\mathrm{r}} - \sum_{\ell=1}^{N} g_{1,\ell,3} = (-k_{\mathrm{PLL}}^{p} v_{\mathrm{PLL}}^{\mathrm{r}} + k_{\mathrm{PLL}}^{i} \phi_{\mathrm{PLL}}^{\mathrm{r}}) i_{\mathrm{o}}^{\mathrm{q,r}} - \frac{\widehat{\kappa}}{L_g} v_g^{\mathrm{d}}(x^{\mathrm{r}}, u_2^{\mathrm{r}})$$

$$
\begin{aligned}
&\quad - \sum_{\ell=1}^{N}((-k^p_{\mathrm{PLL}} v_{\mathrm{PLL},\ell} + k^i_{\mathrm{PLL}} \phi_{\mathrm{PLL},\ell}) i^{\mathrm{q}}_{\mathrm{o},\ell} - \frac{\kappa_\ell}{L_g} v^{\mathrm{d}}_g(x_\ell, u_2)) \\
&= (-k^p_{\mathrm{PLL}} v^{\mathrm{r}}_{\mathrm{PLL}} + k^i_{\mathrm{PLL}} \phi^{\mathrm{r}}_{\mathrm{PLL}}) z_{1,3}, \qquad \text{(B.12)}
\end{aligned}
$$

$$
\begin{aligned}
g^{\mathrm{r}}_{1,4} - \sum_{\ell=1}^{N} g_{1,\ell,4} &= (k^p_{\mathrm{PLL}} v^{\mathrm{r}}_{\mathrm{PLL}} - k^i_{\mathrm{PLL}} \phi^{\mathrm{r}}_{\mathrm{PLL}}) i^{\mathrm{d,r}}_{\mathrm{o}} - \frac{\widehat{\kappa}}{L_g} v^{\mathrm{q}}_g(x^{\mathrm{r}}, u^{\mathrm{r}}_2) \\
&\quad - \sum_{\ell=1}^{N}((k^p_{\mathrm{PLL}} v_{\mathrm{PLL},\ell} - k^i_{\mathrm{PLL}} \phi_{\mathrm{PLL},\ell}) i^{\mathrm{d}}_{\mathrm{o},\ell} - \frac{\kappa_\ell}{L_g} v^{\mathrm{q}}_g(x_\ell, u_2)) \\
&= (k^p_{\mathrm{PLL}} v^{\mathrm{r}}_{\mathrm{PLL}} - k^i_{\mathrm{PLL}} \phi^{\mathrm{r}}_{\mathrm{PLL}}) z_{1,4}, \qquad \text{(B.13)}
\end{aligned}
$$

$$
g^{\mathrm{r}}_{1,5} - \sum_{\ell=1}^{N} g_{1,\ell,5} = 0, \quad g^{\mathrm{r}}_{1,6} - \sum_{\ell=1}^{N} g_{1,\ell,6} = 0, \qquad \text{(B.14)}
$$

$$
\begin{aligned}
g^{\mathrm{r}}_{1,7} - \sum_{\ell=1}^{N} g_{1,\ell,7} &= \frac{3}{2}\omega_{\mathrm{c,PC}}(v^{\mathrm{d}}_g(x^{\mathrm{r}}, u^{\mathrm{r}}_2) i^{\mathrm{d,r}}_{\mathrm{o}} + v^{\mathrm{q}}_g(x^{\mathrm{r}}, u^{\mathrm{r}}_2) i^{\mathrm{q,r}}_{\mathrm{o}}) \\
&\quad - \frac{3}{2}\omega_{\mathrm{c,PC}} \sum_{\ell=1}^{N}(v^{\mathrm{d}}_g(x_\ell, u_2) i^{\mathrm{d}}_{\mathrm{o},\ell} + v^{\mathrm{q}}_g(x_\ell, u_2) i^{\mathrm{q}}_{\mathrm{o},\ell}) \\
&= \frac{3}{2}\omega_{\mathrm{c,PC}}(v^{\mathrm{d}}_g(x^{\mathrm{r}}, u_2) z_{1,3} + v^{\mathrm{q}}_g(x^{\mathrm{r}}, u_2) z_{1,4}), \qquad \text{(B.15)}
\end{aligned}
$$

$$
\begin{aligned}
g^{\mathrm{r}}_{1,8} - \sum_{\ell=1}^{N} g_{1,\ell,8} &= \frac{3}{2}\omega_{\mathrm{c,PC}}(v^{\mathrm{q}}_g(x^{\mathrm{r}}, u^{\mathrm{r}}_2) i^{\mathrm{d,r}}_{\mathrm{o}} - v^{\mathrm{d}}_g(x^{\mathrm{r}}, u^{\mathrm{r}}_2) i^{\mathrm{q,r}}_{\mathrm{o}}) \\
&\quad - \frac{3}{2}\omega_{\mathrm{c,PC}} \sum_{\ell=1}^{N}(v^{\mathrm{q}}_g(x_\ell, u_2) i^{\mathrm{d}}_{\mathrm{o},\ell} - v^{\mathrm{d}}_g(x_\ell, u_2) i^{\mathrm{q}}_{\mathrm{o},\ell}) \\
&= \frac{3}{2}\omega_{\mathrm{c,PC}}(v^{\mathrm{q}}_g(x^{\mathrm{r}}, u_2) z_{1,3} - v^{\mathrm{d}}_g(x^{\mathrm{r}}, u_2) z_{1,4}), \qquad \text{(B.16)}
\end{aligned}
$$

$$
g^{\mathrm{r}}_{1,9} - \sum_{\ell=1}^{N} g_{1,\ell,9} = 0, \quad g^{\mathrm{r}}_{1,10} - \sum_{\ell=1}^{N} g_{1,\ell,10} = 0, \qquad \text{(B.17)}
$$

and the entries of $\widehat{\kappa} g^{\mathrm{r}}_2(x^{\mathrm{r}}, u^{\mathrm{r}}_2) - \sum_{\ell=1}^{N} \kappa_\ell g_{1,\ell}(x_\ell, u_2)$ are:

$$
\begin{aligned}
\widehat{\kappa} g^{\mathrm{r}}_{2,1} - \sum_{\ell=1}^{N} \kappa_\ell g_{2,\ell,2} &= \widehat{\kappa}(-k^p_{\mathrm{PLL}} v^{\mathrm{r}}_{\mathrm{PLL}} + k^i_{\mathrm{PLL}} \phi^{\mathrm{r}}_{\mathrm{PLL}})(-\frac{R_{\mathrm{f}}}{\widehat{\kappa}} i^{\mathrm{q,r}}_{\mathrm{i}} + v^{\mathrm{q,r}}_{\mathrm{f}}) + \frac{R_{\mathrm{f}}}{L_g} v^{\mathrm{d}}_g(x^{\mathrm{r}}, u^{\mathrm{r}}_2)) \\
&\quad - \sum_{\ell=1}^{N} \kappa_\ell((-k^p_{\mathrm{PLL}} v_{\mathrm{PLL},\ell} + k^i_{\mathrm{PLL}} \phi_{\mathrm{PLL},\ell})(-\frac{R_{\mathrm{f}}}{\kappa_\ell} i^{\mathrm{q}}_{\mathrm{i},\ell} + v^{\mathrm{q}}_{\mathrm{f},\ell}) + \frac{R_{\mathrm{f}}}{L_g} v^{\mathrm{d}}_g(x_\ell, u_2))
\end{aligned}
$$

$$= (-k^p_{\mathrm{PLL}} v^{\mathrm{r}}_{\mathrm{PLL}} + k^i_{\mathrm{PLL}} \phi^{\mathrm{r}}_{\mathrm{PLL}})(-R_{\mathrm{f}} z_{1,2} + z_{2,2}), \tag{B.18}$$

$$\begin{aligned}
\widehat{\kappa} g^{\mathrm{r}}_{2,2} - \sum_{\ell=1}^{N} \kappa_\ell g_{2,\ell,2} &= \widehat{\kappa}(k^p_{\mathrm{PLL}} v^{\mathrm{r}}_{\mathrm{PLL}} - k^i_{\mathrm{PLL}} \phi^{\mathrm{r}}_{\mathrm{PLL}})(-\frac{R_{\mathrm{f}}}{\widehat{\kappa}} i^{\mathrm{d,r}}_{\mathrm{i}} + v^{\mathrm{d,r}}_{\mathrm{f}}) + \frac{R_{\mathrm{f}}}{L_g} v^{\mathrm{q}}_g(x^{\mathrm{r}}, u^{\mathrm{r}}_2)) \\
&\quad - \sum_{\ell=1}^{N} \kappa_\ell ((k^p_{\mathrm{PLL}} v_{\mathrm{PLL},\ell} - k^i_{\mathrm{PLL}} \phi_{\mathrm{PLL},\ell})(-\frac{R_{\mathrm{f}}}{\kappa_\ell} i^{\mathrm{d}}_{\mathrm{i},\ell} + v^{\mathrm{d}}_{\mathrm{f},\ell}) + \frac{R_{\mathrm{f}}}{L_g} v^{\mathrm{q}}_g(x_\ell, u_2)) \\
&= (k^p_{\mathrm{PLL}} v^{\mathrm{r}}_{\mathrm{PLL}} - k^i_{\mathrm{PLL}} \phi^{\mathrm{r}}_{\mathrm{PLL}})(-R_{\mathrm{f}} z_{1,1} + z_{2,1}).
\end{aligned} \tag{B.19}$$

Notice that $z_1 = \mathbb{0}_{10}$ and $z_2 = \mathbb{0}_2$ imply $\dot{z}_1 = \mathbb{0}_{10}$ and $\dot{z}_2 = \mathbb{0}_2$ since the nonlinear parts of the dynamics shown in (B.11)–(B.19) are also zero. Thus, we have $\lambda^{\mathrm{r}}(t) = \sum_{\ell=0}^{N} \lambda_\ell(t)$ and $v^{\mathrm{dq,r}}_{\mathrm{f}}(t) = \sum_{\ell=1}^{N} \frac{\kappa_\ell}{\widehat{\kappa}} v^{\mathrm{dq}}_{\mathrm{f},\ell}(t)$ for $t \geq t_0$ if we initialize them as $\lambda^{\mathrm{r}}(t_0) = \sum_{\ell=0}^{N} \lambda_\ell(t_0)$ and $v^{\mathrm{dq,r}}_{\mathrm{f}}(t_0) = \sum_{\ell=1}^{N} \frac{\kappa_\ell}{\widehat{\kappa}} v^{\mathrm{dq}}_{\mathrm{f},\ell}(t_0)$. This concludes the proof.

Appendix C

Three-phase Photovoltaic Inverter Model Particulars

C.1 Entries of State-space Matrices of Three-phase Photovoltaic Inverter

Partition the state vector as $x = [x_{\mathrm{LCL}}^{\mathrm{T}}, x_{\mathrm{dc}}^{\mathrm{T}}, x_{\mathrm{RC}}^{\mathrm{T}}, x_{\mathrm{CC}}^{\mathrm{T}}, x_{\mathrm{PLL}}^{\mathrm{T}}]^{\mathrm{T}}$, where $x_{\mathrm{LCL}} := [i_{\mathrm{i}}^{\mathrm{d}}, i_{\mathrm{i}}^{\mathrm{q}}, i_{\mathrm{o}}^{\mathrm{d}}, i_{\mathrm{o}}^{\mathrm{q}}, v_{\mathrm{f}}^{\mathrm{d}}, v_{\mathrm{f}}^{\mathrm{q}}]^{\mathrm{T}}$, $x_{\mathrm{dc}} := [e_{\mathrm{dc}}, p_{\mathrm{pv,avg}}, \phi_{\mathrm{dc}}]^{\mathrm{T}}$, $x_{\mathrm{RC}} := [q_{\mathrm{avg}}, \phi_{\mathrm{q}}]^{\mathrm{T}}$, $x_{\mathrm{CC}} := [\gamma^{\mathrm{d}}, \gamma^{\mathrm{q}}]^{\mathrm{T}}$, and $x_{\mathrm{PLL}} := [v_{\mathrm{PLL}}, \phi_{\mathrm{PLL}}, \delta]^{\mathrm{T}}$. The inverter dynamics are

$$\begin{bmatrix} \dot{x}_{\mathrm{LCL}} \\ \dot{x}_{\mathrm{dc}} \\ \dot{x}_{\mathrm{RC}} \\ \dot{x}_{\mathrm{CC}} \\ \dot{x}_{\mathrm{PLL}} \end{bmatrix} = \begin{bmatrix} A_{\mathrm{LCL}} & A_{\mathrm{LCL}}^{\mathrm{dc}} & A_{\mathrm{LCL}}^{\mathrm{RC}} & A_{\mathrm{LCL}}^{\mathrm{CC}} & \mathbb{0}_{6\times 3} \\ \mathbb{0}_{3\times 6} & A_{\mathrm{dc}} & \mathbb{0}_{3\times 2} & \mathbb{0}_{3\times 2} & \mathbb{0}_{3\times 3} \\ \mathbb{0}_{2\times 6} & \mathbb{0}_{2\times 3} & A_{\mathrm{RC}} & \mathbb{0}_{2\times 2} & \mathbb{0}_{2\times 3} \\ A_{\mathrm{CC}}^{\mathrm{LCL}} & A_{\mathrm{CC}}^{\mathrm{dc}} & A_{\mathrm{CC}}^{\mathrm{RC}} & \mathbb{0}_{2\times 2} & \mathbb{0}_{2\times 3} \\ \mathbb{0}_{3\times 6} & \mathbb{0}_{3\times 3} & \mathbb{0}_{3\times 2} & \mathbb{0}_{3\times 2} & A_{\mathrm{PLL}} \end{bmatrix} \begin{bmatrix} x_{\mathrm{LCL}} \\ x_{\mathrm{dc}} \\ x_{\mathrm{RC}} \\ x_{\mathrm{CC}} \\ x_{\mathrm{PLL}} \end{bmatrix} + g(x, u_1, u_2, u_3),$$

where the nonzero submatrices are given by

$$A_{\mathrm{LCL}} = \begin{bmatrix} -\frac{R_{\mathrm{i}}+k^p_{\mathrm{CC}}}{L_{\mathrm{i}}} & 0 & 0 \\ 0 & -\frac{R_{\mathrm{i}}+k^p_{\mathrm{CC}}}{L_{\mathrm{i}}} & 0 \\ 0 & 0 & -\frac{R_g}{L_g} \\ 0 & 0 & -\omega_{\mathrm{nom}} \\ -\frac{R_{\mathrm{f}}(k^p_{\mathrm{CC}}+R_{\mathrm{i}})}{L_{\mathrm{i}}} + \frac{1}{C_{\mathrm{f}}} & -\omega_{\mathrm{nom}}R_{\mathrm{f}} & \frac{R_{\mathrm{f}}R_g}{L_g} - \frac{1}{C_{\mathrm{f}}} \\ \omega_{\mathrm{nom}}R_{\mathrm{f}} & -\frac{R_{\mathrm{f}}(k^p_{\mathrm{CC}}+R_{\mathrm{i}})}{L_{\mathrm{i}}} & 0 \end{bmatrix}$$

$$\begin{bmatrix} 0 & -\frac{1}{L_{\mathrm{i}}} & 0 \\ 0 & 0 & -\frac{1}{L_{\mathrm{i}}} \\ \omega_{\mathrm{nom}} & \frac{1}{L_g} & 0 \\ -\frac{R_g}{L_g} & 0 & \frac{1}{L_g} \\ 0 & -\frac{R_{\mathrm{f}}}{L_{\mathrm{i}}} - \frac{R_{\mathrm{f}}}{L_g} & \omega_{\mathrm{nom}} \\ \frac{R_{\mathrm{f}}R_g}{L_g} - \frac{1}{C_{\mathrm{f}}} & -\omega_{\mathrm{nom}} & -\frac{R_{\mathrm{f}}}{L_{\mathrm{i}}} - \frac{R_{\mathrm{f}}}{L_g} \end{bmatrix},$$

$$A^{\mathrm{dc}}_{\mathrm{LCL}} = \begin{bmatrix} 0 & 0 & \\ \frac{k^p_{\mathrm{CC}}k^p_{\mathrm{VC}}}{L_{\mathrm{i}}} & 0 & -\frac{k^p_{\mathrm{CC}}k^i_{\mathrm{VC}}}{L_{\mathrm{i}}} \\ 0 & 0 & 0 \\ 0 & 0 & 0 \\ \frac{k^p_{\mathrm{CC}}k^p_{\mathrm{VC}}R_{\mathrm{f}}}{L_{\mathrm{i}}} & 0 & -\frac{k^p_{\mathrm{CC}}k^i_{\mathrm{VC}}R_{\mathrm{f}}}{L_{\mathrm{i}}} \end{bmatrix}, \quad A^{\mathrm{RC}}_{\mathrm{LCL}} = \begin{bmatrix} -\frac{k^p_{\mathrm{CC}}k^p_{\mathrm{Q}}}{L_{\mathrm{i}}} & \frac{k^p_{\mathrm{CC}}k^i_{\mathrm{Q}}}{L_{\mathrm{i}}} \\ 0 & 0 \\ 0 & 0 \\ 0 & 0 \\ -\frac{k^p_{\mathrm{CC}}k^p_{\mathrm{Q}}R_{\mathrm{f}}}{L_{\mathrm{i}}} & \frac{k^p_{\mathrm{CC}}k^i_{\mathrm{Q}}R_{\mathrm{f}}}{L_{\mathrm{i}}} \\ 0 & 0 \end{bmatrix},$$

$$A^{\mathrm{CC}}_{\mathrm{LCL}} = \begin{bmatrix} \frac{k^i_{\mathrm{CC}}}{L_{\mathrm{i}}} & 0 \\ 0 & \frac{k^i_{\mathrm{CC}}}{L_{\mathrm{i}}} \\ 0 & 0 \\ 0 & 0 \\ \frac{k^i_{\mathrm{CC}}R_{\mathrm{f}}}{L_{\mathrm{i}}} & 0 \\ 0 & \frac{k^i_{\mathrm{CC}}R_{\mathrm{f}}}{L_{\mathrm{i}}} \end{bmatrix}, \quad A_{\mathrm{dc}} = \begin{bmatrix} 0 & 0 & 0 \\ 0 & -\omega_{\mathrm{c,pv}} & 0 \\ -1 & 0 & 0 \end{bmatrix}, \quad A_{\mathrm{RC}} = \begin{bmatrix} -\omega_{\mathrm{c,Q}} & 0 \\ 0 & -1 \end{bmatrix},$$

$$A^{\mathrm{LCL}}_{\mathrm{CC}} = \begin{bmatrix} -1 & 0 & 0 & 0 & 0 & 0 \\ 0 & -1 & 0 & 0 & 0 & 0 \end{bmatrix}, \quad A^{\mathrm{dc}}_{\mathrm{CC}} = \begin{bmatrix} 0 & 0 & 0 \\ k^p_{\mathrm{VC}} & 0 & -k^i_{\mathrm{VC}} \end{bmatrix},$$

$$A^{\mathrm{RC}}_{\mathrm{CC}} = \begin{bmatrix} -k^p_{\mathrm{Q}} & k^i_{\mathrm{Q}} \\ 0 & 0 \end{bmatrix}, \quad A_{\mathrm{PLL}} = \begin{bmatrix} -\omega_{c,\mathrm{PLL}} & 0 & 0 \\ -1 & 0 & 0 \\ -k^p_{\mathrm{PLL}} & k^i_{\mathrm{PLL}} & 0 \end{bmatrix}.$$

Let g_ℓ denote the ℓ-th entry of the function $g(x, u_1, u_2, u_3)$. The nonzero entries of $g(x, u_1, u_2, u_3)$ are given by

$$
\begin{aligned}
g_2 &= -\frac{k^p_{\mathrm{CC}} k^p_{\mathrm{VC}}}{L_{\mathrm{i}}} v^{\star 2}_{\mathrm{dc}}, \\
g_3 &= (-k^p_{\mathrm{PLL}} v_{\mathrm{PLL}} + k^i_{\mathrm{PLL}} \phi_{\mathrm{PLL}}) i^{\mathrm{q}}_{\mathrm{o}} - \frac{1}{L_g} v^{\mathrm{d}}_g,\ g_{13} = -k^p_{\mathrm{VC}} v^{\star 2}_{\mathrm{dc}} \\
g_4 &= (k^p_{\mathrm{PLL}} v_{\mathrm{PLL}} - k^i_{\mathrm{PLL}} \phi_{\mathrm{PLL}}) i^{\mathrm{d}}_{\mathrm{o}} - \frac{1}{L_g} v^{\mathrm{q}}_g, \\
g_5 &= (-k^p_{\mathrm{PLL}} v_{\mathrm{PLL}} + k^i_{\mathrm{PLL}} \phi_{\mathrm{PLL}})(-R_{\mathrm{f}} i^{\mathrm{q}}_{\mathrm{i}} + v^{\mathrm{q}}_{\mathrm{f}}) + \frac{R_{\mathrm{f}}}{L_g} v^{\mathrm{d}}_g, \\
g_6 &= (k^p_{\mathrm{PLL}} v_{\mathrm{PLL}} - k^i_{\mathrm{PLL}} \phi_{\mathrm{PLL}})(-R_{\mathrm{f}} i^{\mathrm{d}}_{\mathrm{i}} + v^{\mathrm{d}}_{\mathrm{f}}) + \frac{R_{\mathrm{f}}}{L_g} v^{\mathrm{q}}_g - \frac{R_{\mathrm{f}} k^p_{\mathrm{CC}} k^p_{\mathrm{VC}}}{L_{\mathrm{i}}} v^{\star 2}_{\mathrm{dc}}, \\
g_7 &= \frac{1}{C_{\mathrm{dc}}} (\sqrt{e_{\mathrm{dc}}} i_{\mathrm{pv}} - \frac{3}{2} (v^{\mathrm{d}}_{\mathrm{i}} i^{\mathrm{d}}_{\mathrm{i}} + v^{\mathrm{q}}_{\mathrm{i}} i^{\mathrm{q}}_{\mathrm{i}})) \\
g_8 &= \omega_{\mathrm{c,pv}} \sqrt{e_{\mathrm{dc}}} i_{\mathrm{pv}}, \\
g_9 &= v^{\star 2}_{\mathrm{dc}}, \\
g_{10} &= \frac{3}{2} \omega_{\mathrm{c,Q}} (v^{\mathrm{q}}_g i^{\mathrm{d}}_{\mathrm{o}} - v^{\mathrm{d}}_g i^{\mathrm{q}}_{\mathrm{o}}), \\
g_{14} &= \omega_{\mathrm{c,PLL}} v^{\mathrm{d}}_g, \\
g_{16} &= \omega_{\mathrm{nom}}.
\end{aligned}
$$